AD-771 963

AEROELASTIC ANALYSIS OF A TELESCOPING ROTOR BLADE

Raymond G. Carlson, et al

United Aircraft Corporation

Prepared for:

Army Air Mobility Research and Development Laboratory

August 1973

DISTRIBUTED BY:

NTIS

National Technical Information Service
U. S. DEPARTMENT OF COMMERCE
5285 Port Royal Road, Springfield Va. 22151

DEPARTMENT OF THE ARMY
U. S. ARMY AIR MOBILITY RESEARCH & DEVELOPMENT LABORATORY
EUSTIS DIRECTORATE
FORT EUSTIS, VIRGINIA 23604

This report has been reviewed by the Eustis Directorate, U. S. Army Air Mobility and Development Laboratory and is considered to be technically sound. The purpose of the program was to develop an aeroelastic analysis and computer program for predicting the uncoupled flapwise, chordwise, and torsional natural frequencies and mode shapes of a TRAC rotor blade. An analysis and computer program was also developed for calculating the TRAC rotor blade aeroelastic time history.

The technical monitor for this contract was Paul H. Mirick, Aeromechanics, Technology Applications Division.

Project 1F163204D157
Contract DAAJ02-72-C-0025
USAAMRDL Technical Report 73-48
August 1973

AEROELASTIC ANALYSIS OF A TELESCOPING ROTOR BLADE

Final Report

By

Raymond G. Carlson
Sebastian J. Cassarino

Prepared by

United Aircraft Corporation
Sikorsky Aircraft Division
Stratford, Connecticut

for

EUSTIS DIRECTORATE
U.S. ARMY AIR MOBILITY RESEARCH AND DEVELOPMENT LABORATORY
FORT EUSTIS, VIRGINIA

Unclassifed
Security Classification

AD-771963

DOCUMENT CONTROL DATA - R & D

(Security classification of title, body of abstract and indexing annotation must be entered when the overall report is classified)

1. ORIGINATING ACTIVITY (Corporate author) United Aircraft Corporation Sikorsky Aircraft Division Stratford, Connecticut	2a. REPORT SECURITY CLASSIFICATION Unclassified 2b. GROUP

3. REPORT TITLE

AEROELASTIC ANALYSIS OF A TELESCOPING ROTOR BLADE

4. DESCRIPTIVE NOTES (Type of report and inclusive dates)

Final Report

5. AUTHOR(S) (First name, middle initial, last name)

Raymond G. Carlson
Sebastian J. Cassarino

6. REPORT DATE August 1973	7a. TOTAL NO. OF PAGES ~~128~~ 119	7b. NO. OF REFS 8
8a. CONTRACT OR GRANT NO DAAJ02-72-C-0025 b. PROJECT NO. 1F163204D157 c. d.	9a. ORIGINATOR'S REPORT NUMBER(S) USAAMRDL Technical Report 73-48 9b. OTHER REPORT NO(S) (Any other numbers that may be assigned this report)	

10. DISTRIBUTION STATEMENT

Approved for public release; distribution unlimited.

11. SUPPLEMENTARY NOTES	12. SPONSORING MILITARY ACTIVITY Eustis Directorate U.S. Army Air Mobility R&D Laboratory Fort Eustis, Virginia

13. ABSTRACT

Two computer programs were developed to evaluate the aeroelastic response of a telescoping rotor blade (TRAC). The first program calculates the uncoupled blade natural frequencies of flatwise, edgewise, and torsional degrees of freedom. The second program is a forced-response program and is a modification of the computer program provided to the Army under Contract DAAJ02-71-C-0024. It calculates the time history of the response of either a single blade or the complete rotor on a rigid-body airframe. Both steady-state and transient response can be analyzed. The forced-response program uses blade mode shapes and natural frequencies calculated from the natural frequency program. The mathematical model used reflects the unique structure of the TRAC blade, which consists of torque tube, outboard blade, jackscrew, and two tension straps. In determining natural frequencies, each component is considered as a series of lumped mass elements with appropriate constraint equations applied at the interfaces between the structural components. Blade root end fixity, amount of retraction, and rotor speed can all be varied.

Analysis of a TRAC model rotor blade using the blade natural frequency analysis demonstrated the significant effects on natural frequency of coupling between structural components, rotor speed, retraction ratio, and compression in the outboard blade. The natural frequency analysis was also found to compare quite well with the conventional blade natural frequency analysis at low rotor speeds where centrifugal forces are not a significant factor. At high rotor speeds, the compression in the TRAC outboard blade tends to lower blade natural frequencies. Correlation of predicted flatwise moments with model rotor test data showed reasonably good correlation for all retraction ratios and rotor speeds. Measured torsional moments were, however, much larger than predicted. Edgewise moment predictions could not be correlated because of an extraneous vibration which dominated the test data for the selected cases. All test data were obtained under Contract DAAJ02-68-C-0074. The correlation study considered variations in retraction ratio, rotor speed, airspeed, and root end fixity.

DD FORM 1 NOV 65 1473 REPLACES DD FORM 1473, 1 JAN 64, WHICH IS OBSOLETE FOR ARMY USE.

Unclassified
Security Classification

14 KEY WORDS	LINK A		LINK B		LINK C	
	ROLE	WT	ROLE	WT	ROLE	WT
Telescoping Rotor Blade (TRAC) Aeroelastic Analysis of a TRAC Blade Natural Frequency Calculations for a TRAC Blade Mode Shape Calculations for a TRAC Blade Forced-Response Characteristics of a TRAC Blade Correlation of Experimental and Theoretical Data for a TRAC Blade						

SUMMARY

Two computer programs were developed to evaluate the aeroelastic response of a telescoping rotor blade (TRAC). The first program calculates the uncoupled blade natural frequencies for flatwise, edgewise, and torsional degrees of freedom. The second program is a forced-response program and is a modification of the computer program provided to the Army under Contract DAAJ02-71-C-0024. It calculates the time history of the response of either a single blade or the complete rotor on a rigid-body airframe. Both steady-state and transient response can be analyzed. The forced-response program uses blade mode shapes and natural frequencies calculated from the natural frequency program. The mathematical model used reflects the unique structure of the TRAC blade, which consists of torque tube, outboard blade, jackscrew, and two tension straps. In determining natural frequencies, each component is considered as a series of lumped mass elements with appropriate constraint equations applied at the interfaces between the structural components. Blade root end fixity, amount of retraction, and rotor speed can all be varied.

Analysis of a TRAC model rotor blade using the blade natural frequency analysis demonstrated the significant effects on natural frequency of coupling between structural components, rotor speed, retraction ratio, and compression in the outboard blade. The natural frequency analysis was also found to compare quite well with the conventional blade natural frequency analysis at low rotor speeds where centrifugal forces are not a significant factor. At high rotor speeds, the compression in the TRAC outboard blade tends to lower blade natural frequencies. Correlation of predicted flatwise moments with model rotor test data showed reasonably good correlation for all retraction ratios and rotor speeds. Measured torsional moments were, however, much larger than predicted. Edgewise moment predictions could not be correlated because of an extraneous vibration which dominated the test data for the selected cases. All test data were obtained under Contract DAAJ02-68-C-0074. The correlation study considered variations in retraction ratio, rotor speed, airspeed, and root end fixity.

FOREWORD

This work was performed for the Eustis Directorate, U. S. Army Air Mobility Research and Development Laboratory, Fort Eustis, Virginia, under Contract DAAJ02-72-C-0025. Technical monitor for the Army was Paul Mirick. The equations of motion for this study were developed by Sebastian Cassarino, and the programming and correlation of results were done by Russell Bergquist.

TABLE OF CONTENTS

LIST OF ILLUSTRATIONS

Figure		Page

Figure		Page

LIST OF TABLES

LIST OF SYMBOLS

$\mathbf{A}$ three-by-three transformation matrix

C_{C1} effective angular spring between the torque tube and the outboard blade at the beginning of the overlapped region, ft-lb/rad

C_{C2} effective angular spring between the torque tube and the outboard blade at the end of the overlapped region, ft-lb/rad

C_n standard four-by-four transfer matrix between the n^{th} and $(n-1)^{th}$ segments

C_T/σ rotor thrust coefficient-solidity ratio

D external force in the edgewise equations, lb

e hinge offset, ft

F_x D'Alembert's force along a longitudinal blade axis, lb

F_y D'Alembert's force along a chordwise blade axis, lb

F_z D'Alembert's force along a vertical blade axis, lb

$I_{x\beta}$ mass moment of inertia of a blade segment about the vertical blade axis, $\int_{-l_n/2}^{l_n/2} x_{4n}^2 dm_n$, slug-ft^2

$I_{z\beta}$ mass moment of inertia of a blade segment about the longitudinal axis of the blade, $\int_{-l_n/2}^{l_n/2} z_{4n}^2 dm_n$, slug-ft^2

I_F effective moment of inertia of a blade segment associated with the blade propeller moment, $(I_{x\beta}-I_{z\beta})$, slug-ft^2

I_β flatwise polar moment of inertia of blade segment, $(I_{x\beta}+I_{z\beta})$, slug-ft^2

I_γ edgewise polar moment of inertia of a blade segment, $\int_{-l_n/2}^{l_n/2} (y_{4n}^2 + z_{4n}^2) dm_n$, slug-ft^2

K_n effective elastic spring between the n^{th} and $(n-1)^{th}$ segments, ft-lb/rad

K_x effective linear spring at the inboard end of the tension straps, lb/ft

L_s distance between leading and lagging straps, ft

l length of a blade segment, ft

M elastic bending moment acting at one end of a blade segment defined in terms of the effective spring and the difference in the angular displacements of two adjacent segments, ft-lb

M_y D'Alembert's moment along a chordwise blade axis, ft-lb

M_z D'Alembert's moment along a vertical blade axis, ft-lb

m mass of a blade segment, slug

N total number of segments in a major blade element (chosen as 10 for all elements)

p_n column vector for the n^{th} blade segment used in the development of the transfer matrix method, $\begin{Bmatrix} \beta_n \\ z_{2n} \\ S_n^R \\ M_n^R \end{Bmatrix}$

Q external force in the flatwise equations, lb

$\vec{q}_n$ vectorial representation of the n^{th} axis system, $\begin{Bmatrix} x_n \\ y_n \\ z_n \end{Bmatrix}$

R rotor radius, ft

R_o fully-extended rotor radius, ft

$\bar{r}$ blade section radial coordinate divided by R

S normal shear acting at one end of a blade segment, lb

T tension acting at one end of a blade segment, lb

t real time, sec

V forward velocity, kt

x coordinate along a longitudinal blade axis, ft

y	coordinate along a chordwise blade axis, ft
z	coordinate along a vertical blade axis, ft
ω	blade natural frequency, rad/sec
α_s	rotor shaft angle, positive when shaft is tilted aft, deg
β	flapping angle, rad
γ	lead-lag or inplane angle, rad
σ	rotor solidity, ratio of blade area to rotor disc area
Ψ	rotor rotational displacement, rad
Ω	rotor speed, $d\Psi/dt$, rad/sec

SUBSCRIPTS

i	associated with the outboard blade segment in contact with the torque tube last segment
j	associated with the torque tube segment in contact with the outboard blade first segment
k	associated with the jackscrew segment containing the nut assembly
N_B	last segment of the outboard blade
N_J	last segment of the jackscrew
N_{LS}	last segment of the lagging strap
N_{RS}	last segment of the leading strap
N_T	last segment of the torque tube
n	index associated with a general blade segment
0	associated with the blade root segment
TIP	associated with the blade tip segment
1, 2, 3, 4	refer to coordinate axis

SUPERSCRIPTS

The following letters are used as right superscripts:

R	refers to the right side of a blade segment
L	refers to the left side of a blade segment

The following letters are used as left superscripts:

B	refers to the outboard blade
J	refers to the jackscrew
LS	refers to the lagging strap
RS	refers to the leading strap
T	refers to the torque tube

INTRODUCTION

A rotor configuration which offers significant potential of extending the operating capabilities of rotary-wing aircraft is the Telescoping Rotor Aircraft Concept (TRAC). The TRAC rotor blade is shown schematically in Figure 1 and is discussed in more detail in Reference 1. As might be expected, the structural arrangement of the TRAC blade differs considerably from that of conventional blades. For example, the outboard portion of the blade is under compressive loading since it is restrained in the radial direction by strap members at its outermost point. In addition, the blade is composed of multiple structural elements rather than a single primary element usually found in helicopter rotor blades. For these reasons, available analytical methods such as the Sikorsky Y200 Normal Modes Program (References 2 and 3) are not generally applicable to the TRAC system.

A preliminary analysis applicable to the TRAC blade was developed at Sikorsky Aircraft in 1964 to determine the flatwise natural frequencies and modes shapes and flatwise aeroelastic responses of a fully-extended TRAC rotor blade. A schematic of the aeroelastic representation of the blade appears in Figure 2. The analysis considered only two major structural components: the inboard element representing the combination of the torque tube and jackscrew, and the outboard blade. The tension strap was represented mathematically as a weightless string attaching the blade tip to the end of the jackscrew. The analysis represented each structural element as made up of rigid, finite-length segments with lumped masses and elastically equivalent springs between adjacent segments. The aerodynamic forces acting on the outboard blade and torque tube were included using conventional strip-theory and steady-state, two-dimensional airfoil data, including stall and Mach number effects. The analysis was extremely valuable in the preliminary design of the TRAC structural components.

The 1964 flatwise aeroelastic analysis was extended in 1967 to include the internal components, i.e., the jackscrew and a single tension strap as shown schematically in Figure 3. The same basic mathematical approach was used as in the two-element 1964 analysis except that the jackscrew and strap were given their own masses, stiffnesses, and degrees of freedom independent of the external components.

There are two primary limitations of the 1967 mathematical model discussed above. First, it does not consider the blade edgewise and torsional motions. Second, it is restricted to a fully-extended rotor for which the overlapped region between the torque tube and the outboard blade is a minimum. The aeroelastic analysis developed under this contract provides a more general analytical tool without these limitations. A schematic of the present representation of the TRAC blade is illustrated in Figure 4. From this figure it is noted that the overlapped region can be varied to represent all blade retraction radii and that two tension straps are used to connect the blade tip and the nut assembly.

DESCRIPTION OF THE TRAC ROTOR SYSTEM

The structural components of the TRAC rotor system are shown in the detailed schematic of Figure 5. The retraction mechanism is actuated by a jackscrew, which acts as the primary tension element of the blade. When rotated, the jackscrew imparts a linear retraction or extension motion to the retention nut and through the tension straps to the outboard blade. The jackscrew is inside a torque tube which transmits control motions to the outboard blade. The torque tube also carries the bending moments that are transmitted from the outboard blade, and it serves as an airfoil when the blade is extended.

The TRAC blade structure for a full-scale design, which appears in Figure 5, was based to a large extent on the two-element aeroelastic analysis discussed in the Introduction. The outboard blade is an NACA 63_2A016 airfoil section, while the torque tube has a 33-percent-thick elliptical section. Two bearing blocks are utilized for the sliding contacts between the outboard blade and the torque tube and the other to the inboard end of the outer blade. The jackscrew and the tension straps represent the main structural load path for centrifugal loads. A bearing block, not shown in Figure 5, attaches the outboard end of the jackscrew to the inner walls of the torque tube.

MATHEMATICAL MODEL OF THE TRAC BLADE

MATHEMATICAL MODEL OF A BLADE ELEMENT

The analytical technique used to compute the TRAC blade uncoupled flatwise and edgewise natural frequencies and mode shapes assumes that the various blade elastic elements (outboard blade, torque tube, jackscrew, and tension straps) can be represented by a finite number of rigid members or segments. The segments are joined by frictionless hinges and equivalent springs which simulate the elastic properties of the continuous blade element. For a uniform blade, the equivalent elastic spring between two segments is directly proportional to the flexural rigidity (EI) and inversely proportional to the total length of the segments. A schematic of the mathematical model of a TRAC blade element of given mass moment of inertia and length appears in Figure 6. The mass and area moments of inertia of the individual segments are uniform along a segment but can vary arbitrarily among the various segments. The lengths of the rigid members are also arbitrary. While an infinite number of segments is needed to represent theoretically a continuous element, it is found in practice that ten segments are sufficient to determine accurately the elastic behavior of the element. Structural damping effects are neglected in the development of the natural frequency analysis.

DESCRIPTION OF CRITICAL POINTS ALONG THE TRAC BLADE

In the development of the aeroelastic analysis of the TRAC blade, the five major structural elements are treated as elastic beams and are represented mathematically as discussed in the previous section. The following components, however, are assumed to behave as rigid bodies: blade root, blade tip cap, nut assembly, and bearing blocks between the major structural elements.

The various contact and attachment points which are present among the TRAC blade major components are shown in Figure 7. These are as follows:

1. Inboard sliding contact between the outer surface of the torque tube and the inner end of the outboard blade.
2. Outboard sliding contact between the end of the torque tube and the inner surface of the outboard blade.
3. Sliding contact between the jackscrew nut assembly and the torque tube.
4. Cantilevered attachment of tension straps to the nut assembly.
5. Attachment of jackscrew outboard end to the torque tube.
6. Attachment of outboard blade and tension straps to the blade tip cap.

7. Attachment of the torque tube and jackscrew inboard ends to the rotor head.

The first three critical points listed above represent sliding contacts between two elements of the TRAC blade. It is assumed that only normal shears and bending moments are transmitted through the bearing blocks present in the contact areas. When the segment approach is used to represent mathematically the blade elements, a contact area is described by a common segment for the two elements in contact. Angular flexibility of the contact area can be represented by an equivalent spring of variable stiffness to account for the local bending moment. We note then that the equations of motion describing the elastic behavior of the outboard blade and the torque tube are coupled through the first two contact points, while the torque tube and jackscrew are coupled through the third contact point. It should be pointed out that the nut assembly is treated as a rigid extension of the jackscrew. The jackscrew segment distribution is such that one of the segments represents the nut assembly. The contact between the nut assembly and the torque tube (point 3 above) is present only in the flatwise equations of motion and exists as soon as the blade begins to flap.

The remaining critical points represent various attachments along the TRAC blade. The inboard ends of the tension straps are attached to the center of the nut assembly (point 4), while the outboard ends are attached to the blade tip cap (point 6). It is assumed that the straps are located symmetrically about a longitudinal axis through the center of the jackscrew. The outboard end of the jackscrew is supported by a bearing block which connects it to the torque tube (point 5). The normal shear which is present between the two elements is accounted for in the analysis. The inboard ends of the torque tube and jackscrew are connected to the root segment (point 7).

BOUNDARY CONDITIONS ALONG THE TRAC BLADE

The boundary conditions which must be satisfied at the critical points (one through seven) shown in Figure 7 are discussed below:

1. The linear displacements (z for flatwise motion and y for edgewise motion) are the same for the first segment of the outboard blade and the segment of the torque tube which is in contact with the blade at point 1. The angular displacements (β for flatwise motion and γ for edgewise motion) are related through an angular spring located at the center of common segment.

2. The linear displacement of the last segment of the torque tube is identical to the displacement of the outboard blade segment in contact with the torque tube at point 2. The angular displacements are related through an angular spring located at the center of the common segment.

3. The linear (only z for flatwise motion) and angular displacements of the jackscrew segment containing the nut assembly are

the same as the displacements associated with the torque tube segment in contact with the jackscrew at point 3.

4. The linear displacement of the inboard end of the straps' first segment is the same as the displacement of the center of the jackscrew segment which includes the nut assembly. In addition, the angular displacements of the two segments are identical.

5. The linear displacements of the outboard ends of the jackscrew and torque tube are the same since they are rigidly attached at that point.

6. Since both the straps and the outboard blade are attached to the tip segment, then the linear displacement of the tip segment can be described by three continuity equations. These relations apply respectively to each strap and to the outboard blade.

7. Both the torque tube and jackscrew first segments are attached to the root segment. It follows that the angular displacements of these segments are defined in terms of the angular motion of the blade root and the equivalent springs at the segment junctions. The linear displacement of the segments is also defined in terms of the root linear displacement.

In the discussion of the boundary conditions applicable at critical points 1 and 2, it has been assumed that the outboard blade and torque tube walls in the contact areas have infinite stiffness in the normal direction. Angular flexibility of the two elements is accounted for by a linear relationship between the angular displacement and the local bending moment.

BLADE ROOT AND TIP BOUNDARY CONDITIONS

The inboard end of the root segment is attached to the flapping hinge for flatwise motion or to the lead-lag hinge for inplane motion by an angular spring. For an articulated rotor blade, the spring stiffness is zero, corresponding to the root condition of zero moment; while for a rigid blade, the stiffness becomes infinite, which is represented mathematically by the root condition of zero slope. For a stiffness value between zero and infinity, the boundary condition at the blade root is satisfied by a linear relation between root slope and moment. The second root boundary condition is that the linear displacement (z for flatwise motion and y for edgewise motion) at the hinge is zero.

The boundary conditions which apply to the outboard end of the TRAC blade are the standard conditions for a free end, i.e., zero shear and moment. These conditions are applied to the equations of motion of the blade tip segment. The linear displacement of the blade tip is used to normalize the blade motions in the calculations of the mode shapes.

TRAC BLADE FLATWISE EQUATIONS OF MOTION

COORDINATE AXES AND TRANSFORMATIONS

The axis systems employed in the development of the TRAC blade flatwise equations of motion are presented schematically in Figure 8 and are discussed below.

Nonrotating Rotor Hub Axis System: x_1, y_1, z_1

This axis system is located at the rotor hub center and does not rotate with respect to the aircraft. The axis z_1 is parallel to the rotor shaft and is positive up; x_1 is normal to the rotor shaft, lies in the plane formed by z_1 and the air velocity vector and is positive aft; y_1 is orthogonal to x_1 and z_1 and is positive toward the advancing side of the rotor. This axis system is Newtonian, having at most a steady translational velocity.

Rotating Rotor Hub Axis System: x_2, y_2, z_2

This axis system has its origin at the rotor hub center and rotates with the rotor blades. It is related to the "1" axis system as follows:

$$\vec{q}_1 = A_\psi \vec{q}_2 \qquad (1)$$

where the following definitions apply:

$$\vec{q}_n = \begin{Bmatrix} x_n \\ y_n \\ z_n \end{Bmatrix} \quad \text{and} \quad A_\psi = \begin{bmatrix} \cos\psi & -\sin\psi & 0 \\ \sin\psi & \cos\psi & 0 \\ 0 & 0 & 1 \end{bmatrix} \qquad (2)$$

Local Segment Axis System: x_{3n}, y_{3n}, z_{3n}

This axis system is located at the center of gravity of the n^{th} segment along the rotor blade. It is obtained by translations along each axis of the "2" system as shown below:

$$\vec{q}_2 = \vec{q}_{2n} + \vec{q}_{3n} \qquad (3)$$

Flapping Angle Axis System: x_{4n}, y_{4n}, z_{4n}

This axis system has its origin at the center of gravity of the n^{th} segment and is related to the "3n" system through the flapping angle β_n, which is defined as positive up.

$$\vec{q}_{3n} = A_{\beta_n} \vec{q}_{4n} \qquad (4)$$

where

$$A_{\beta_n} = \begin{bmatrix} \cos\beta_n & 0 & \sin\beta_n \\ 0 & 1 & 0 \\ \sin\beta_n & 0 & \cos\beta_n \end{bmatrix} \tag{5}$$

VELOCITY AND ACCELERATION VECTORS

Combining relations (1), (3), and (4) gives

$$\vec{q}_1 = A_\psi A_{\beta_n} \vec{q}_{4n} + A_\psi \vec{q}_{2n} \tag{6}$$

The velocity of an arbitrary point in the n^{th} blade segment is given by the following relation in the inertial coordinate system:

$$\dot{\vec{q}}_1 = A'_\psi A_{\beta_n} \vec{q}_{4n} \Omega + A_\psi A'_{\beta_n} \vec{q}_{4n} \dot{\beta}_n + A'_\psi \vec{q}_{2n} \Omega + A_\psi \dot{\vec{q}}_{2n} \tag{7}$$

where the following definitions were used:

$$\left.\begin{array}{l} 1.\ \dfrac{dA_\psi}{dt} = \dfrac{dA_\psi}{d\psi}\dfrac{d\psi}{dt} = A'_\psi \dot{\psi} \\ 2.\ \dfrac{d\psi}{dt} = \Omega = \text{constant} \end{array}\right\} \tag{8}$$

Also $\dot{\vec{q}}_{4n} = 0$ since an arbitrary point on the n^{th} blade segment is not moving relative to the center of gravity of the segment. The acceleration of the arbitrary point is obtained by differentiation of relation (7) above, which yields

$$\begin{aligned} \ddot{\vec{q}}_1 = {} & \ddot{\beta}_n A_\psi A'_{\beta_n} \vec{q}_{4n} + \dot{\beta}_n^2 A_\psi A''_{\beta_n} \vec{q}_{4n} + 2\Omega \dot{\beta}_n A'_\psi A'_{\beta_n} \vec{q}_{4n} \\ & + A_\psi \ddot{\vec{q}}_{2n} + 2\Omega A'_\psi \dot{\vec{q}}_{2n} + \Omega^2 A''_\psi \left[A_{\beta_n} \vec{q}_{4n} + \vec{q}_{2n} \right] \end{aligned} \tag{9}$$

In order to write the individual element equations of motion, the components of the total acceleration in the direction of the "4n" axis system must be found. These are obtained by the inverse transformations shown below:

$$\ddot{\vec{q}}_{4n} = A_{\beta_n}^{-1} A_\psi^{-1} \ddot{\vec{q}}_1 = \begin{Bmatrix} \ddot{x}_{4n} \\ \ddot{y}_{4n} \\ \ddot{z}_{4n} \end{Bmatrix} \tag{10}$$

where $A_{\beta_n}^{-1}$ and A_{ψ}^{-1} are the inverses of the matrices A_{β_n} and A_{ψ} respectively.

Substitution of relation (9) into (10) above and performing the various matrix multiplications yields the following expressions for the individual accelerations:

$$\ddot{x}_{4n} = -\ddot{\beta}_n z_{4n} - \dot{\beta}_n^2 x_{4n} + \Omega^2\left(-x_{4n}\cos^2\beta_n + z_{4n}\cos\beta_n \sin\beta_n - x_{2n}\cos\beta_n\right) + \ddot{x}_{2n}\cos\beta_n + \ddot{z}_{2n}\sin\beta_n - 2\Omega\dot{y}_{2n}\cos\beta_n \tag{11}$$

$$\ddot{y}_{4n} = -2\Omega\dot{\beta}_n\left(x_{4n}\sin\beta_n + z_{4n}\cos\beta_n\right) - \Omega^2\left(y_{2n} + y_{4n}\right) + \ddot{y}_{2n} + 2\Omega\dot{x}_{2n} \tag{12}$$

$$\ddot{z}_{4n} = \ddot{\beta}_n x_{4n} - \dot{\beta}_n^2 z_{4n} + \Omega^2\left(x_{4n}\sin\beta_n\cos\beta_n - z_{4n}\sin^2\beta_n + x_{2n}\sin\beta_n\right) - \ddot{x}_{2n}\sin\beta_n + \ddot{z}_{2n}\cos\beta_n + 2\Omega\dot{y}_{2n}\sin\beta_n \tag{13}$$

Since the equations of motion are uncoupled, the expression for $\ddot{y}_{4n}$ is ignored and the velocity $\dot{y}_{2n}$ is set to zero. Thus, the radial and vertical accelerations for a blade segment flatwise equation of motion become, respectively,

$$\ddot{x}_{4n} = -\ddot{\beta}_n z_{4n} - \dot{\beta}_n^2 x_{4n} + \Omega^2\left(-x_{4n}\cos^2\beta_n + z_{4n}\cos\beta_n\sin\beta_n - x_{2n}\cos\beta_n\right) + \ddot{x}_{2n}\cos\beta_n + \ddot{z}_{2n}\sin\beta_n \tag{14}$$

$$\ddot{z}_{4n} = \ddot{\beta}_n x_{4n} - \dot{\beta}_n^2 z_{4n} + \Omega^2\left(x_{4n}\sin\beta_n\cos\beta_n - z_{4n}\sin^2\beta_n + x_{2n}\sin\beta_n\right) - \ddot{x}_{2n}\sin\beta_n + \ddot{z}_{2n}\cos\beta_n \tag{15}$$

D'ALEMBERT'S FORCES AND MOMENT

By D'Alembert's principle, the incremental forces and moment on the n^{th} blade segment are as follows:

$$\left.\begin{aligned} dF_{x_{4n}} &= \ddot{x}_{4n}\, dm_n \\ dF_{z_{4n}} &= \ddot{z}_{4n}\, dm_n \\ dM_{y_{4n}} &= x_{4n}\, dF_{z_{4n}} - z_{4n}\, dF_{x_{4n}} \end{aligned}\right\} \tag{16}$$

Integration along the entire length of the blade segment yields the total forces and moment acting on the element center of gravity. The following relations are utilized:

$$\left.\begin{array}{ll}
1. & \displaystyle\int_{-\frac{\ell_n}{2}}^{\frac{\ell_n}{2}} dm_n = m_n \\[2ex]
2. & \displaystyle\int_{-\frac{\ell_n}{2}}^{\frac{\ell_n}{2}} x_{4n}\, dm_n = \int_{-\frac{\ell_n}{2}}^{\frac{\ell_n}{2}} z_{4n}\, dm_n = 0 \\[2ex]
3. & \displaystyle\int_{-\frac{\ell_n}{2}}^{\frac{\ell_n}{2}} x_{4n}^2\, dm_n = I_{x\beta_n} \\[2ex]
4. & \displaystyle\int_{-\frac{\ell_n}{2}}^{\frac{\ell_n}{2}} z_{4n}^2\, dm_n = I_{z\beta_n} \\[2ex]
5. & \displaystyle\int_{-\frac{\ell_n}{2}}^{\frac{\ell_n}{2}} x_{4n} z_{4n}\, dm_n = 0
\end{array}\right\} \quad (17)$$

The second relation states that the center of the segment is the center of gravity of the element. The last relation assumes that the product moment of inertia is zero.

The inertial force along the x_{4n} direction is given by

$$F_{x_{4n}} = \int_{-\frac{\ell_n}{2}}^{\frac{\ell_n}{2}} \ddot{x}_{4n}\, dm_n = m_n\left(-\Omega^2 x_{2n}\cos\beta_n + \ddot{x}_{2n}\cos\beta_n + \ddot{z}_{2n}\sin\beta_n\right) \quad (18)$$

The inertial force along the z_{4n} direction is given by

$$F_{z_{4n}} = \int_{-\frac{\ell_n}{2}}^{\frac{\ell_n}{2}} \ddot{z}_{4n}\, dm_n = m_n\left(\Omega^2 x_{2n}\sin\beta_n - \ddot{x}_{2n}\sin\beta_n + \ddot{z}_{2n}\cos\beta_n\right) \quad (19)$$

The flapping inertial moment is given by

$$M_{y_{4n}} = \int_{-\frac{\ell_n}{2}}^{\frac{\ell_n}{2}} (x_{4n}\ddot{z}_{4n} - z_{4n}\ddot{x}_{4n})\,dm_n = \ddot{\beta}_n (I_{x\beta_n} + I_{z\beta_n}) + \Omega^2 (I_{x\beta_n} - I_{z\beta_n}) \cos\beta_n \sin\beta_n \qquad (20)$$

In the following derivation of the flatwise equations of motion, the "4n" axis system will be referred to simply as the "n" axis system (see Figure 9).

FLATWISE EQUATIONS OF MOTION FOR THE n^{th} BLADE SEGMENT

The flatwise equations of motion for a typical blade segment can be derived from the equilibrium of forces and moments applicable to the free-body diagram illustrated in Figure 9. The subscript "n" indicates the number of the segment, while the right superscript denotes the right side (R) or the left side (L) of the segment. The balance of forces in the x_n direction yields

$$T_n^R = T_n^L + F_{x_n} \qquad (21)$$

which becomes, using relation (18) for F_{x_n},

$$T_n^R - T_n^L = m_n \left(-\Omega^2 x_{2n} \cos\beta_n + \ddot{x}_{2n} \cos\beta_n + \ddot{z}_{2n} \sin\beta_n\right) \qquad (22)$$

The balance of forces in the z_n direction gives

$$S_n^R + Q_n = S_n^L + F_{z_n} \qquad (23)$$

The force Q_n represents the aerodynamic loading on the n^{th} segment. After substitution for F_{z_n} from relation (19), this equation becomes

$$S_n^R - S_n^L = m_n \left(\Omega^2 x_{2n} \sin\beta_n - \ddot{x}_{2n} \sin\beta_n + \ddot{z}_{2n} \cos\beta_n\right) - Q_n \qquad (24)$$

The balance of moments about the n^{th} segment center of gravity yields

$$M_n^R - M_n^L + \frac{\ell_n}{2}\left(S_n^R + S_n^L\right) - M_{y_n} = 0 \qquad (25)$$

which with the use of relation (20) becomes

$$M_n^R - M_n^L + \frac{\ell_n}{2}\left(S_n^R + S_n^L\right) = \ddot{\beta}_n \left(I_{x\beta_n} + I_{z\beta_n}\right) + \Omega^2\left(I_{x\beta_n} - I_{z\beta_n}\right) \cos\beta_n \sin\beta_n \qquad (26)$$

The balance of forces between the n^{th} and $(n-1)^{th}$ segment provides two more relations as follows:

$$S_n^L = S_{n-1}^R \cos(\beta_n - \beta_{n-1}) - T_{n-1}^R \sin(\beta_n - \beta_{n-1}) \qquad (27)$$

$$T_n^L = T_{n-1}^R \cos(\beta_n - \beta_{n-1}) + S_{n-1}^R \sin(\beta_n - \beta_{n-1}) \tag{28}$$

The elastic moment M_n^L is determined from the following expression:

$$M_n^L = K_n(\beta_n - \beta_{n-1}) \tag{29}$$

The continuity of moment between the n^{th} and $(n-1)^{th}$ segments provides another relation, which is

$$M_n^L = M_{n-1}^R \tag{30}$$

Two more relations are obtained from the continuity of the radial and vertical displacements of the n^{th} segment center of gravity. These relations are shown below:

$$x_{2n} = x_{2(n-1)} + \frac{\ell_{n-1}}{2}\cos\beta_{n-1} + \frac{\ell_n}{2}\cos\beta_n \tag{31}$$

$$z_{2n} = z_{2(n-1)} + \frac{\ell_{n-1}}{2}\sin\beta_{n-1} + \frac{\ell_n}{2}\sin\beta_n \tag{32}$$

Thus a total of nine equations is obtained describing the flatwise response of the blade n^{th} segment with respect to the previous segment. Equations (21) through (32) can be used in their present nonlinear form to analyze the time-history response of the TRAC blade. To obtain the blade natural frequencies and mode shapes, the equations of motion are linearized and the aerodynamic forcing term is set to zero.

LINEARIZATION OF THE FLATWISE EQUATIONS OF MOTION FOR THE n^{th} BLADE SEGMENT

In the linearization of the flatwise equations of motion, the following approximations are made:

$$\left.\begin{array}{ll} 1. & \cos\beta_n = 1 \\ 2. & \sin\beta_n = \beta_n \\ 3. & \cos(\beta_n - \beta_{n-1}) = 1 \\ 4. & \sin(\beta_n - \beta_{n-1}) = \beta_n - \beta_{n-1} \\ 5. & \beta_n \beta_m \ll 1 \text{ for any } n, m \end{array}\right\} \tag{33}$$

Relation (31) then becomes

$$x_{2n} = x_{2(n-1)} + \frac{\ell_{n-1} + \ell_n}{2} \tag{34}$$

Repeated application of relation (34) yields that the displacement, x_{2n},

of an arbitrary blade segment is a constant quantity. Then the acceleration $\ddot{x}_{2n}$, which appears explicitly in equations (22) and (24), becomes zero. Use of approximation (33) above reduces relation (32) to the following form:

$$z_{2n} = z_{2(n-1)} + \frac{l_{n-1}}{2}\beta_{n-1} + \frac{l_n}{2}\beta_n \tag{35}$$

Equation (22) then is

$$T_n^R - T_n^L = m_n\left(-x_{2n}\Omega^2 + \ddot{z}_{2n}\beta_n\right) \tag{36}$$

The term $(\ddot{z}_{2n}\ \beta_n)$ is a second-order term in the flapping angle when equation (35) is substituted for z_{2n}, and the term is neglected with respect to the centrifugal term $x_{2n}\Omega^2$.

Equation (24) is now

$$S_n^R - S_n^L = m_n\left(x_{2n}\beta_n\Omega^2 + \ddot{z}_{2n}\right) \tag{37}$$

By use of the definitions

$$I_{\beta_n} = I_{x\beta_n} + I_{z\beta_n} \quad \text{and} \quad I_{Fn} = I_{x\beta_n} - I_{z\beta_n} \tag{38}$$

equation (26) reduces to

$$M_n^R - M_n^L + \frac{l_n}{2}\left(S_n^R + S_n^L\right) = \ddot{\beta}_n I_{\beta n} + \Omega^2\beta_n I_{Fn} \tag{39}$$

The force continuity equations (27) and (28) become

$$S_n^L = S_{n-1}^R - T_{n-1}^R\left(\beta_n - \beta_{n-1}\right) \tag{40}$$

$$T_n^L = T_{n-1}^R + S_{n-1}^R\left(\beta_n - \beta_{n-1}\right) \tag{41}$$

Equations (29) and (30) are not affected by the linearization technique. It should be noted that the normal shear equation (37) is a first-order equation in the flapping angle β_n when equation (35) is substituted for $\ddot{z}_{2n}$. Thus the product of the normal shear and the difference in the flapping angles β_n and β_{n-1} appearing in equation (41) is a second-order term and is neglected with respect to the tension T_{n-1}^R. This approximation uncouples the tensions from the normal shears. Therefore, equations (41) and (36) become, respectively,

$$T_n^{L} = T_{n-1}^{R} \tag{42}$$

and

$$T_n^{R} = T_{n-1}^{R} - m_n x_{2n} \Omega^2 \tag{43}$$

The blade natural frequencies are found by assuming harmonic behavior for the blade displacements, shears, and moments. Thus, with the substitutions

$$\left.\begin{aligned} \beta_n &= \bar{\beta}_n \sin \omega t \\ z_{2n} &= \bar{z}_{2n} \sin \omega t \\ S_n &= \bar{S}_n \sin \omega t \\ M_n &= \bar{M}_n \sin \omega t \end{aligned}\right\} \tag{44}$$

the blade flatwise equations become

$$\bar{S}_n^{R} - \bar{S}_n^{L} = m_n \left(x_{2n} \bar{\beta}_n \Omega^2 - \omega^2 \bar{z}_{2n} \right) \tag{45}$$

$$\bar{M}_n^{R} - \bar{M}_n^{L} + \frac{l_n}{2}\left(\bar{S}_n^{R} + \bar{S}_n^{L} \right) = \bar{\beta}_n \left(-\omega^2 I_{\beta_n} + \Omega^2 I_{Fn} \right) \tag{46}$$

$$\bar{S}_n^{L} = \bar{S}_{n-1}^{R} - T_{n-1}^{R} \left(\bar{\beta}_n - \bar{\beta}_{n-1} \right) \tag{47}$$

$$\bar{M}_n^{L} = k_n \left(\bar{\beta}_n - \bar{\beta}_{n-1} \right) \tag{48}$$

$$\bar{M}_n^{L} = \bar{M}_{n-1}^{R} \tag{49}$$

$$\bar{z}_{2n} = \bar{z}_{2(n-1)} + \frac{l_{n-1}}{2} \bar{\beta}_{n-1} + \frac{l_n}{2} \bar{\beta}_n \tag{50}$$

This system of equations is used to develop the flatwise transfer matrix method. In the subsequent presentation of equations (45) through (50), the bars will be left out.

DERIVATION OF THE TRANSFER MATRIX FOR THE FLATWISE EQUATIONS OF MOTION

A transfer matrix approach as discussed in Reference 4 is employed to develop a system of linear equations describing the five major components of

the TRAC blade. These coupled linear equations are solved simultaneously to determine the blade natural frequencies and mode shapes. Three adjacent segments of a continuous blade structural component are shown in the sketch below:

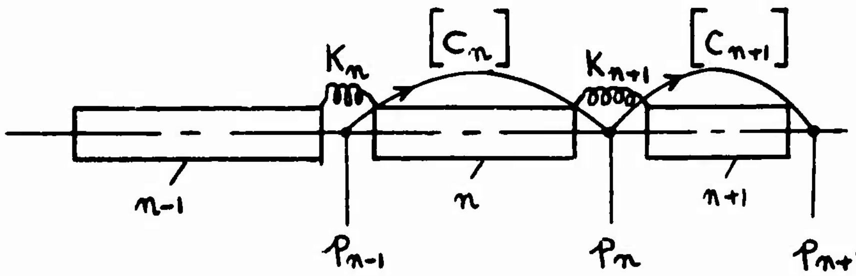

The vector p_n is made up of the flapping angle and vertical displacement of the center of gravity of the n^{th} segment and of the normal shear and bending moment acting on the right-hand side of the n^{th} segment. The transfer matrix C_n is a four-by-four matrix which relates the p_n and p_{n-1} vectors. Thus,

$$\left\{ p_n \right\} = \left[C_n \right] \left\{ p_{n-1} \right\} \qquad \text{where} \quad \left\{ p_n \right\} = \begin{Bmatrix} \beta_n \\ z_{2n} \\ S_n^R \\ M_n^R \end{Bmatrix} \tag{51}$$

It is seen that repeated application of equation (51) will eventually relate the conditions at the tip of the blade to those at the root of the blade. Once the boundary conditions applicable at the blade tip and root are introduced, the blade frequencies and mode shapes can be found. The transfer matrix $\left[C_n\right]$ is derived below from a manipulation of the system of equations (45) through (50) as follows:

1. Substitute for S_n^L and z_{2n} in equation (45) using equations (47) and (50) respectively.

2. Substitute for M_n^L and S_n^L in equation (46) using equations (49) and (47) respectively.

3. Substitute for M_n^L in equation (48) using equation (49).

4. Rearrange equation (50).

The system of equations (45) through (50) can then be expressed in a condensed form:

$$\beta_n \left[T_{n-1}^R + m_n \left(\omega^2 \frac{l_n}{2} - x_{2n} \Omega^2 \right) \right] + S_n^R =$$

$$\beta_{n-1} \left[T_{n-1}^R - m_n \frac{l_{n-1}}{2} \omega^2 \right] - m_n \omega^2 z_{2(n-1)} + S_{n-1}^R \tag{52}$$

$$\beta_n\left[I_{\beta n}\omega^2 - I_{Fn}\Omega^2 - \frac{\ell_n}{2}T^R_{n-1}\right] + \frac{\ell_n}{2}S^R_n + M^R_n = -\frac{\ell_n}{2}T^R_{n-1}\beta_{n-1} - \frac{\ell_n}{2}S^R_{n-1} + M^R_{n-1} \tag{53}$$

$$\beta_n = \beta_{n-1} + \frac{M^R_{n-1}}{K_n} \tag{54}$$

$$-\frac{\ell_n}{2}\beta_n + z_{2n} = \frac{\ell_{n-1}}{2}\beta_{n-1} + z_{2(n-1)} \tag{55}$$

The above system of equations can be represented in matrix form as follows:

$$\left[A_n\right]\begin{Bmatrix}\beta_n\\ z_{2n}\\ S^R_n\\ M^R_n\end{Bmatrix} = \left[B_n\right]\begin{Bmatrix}\beta_{n-1}\\ z_{2(n-1)}\\ S^R_{n-1}\\ M^R_{n-1}\end{Bmatrix} \quad \text{or} \quad \left[A_n\right]\left\{p_n\right\} = \left[B_n\right]\left\{p_{n-1}\right\} \tag{56}$$

where $\left[A_n\right]$ and $\left[B_n\right]$ are four-by-four matrices readily obtained from an inspection of equations (52) through (55) The transfer matrix $\left[C_n\right]$ from equation (51) is then defined from the relation

$$\left[C_n\right] = \left[A_n\right]^{-1}\left[B_n\right] \tag{57}$$

and is shown explicitly below:

$$\left[C_n\right] = \begin{bmatrix} 1 & 0 & 0 & \frac{1}{K_n} \\ \frac{\ell_{n-1}+\ell_n}{2} & 1 & 0 & \frac{\ell_n}{2K_n} \\ C_{31,n} & -m_n\omega^2 & 1 & C_{34,n} \\ C_{41,n} & \frac{m_n\ell_n\omega^2}{2} & -\ell_n & C_{44,n} \end{bmatrix} \tag{58}$$

where $\quad C_{31,n} = -m_n\left[\frac{\omega^2}{2}\left(\ell_n + \ell_{n-1}\right) - x_{2n}\Omega^2\right]$

$$C_{34,n} = -\frac{1}{h_n}\left[T_{n-1}^{R} + m_n\left(\omega^2\frac{l_n}{2} - x_n\Omega^2\right)\right]$$

$$C_{41,n} = -\frac{l_n}{2}C_{31,n} + I_{F_n}\Omega^2 - I_{\beta_n}\omega^2$$

$$C_{44,n} = 1 + \frac{1}{h_n}\left[-I_{\beta_n}\omega^2 + I_{F_n}\Omega^2 + l_n T_{n-1}^{R} + \frac{m_n l_n}{2}\left(\frac{\omega^2 l_n}{2} - X_{2n}\Omega^2\right)\right]$$

The tension T_{n-1}^{R} which appears in the transfer matrix above is found from equation (43) as shown in Appendix III.

The validity of the transfer matrix technique was checked out for a conventional articulated rotor blade. Repeated application of equation (51) results in the following expression:

$$\{P_N\} = [C_N][C_{N-1}]\cdots[C_2][C_1]\{q_0\} \tag{59}$$

where N denotes the blade last segment and the subscript "0" refers to the quantities at the blade root. With the tip boundary conditions of zero shear and moment, i.e., $S_N^R = M_N^R = 0$, and the root conditions of zero displacement and moment, i.e., $z_0 = M_0 = 0$, then the above system of equations becomes

$$\beta_N = a_{11}\beta_0 + a_{13}S_0 \tag{60}$$

$$z_N = a_{21}\beta_0 + a_{23}S_0 \tag{61}$$

$$0 = a_{31}\beta_0 + a_{33}S_0 \tag{62}$$

$$0 = a_{41}\beta_0 + a_{43}S_0 \tag{63}$$

The system natural frequencies are obtained from equations (62) and (63), which yield the following relation:

$$a_{31}a_{43} - a_{33}a_{41} = 0 \tag{64}$$

Once a frequency, ω_i, has been found, then three of the four variables are defined in terms of one of the variables. If, for example, the root shear is arbitrarily chosen as the normalizing factor, then

$$\beta_0/S_0 = -a_{33}/a_{31} \tag{65}$$

$$z_N/S_i = (a_{23}a_{31} - a_{21}a_{33})/a_{31} \quad (66)$$

$$\beta_N/S_i = (a_{13}a_{31} - a_{11}a_{33})/a_{31} \quad (67)$$

The mode shapes corresponding to the i^{th} blade natural frequency can be calculated from equations (65) through (67) and the transfer matrix (51). The frequencies and mode shapes obtained from the transfer matrix technique agreed very well with similar calculations using the "Normal Modes Transient Analysis" from Reference 1.

DERIVATION OF THE FLATWISE EQUATIONS OF MOTION FOR THE TRAC BLADE

The derivation of the TRAC blade flatwise equations of motion must take into account the various boundary conditions which are applicable at points one through seven from Figure 7, as discussed previously. At these points the transfer matrix relation (51) is modified to include the coupling effects among the various blade components. The flatwise equations of motion are derived in terms of only those parameters (vertical displacement, flapping angle, normal shear, and bending moment) which are affected by the boundary conditions. The critical segments which are illustrated in Figure 10 are listed below:

1. blade tip segment, subscripted TIP
2. outboard blade last segment, subscripted N
3. outboard blade segment in contact with the last segment of the torque tube, subscripted i
4. first blade segment, subscripted 1
5. strap last segment, subscripted N
6. strap first segment, subscripted 1
7. torque tube last segment, subscripted N
8. torque tube segment in contact with the outboard blade first segment and with the nut assembly, subscripted j
9. torque tube first segment, subscripted 1
10. jackscrew last segment, subscripted N
11. jackscrew segment containing the nut assembly which is in contact with the torque tube, subscripted k
12. jackscrew first segment, subscripted 1
13. blade root segment, subscripted 0

The procedure employed to derive the system of flatwise equations needed to determine the blade frequencies and mode shapes is to proceed along the blade from the tip to the root, specifying the transfer matrices as applicable from segment to segment. Special care must be exercised in the treatment of the thirteen segments listed above. The final system of flatwise equations, which consists of 65 variables, is shown in Appendix I. The tensions along the major blade elements are obtained from the results of Appendix III.

TRAC BLADE EDGEWISE EQUATIONS OF MOTION

COORDINATE AXES AND TRANSFORMATIONS

The following axis systems, which were used in the development of the flatwise equation of motion, are also used for the edgewise equations: nonrotating rotor hub axis system (x_1, y_1, z_1), rotating rotor hub axis system (x_2, y_2, z_2), and local segment axis system (x_{3n}, y_{3n}, z_{3n}). The lead-lag angle axis system (x_{4n}, y_{4n}, z_{4n}) is introduced in the uncoupled edgewise motion. It is related to the local segment axis system by the following relations:

$$\vec{q}_{3n} = A_{\gamma_n} \vec{q}_{4n} \tag{68}$$

where

$$A_{\gamma_n} = \begin{bmatrix} \cos\gamma_n & -\sin\gamma_n & 0 \\ \sin\gamma_n & \cos\gamma_n & 0 \\ 0 & 0 & 1 \end{bmatrix} \tag{69}$$

The lead-lag angle, γ_n, is defined positive in the same direction as the rotor rotation, Ψ.

VELOCITY AND ACCELERATION VECTORS

Following the procedure outlined for the flatwise equations of motion, it is found that the velocity and acceleration vectors are, respectively,

$$\dot{\vec{q}}_1 = A'_\psi A_{\gamma_n} \vec{q}_{4n} \Omega + A_\psi A'_{\gamma_n} \vec{q}_{4n} \dot{\gamma}_n + A'_\psi \vec{q}_{2n} \Omega + A_\psi \dot{\vec{q}}_{2n} \tag{70}$$

$$\ddot{\vec{q}}_1 = \ddot{\gamma}_n A_\psi A'_{\gamma_n} \vec{q}_{4n} + \dot{\gamma}_n^2 A_\psi A''_{\gamma_n} \vec{q}_{4n} + 2\Omega \dot{\gamma}_n A'_\psi A'_{\gamma_n} \vec{q}_{4n}$$
$$+ A_\psi \ddot{\vec{q}}_{2n} + 2\Omega A'_\psi \dot{\vec{q}}_{2n} + \Omega^2 A''_\psi \left[A_{\gamma_n} \vec{q}_{4n} + \vec{q}_{2n} \right] \tag{71}$$

The components of the total acceleration in the direction of the "4n" axis system are given by

$$\ddot{\vec{q}}_{4n} = A_{\gamma_n}^{-1} A_\psi^{-1} \ddot{\vec{q}}_1 = \begin{Bmatrix} \ddot{x}_{4n} \\ \ddot{y}_{4n} \\ \ddot{z}_{4n} \end{Bmatrix} \tag{72}$$

After the matrix operations are performed, the accelerations are

$$\ddot{x}_{4n} = -\ddot{\gamma}_n y_{4n} - \dot{\gamma}_n^2 x_{4n} - 2\Omega\dot{\gamma}_n x_{4n} - \Omega^2\left(x_{4n} + y_{2n}\sin\gamma_n + x_{2n}\cos\gamma_n\right)$$
$$+ 2\Omega\left(\dot{x}_{2n}\sin\gamma_n - \dot{y}_{2n}\cos\gamma_n\right) + \ddot{x}_{2n}\cos\gamma_n + \ddot{y}_{2n}\sin\gamma_n \tag{73}$$

$$\ddot{y}_{4n} = \ddot{\gamma}_n x_{4n} - \dot{\gamma}_n^2 y_{4n} - 2\Omega\dot{\gamma}_n y_{4n} + \Omega^2\left(x_{2n}\sin\gamma_n - y_{2n}\cos\gamma_n\right)$$
$$+ 2\Omega\left(\dot{x}_{2n}\cos\gamma_n + \dot{y}_{2n}\sin\gamma_n\right) - \ddot{x}_{2n}\sin\gamma_n + \ddot{y}_{2n}\cos\gamma_n \tag{74}$$

$$\ddot{z}_{4n} = \ddot{z}_{2n} \tag{75}$$

D'ALEMBERT'S FORCES AND MOMENTS

Application of D'Alembert's principle to the nth blade segment results in the following expressions:

$$\left.\begin{aligned} dF_{x_{4n}} &= \ddot{x}_{4n}\, dm_n \\ dF_{y_{4n}} &= \ddot{y}_{4n}\, dm_n \\ dM_{z_{4n}} &= -y_{4n}\, dF_{x_{4n}} + x_{4n}\, dF_{y_{4n}} \end{aligned}\right\} \tag{76}$$

Using relations (17) for the flatwise equations (with z_{4n} replaced by y_{4n}) gives for the inertial forces and the inplane moment, respectively,

$$F_{x_{4n}} = m_n\Big[-\Omega^2\left(y_{2n}\sin\gamma_n + x_{2n}\cos\gamma_n\right) + 2\Omega\big(\dot{x}_{2n}\sin\gamma_n$$
$$- \dot{y}_{2n}\cos\gamma_n\big) + \ddot{x}_{2n}\cos\gamma_n + \ddot{y}_{2n}\sin\gamma_n\Big] \tag{77}$$

$$F_{y_{4n}} = m_n\Big[\Omega^2\left(x_{2n}\sin\gamma_n - y_{2n}\cos\gamma_n\right) + 2\Omega\big(\dot{x}_{2n}\cos\gamma_n$$
$$+ \dot{y}_{2n}\sin\gamma_n\big) - \ddot{x}_{2n}\sin\gamma_n + \ddot{y}_{2n}\cos\gamma_n\Big] \tag{78}$$

$$M_{z_{4n}} = \ddot{\gamma}_n \int_{-\frac{\ell_n}{2}}^{\frac{\ell_n}{2}} \left(y_{4n}^2 + x_{4n}^2\right) dm_n = I_{\gamma_n}\ddot{\gamma}_n \tag{79}$$

In the following derivation of the edgewise equations of motion, the subscript "4" in the "4n" axis system will be left out (see Figure 11).

EDGEWISE EQUATIONS OF MOTION FOR THE n^{th} BLADE SEGMENT

From Figure 11, equilibrium of forces in the x_n and y_n directions and equilibrium of moments about the z_n axis results in the following equations:

$$T_n^R - T_n^L = F_{x_n} = m_n \Big[-\Omega^2 \left(y_{2n} \sin\gamma_n + x_{2n} \cos\gamma_n \right) + 2\Omega \left(\dot{x}_{2n} \sin\gamma_n - \dot{y}_{2n} \cos\gamma_n \right) + \ddot{x}_{2n} \cos\gamma_n + \ddot{y}_{2n} \sin\gamma_n \Big] \tag{80}$$

$$S_n^R - S_n^L = F_{y_n} + D_n = m_n \Big[\Omega^2 \left(x_{2n} \sin\gamma_n - y_{2n} \cos\gamma_n \right) + 2\Omega \left(\dot{x}_{2n} \cos\gamma_n + \dot{y}_{2n} \sin\gamma_n \right) - \ddot{x}_{2n} \sin\gamma_n + \ddot{y}_{2n} \cos\gamma_n \Big] + D_n \tag{81}$$

$$M_n^R - M_n^L + \frac{l_n}{2} \left(S_n^R + S_n^L \right) = M_{z_n} = I_{\gamma_n} \ddot{\gamma}_n \tag{82}$$

The balance of forces between the n^{th} and $(n-1)^{th}$ segments provides the following additional relations:

$$S_n^L = S_{n-1}^R \cos(\gamma_n - \gamma_{n-1}) - T_{n-1}^R \sin(\gamma_n - \gamma_{n-1}) \tag{83}$$

$$T_n^L = T_{n-1}^R \cos(\gamma_n - \gamma_{n-1}) + S_{n-1}^R \sin(\gamma_n - \gamma_{n-1}) \tag{84}$$

The elastic moment at the left side of the n^{th} segment is

$$M_n^L = K_n (\gamma_n - \gamma_{n-1}) \tag{85}$$

The moment continuity relation between the n^{th} and $(n-1)^{th}$ segments is

$$M_n^L = M_{n-1}^R \tag{86}$$

The continuity equations for the coordinates of the center of the n^{th} segment are given below:

$$x_{2n} = x_{2(n-1)} + \frac{\ell_{n-1}}{2}\cos\gamma_{n-1} + \frac{\ell_n}{2}\cos\gamma_n \qquad (87)$$

$$y_{2n} = y_{2(n-1)} + \frac{\ell_{n-1}}{2}\sin\gamma_{n-1} + \frac{\ell_n}{2}\sin\gamma_n \qquad (88)$$

After equations (80) through (87) are linearized and the aerodynamic forcing term, D_n, which appears in equation (81), is set to zero, the resulting equations are used to develop the transfer matrix method.

LINEARIZATION OF THE EDGEWISE EQUATIONS OF MOTION FOR THE n^{th} BLADE SEGMENT

The approximations made for the flatwise equations are also used for the edgewise equations (with β_n replaced by γ_n). The continuity relations (87) and (88) then become

$$x_{2n} = x_{2(n-1)} + \frac{\ell_{n-1} + \ell_n}{2} = \text{constant} \qquad (89)$$

$$y_{2n} = y_{2(n-1)} + \frac{\ell_{n-1}}{2}\gamma_{n-1} + \frac{\ell_n}{2}\gamma_n \qquad (90)$$

Equation (80) now becomes

$$T_n^R - T_n^L = m_n\left[-\Omega^2(\gamma_n y_{2n} + x_{2n}) - 2\Omega\dot{y}_{2n} + \gamma_n \ddot{y}_{2n}\right] \qquad (91)$$

The terms $\gamma_n y_{2n}$ and $\gamma_n \ddot{y}_{2n}$, using equation (90), are second-order terms in the lead-lag angle and can be negelcted with respect to the centrifugal term, $x_{2n}\Omega^2$, and the Coriolis term, $2\Omega\dot{y}_{2n}$. A comparison of the centrifugal and Coriolis terms shows that the Coriolis term can be neglected with the assumption that the rotor speed, Ω, is much greater than the lead-lag velocity term, $2\dot{\gamma}_n$.

Then the tension equation becomes

$$T_n^R - T_n^L = -m_n\Omega^2 x_{2n} \qquad (92)$$

The shear equation can be expressed as follows:

$$S_n^R - S_n^L = m_n\left[\Omega^2\left(x_{2n}\gamma_n - y_{2n}\right) + \ddot{y}_{2n}\right] \tag{93}$$

The moment equation (82) and equations (85) and (86) remain unchanged. The continuity equations for the tension and shear forces reduce to

$$S_n^L = S_{n-1}^R - T_{n-1}^R\left(\gamma_n - \gamma_{n-1}\right) \tag{94}$$

and

$$T_n^L = T_{n-1}^R \tag{95}$$

As for the flatwise equations, the approximations made in the linearization of the edgewise equations uncouple the segment tensions from the normal shears, as seen from equations (92) and (95).

The edgewise natural frequencies are found by assuming harmonic motions, as given by relation (44) for the flatwise equations. The edgewise equations of motion then become (with β_n and z_n replaced by γ_n and y_n respectively)

$$\bar{S}_n^R - \bar{S}_n^L = m_n\left[\Omega^2\left(x_{2n}\bar{\gamma}_n - \bar{y}_{2n}\right) - \omega^2\bar{y}_{2n}\right] \tag{96}$$

$$\bar{M}_n^R - \bar{M}_n^L + \frac{\ell_n}{2}\left(\bar{S}_n^R + \bar{S}_n^L\right) = -\omega^2 I_{\gamma_n}\bar{\gamma}_n \tag{97}$$

$$\bar{S}_n^L = \bar{S}_{n-1}^R - T_{n-1}^R\left(\bar{\gamma}_n - \bar{\gamma}_{n-1}\right) \tag{98}$$

$$\bar{M}_n^L = K_n\left(\bar{\gamma}_n - \bar{\gamma}_{n-1}\right) \tag{99}$$

$$\bar{M}_n^L = \bar{M}_{n-1}^R \tag{100}$$

$$\bar{z}_{2n} = \bar{z}_{2(n-1)} + \frac{\ell_{n-1}}{2}\bar{\gamma}_{n-1} + \frac{\ell_n}{2}\bar{\gamma}_n \tag{101}$$

This system of equations is the basic system used to develop the edgewise transfer matrix method. In the subsequent use of equations (96) through (101), the bars will be left out.

DERIVATION OF THE TRANSFER MATRIX FOR THE EDGEWISE EQUATIONS OF MOTION

The procedure used for the edgewise equations is the same as that used to develop the transfer matrix for the flatwise equations. The basic system of equations needed for the edgewise transfer matrix is presented below:

$$\gamma_n\left(-m_n x_{2n}\Omega^2+T_{n-1}^R\right)+y_{2n}m_n\left(\omega^2+\Omega^2\right)+S_n^R=T_{n-1}^R\gamma_{n-1}+S_{n-1}^R \tag{102}$$

$$\gamma_n\left(\omega^2 I_{\gamma_n}-\frac{\ell_n}{2}T_{n-1}^R\right)+\frac{\ell_n}{2}S_n^R+M_n^R=-T_{n-1}^R\frac{\ell_n}{2}\gamma_{n-1}-\frac{\ell_n}{2}S_{n-1}^R+M_{n-1}^R \tag{103}$$

$$\gamma_n=\gamma_{n-1}+\frac{M_{n-1}^R}{K_n} \tag{104}$$

$$-\frac{\ell_n}{2}\gamma_n+y_{2n}=\frac{\ell_{n-1}}{2}\gamma_{n-1}+y_{2(n-1)} \tag{105}$$

The system of equations above can be represented in matrix form as follows:

$$\left[A_n\right]\left\{p_n\right\}=\left[B_n\right]\left\{p_{n-1}\right\} \tag{106}$$

The transfer matrix is then found from

$$\left[C_n\right]=\left[A_n\right]^{-1}\left[B_n\right] \tag{107}$$

The edgewise transfer matrix is shown below:

$$\left[C_n\right]\begin{bmatrix} 1 & 0 & 0 & \frac{1}{K_n} \\ \frac{\ell_{n-1}+\ell_n}{2} & 1 & 0 & \frac{\ell_n}{2\cdot K_n} \\ c_{31,n} & -m_n\left(\omega^2+\Omega^2\right) & 1 & c_{34,n} \\ c_{41,n} & \frac{m_n\ell_n}{2}\left(\omega^2+\Omega^2\right) & -\ell_n & c_{44,n} \end{bmatrix} \tag{108}$$

where

$$c_{31,n}=-m_n\left[\left(\omega^2+\Omega^2\right)\frac{\ell_{n-1}+\ell_n}{2}-x_{2n}\Omega^2\right]$$

$$c_{34,n}=-\frac{1}{K_n}\left[T_{n-1}^R+m_n\frac{\ell_n}{2}\left(\omega^2+\Omega^2\right)-m_n x_{2n}\Omega^2\right]$$

$$c_{41,n}=-\frac{\ell_n}{2}c_{31,n}-I_{\gamma_n}\omega^{-2}$$

$$c_{44,n}=1+\frac{1}{K_n}\left[-I_{\gamma_n}\omega^2+\ell_n T_{n-1}^R+m_n\frac{\ell_n^2}{2}\left(\omega^2+\Omega^2\right)-m_n\frac{\ell_n}{2}x_{2n}\Omega^2\right]$$

DERIVATION OF THE EDGEWISE EQUATIONS OF MOTION FOR THE TRAC BLADE

A comparison of the standard transfer matrices derived for the flatwise equations of motion (58) and for the edgewise equations (108) reveals that the flatwise equations can be transformed into the edgewise equations by simply replacing the frequency squared term ω^2 by $(\omega^2 + \Omega^2)$ with the exception that the inertial term $I_{\beta_n}\omega^2$ appearing in the moment equation becomes $I_{\gamma_n}\omega^2$. In addition, the moment of inertia I_{Fn} is set to zero for the edgewise equations.

One important difference between the flatwise and edgewise equations is that the contact between the nut assembly and the torque tube denoted by point 3 in Figure 10, is not present in the edgewise motion of the TRAC blade. Thus the contact force F_{C3} and the bending moment M_{C3} are zero for the edgewise equations. It follows that the boundary conditions applicable at point 3 which are defined by equations (148) and (149) in Appendix I are not used in the edgewise equations. Thus, the total number of equations and of variables reduces to sixty-three.

Another important difference between the flatwise and edgewise equations of motion is that the tension along the leading and lagging strap is not the same as the blade bends in the inplane direction. As shown in Figure 12, as the blade bends forward, the lagging strap is subject to a greater tensile loading than the leading strap. The differential tension is defined in terms of an effective linear spring present in each strap and the net linear displacement resulting from the relative angular motions of the blade tip segment and the jackscrew segment containing the nut assembly. The bending moment due to the difference in the strap tensions is accounted for in the edgewise equations of motion of the blade tip and jackscrew segments (equations (111) and (145) respectively from Appendix I). A summary of the modifications necessary to reduce the flatwise equations to the edgewise equations can be found in Appendix II.

TRAC BLADE TORSIONAL EQUATIONS OF MOTION

The structural design of the TRAC blade is such that the torque tube and the outboard blade are the main components which supply significant torsional stiffness and torsional inertia for the entire blade. The jackscrew and the tension straps provide little torsional stiffening. Thus, only the torque tube and outboard blade are considered in the torsional frequency calculations. The torsional equations which are utilized to compute the TRAC blade torsional frequencies can be found in Reference 3. An effective torsional inertia is calculated for the overlap. The airfoil chord used in this region is that of the outboard blade. The total torsional mass moment of inertia of the blade is constant, independent of the amount of blade retraction. At any given radial location, the inertias of all components present are added together.

TRAC BLADE NATURAL FREQUENCIES AND MODE SHAPES

DESCRIPTION OF COMPUTER PROGRAM USED TO CALCULATE THE TRAC BLADE NATURAL FREQUENCIES AND MODE SHAPES

A computer program has been developed to evaluate specifically the flatwise and edgewise natural frequencies of the TRAC blade. The equations summarized in Appendix I and the expressions for the tensions derived for all major components in Appendix III have been programmed for the Univac 1108 computer system. A description of the computer program can be found in Reference 5. Basically, the procedure employed to determine the blade natural frequencies is as follows:

1. The lower bound for the blade frequency is chosen by the user.

2. The determinant of the homogeneous system of 65 equations for the flatwise motion or 63 equations for the edgewise motion is found using a modified version of the Gauss-Jordan matrix reduction technique.

3. The blade frequency is increased by a small amount specified by the user and the determinant is again calculated. The sign of the determinant is then compared to that obtained in step 2. Care must be exercised in the choice of the frequency increment since too large an increment could result in missing two frequencies very close to each other.

4. If the sign of the determinants found in steps 2 and 3 is the same, then step 3 is repeated until a change in sign is found.

5. Once a change in the sign of the determinant occurs, then the blade natural frequency is found by converging on the frequency which drives the determinant to zero within a numerical tolerance of .000001 rad/sec.

6. Higher blade frequencies are found by repeating the process above using as a lower bound the last natural frequency increased by one frequency increment.

The mode shapes for the TRAC blade are calculated once the natural frequency is known. The system of "n" homogeneous equations is reduced by one; the remaining variables are all defined in terms of the displacement of the tip segment. The (n-1) linear coupled equations are solved simultaneously using the Gauss-Jordan method. The extra equation, which is not used in the mode shape calculations but which must be satisfied by definition, is chosen as the first equation in Appendix I. In order to be consistent with the definition of blade mode shapes found in the literature, the TRAC blade variables are finally normalized by the displacement of the right-hand side of the tip segment.

The computer program is designed to handle any amount of overlap between the torque tube and outboard blade corresponding to rotor conditions from fully-extended (100% radius) to fully-retracted (near 60% radius).

The mass and area moments of inertia of each major component are arbitrary. The number of segments chosen to represent each blade component is ten. With the addition of the blade tip and root segments, the total number of blade segments handled by the analysis is 52. A detailed description of the program input parameters will not be attempted here. It can be found in Reference 5.

TRAC BLADE FLATWISE AND EDGEWISE FREQUENCIES

Computed TRAC blade flatwise and edgewise frequencies are presented in the Southwell plots of Figures 13 through 18 for rotor speeds ranging from zero to 216 radians per second and three radius conditions: 100, 80, and 62.5 percent of the fully-extended blade. The blade physical characteristics are for the 4.5-foot model blade design tested by Sikorsky at United Aircraft Research Laboratories in 1972 under Army Contract DAAJ02-68-C-0074, Reference 1. The model blade operating rotor speed is 144 radians per second. The "Normal Modes Analysis", as discussed in Reference 2, is also used to calculate the blade natural frequencies and mode shapes. This analysis applies only to a conventional rotor blade which is in tension throughout its entire length. Comparison of the results with those obtained for the TRAC blade from the newly developed frequency analysis shows the effect of the compressive loading of the outer end and of the addition of the jackscrew and straps as separate elements. The results from the "Normal Modes Analysis" are also shown in Figures 13 through 18.

A decrease in rotor speed causes a decrease in the flatwise and edgewise natural frequencies for all modes and rotor conditions investigated with both theories. This result is caused mainly by the reduction in centrifugal blade stiffening as the rotor is slowed down. Since the TRAC blade behaves more like a conventional rotor blade at low rotor speeds due to the decrease in centrifugal effects, it can be expected that the natural frequencies calculated from the two theories will be close as the rotor slows down. This is generally true from an inspection of Figures 13 through 18. The frequencies calculated from the TRAC analysis are usually higher than those from the "Normal Modes Analysis" when another blade natural frequency, usually associated with a strap mode, is in the vicinity. From Figures 13 through 18 it is noted that at rotor speeds higher than 120 radians per second, the TRAC blade natural frequency is lower than that calculated for the blade as a conventional rotor. The difference in the frequencies becomes more pronounced as rotor speed is increased even further as a result of the increasing compressive loading on the outboard motion. Buckling can occur at sufficiently high rotor speeds. When buckling (or static divergence)occurs, the natural frequency would drop to zero. This behavior was also predicted by the TRAC blade two-element analysis discussed in the Introduction.

The effect of retracting the rotor to 80 and 62.5 percent of the fully-extended radius on the blade natural frequency can be seen from a comparison of Figures 13 through 15 for the flatwise motion and Figures 16 through 18 for the edgewise motion. As the rotor is retracted, the overlapped region between the torque tube and the outboard blade increases with a subsequent increase in the local mass and moments of inertia. The retracted blade is effectively stiffer, which leads to an increase in the blade

natural frequency. This effect is illustrated in Figure 19 for the first two flatwise bending frequencies calculated with the TRAC frequency program at rotor speeds of 100 percent (which corresponds to 144 rad/sec) and zero. The variation of natural frequency with percentage of fully-retracted rotor seems independent of rotor speed. However, the effect of blade retraction on frequency is much more pronounced for the higher frequency modes. The behavior shown in Figure 19 for the flatwise frequencies is also exhibited by the edgewise frequencies.

One important characteristic of the TRAC blade is the presence of natural frequencies which can be associated with the straps or the jackscrew elements. This is suggested from an investigation of the mode shapes which in such cases exhibit predominant motions in the straps or the jackscrew. These mode shapes are present for both flatwise and edgewise motions at all rotor extensions investigated. The frequency associated with a strap mode decreases rapidly with rotor speed, while a jackscrew mode shows a more gradual decrease. The reduction in frequency is due to the decrease in centrifugal stiffening at lower rotor speeds. This effect is greater for the straps since the structural stiffness of the straps is an order of magnitude less than that of the jackscrew. As the rotor radius is retracted to 80 and 62.5 percent of its full value, the effect of the straps and jackscrew becomes greater. A comparison of Figures 13, 14, and 15 for the TRAC blade flatwise frequencies shows that only one strap mode is present for the fully-extended rotor, while two strap modes can be seen for 80 percent radius and an additional jackscrew mode becomes apparent for the 62.5 percent rotor. Similar conclusions can be drawn from Figures 16, 17, and 18 for the edgewise frequencies.

A brief investigation of the effect of changes in the moment of inertia of the straps or the jackscrew on the blade natural frequencies and mode shapes was conducted for the edgewise case at a rotor speed of 108 radians per second and a fully-extended radius. Figure 20 shows that at this condition, a jackscrew mode is present at 1000 rad/sec while a strap mode exists at 1100 rad/sec. The first and second edgewise bending frequencies are 400 and 1190 rad/sec respectively. It is seen in Figure 20 that increasing the edgewise moment of inertia of the straps by factors of five and ten has no effect on the first and second bending modes, which are associated mainly with motion of the torque tube and the outboard blade. The jackscrew frequency shows an overall increase in frequency of 10 percent. The strap frequency, as expected, shows a large increase with strap moment of inertia. For a strap moment of inertia of ten times its normal value, the jackscrew edgewise moment of inertia is increased by a factor of five. The results shown in Figure 20 indicate slight increases in the first and second bending frequencies, which are now very close to the frequencies calculated from the "Normal Modes Analysis", an increase in strap frequency of 11 percent, and an increase in jackscrew frequency of 31 percent.

TRAC BLADE FLATWISE AND EDGEWISE MODE SHAPES

Flatwise and edgewise mode shapes are illustrated in Figures 21 through 28 for different amounts of blade retractions and rotor speeds. In these

plots, the first mode shape is identified as the rigid-body mode with a flatwise frequency slightly over one per rev or an edgewise frequency near one-third per rev. The first three flatwise bending modes calculated with the TRAC frequency program are shown in Figure 21 for a fully-extended (4.5-foot model) rotor at 100 percent rotor speed (144 radians per second). These mode shapes can be compared with the results obtained from the "Normal Modes Analysis" at the same condition, as shown in Figure 22. The behavior of the torque tube-outboard blade combination is similar from both theories for the first two bending modes. The third bending mode calculated from the TRAC program, however, exhibits twice as much motion for the outboard blade as was given by the "Normal Modes Analysis". In addition, a mode shape, which is referred to as a "strap mode" since the strap motion is the dominant one, occurs at a frequency higher than 9 per rev.

The flatwise mode shapes for the 80 percent extended rotor and for the fully-retracted rotor are presented in Figures 23 and 24 respectively at 100 percent rotor speed. A comparison among Figures 21, 23, and 24 reveals that the characteristics of the first and second bending modes are not affected very much by a change in rotor radius. However, as the blade is retracted, the motion of the jackscrew departs from the torque tube motion. The strap motion shows an increasing dominance as the rotor is retracted; the maximum amplitude of the strap mode shape occurs toward the middle of the element and is greater than the blade tip motion by factors of 3.6, 5.5, and 26 for rotor radii of 100, 80, and 62.5 percent respectively. A jackscrew mode is present for the fully-retracted radius at a frequency near 5 per rev.

A check on the boundary conditions discussed in the section of the report entitled <u>Mathematical Model of the TRAC Blade</u> can be made from the results plotted in Figures 21, 23, and 24. These figures show that the displacement and slope at the beginning and end of the overlap are the same for the torque tube and the outboard blade as discussed for points 1 and 2 in Figure 7. The displacement and slope of the torque tube and the jackscrew segment containing the nut assembly should be the same (point 3). For the model blade design, the nut assembly segment occurs at the beginning of the overlapped region. From these figures it is seen that the above boundary conditions are satisfied. The inboard end of the straps should have the same displacement and slope as the jackscrew segment containing the nut assembly (point 4); this holds true at the beginning of the overlap for all cases. The ends of the torque tube and jackscrew meet to satisfy the boundary condition for point 5 at a radial location of 2.7 feet. The boundary condition at point 6 states that the mode shapes of the outboard blade and the straps will be coincident at the left side of the tip segment. The blade tip segment length was kept constant at .0583 foot for all retractions of the TRAC blade. This boundary condition is also satisfied from an inspection of Figures 21, 23, and 24. The last boundary condition (point 7), which can be interpreted as stating that the displacement of the torque tube and jackscrew will be the same at the right end of the root segment, is met in all cases. In addition, it can be seen that at the blade tip and at the hinge (located at .25 foot), the second derivative of the mode shape, which is proportional to the bending moment, is zero for all modes.

The flatwise mode shapes at zero rotational speed are presented in Figures 25 through 27. The general characteristics discussed for the mode shapes at 100 percent rotor speed are exhibited in these figures. However, the strap and jackscrew modes are more pronounced, especially as the rotor is retracted. This behavior can be expected from the discussion of the Southwell plots of Figures 13 through 15.

The edgewise mode shapes for the fully-extended TRAC rotor are shown in Figure 28 at a rotor speed of 108 radians per second. As indicated from the Southwell plot of Figure 16, a jackscrew mode (Figure 28d) is present at a frequency of 1110 rad/sec and a strap mode at 1008 rad/sec (Figure 28c). The first and second bending modes are shown respectively in Figures 28b and 28e. As discussed in the section on the development of the edgewise equations of motion, the boundary conditions at point 3 are not applicable to the edgewise motion of the TRAC blade. As seen in Figure 28, the displacement and slope of the torque tube and jackscrew are not necessarily the same at the beginning of the overlap, as was true for the flatwise mode shapes presented in Figure 21.

TRAC BLADE TORSIONAL FREQUENCIES AND MODE SHAPES

A Southwell plot of the TRAC blade first torsional frequency is shown in Figure 29 for blade extensions of 100, 80, and 62.5 percent of full radius. The behavior exhibited in this figure by the TRAC blade is similar to that of a conventional blade of similar radius. Due to the decrease in torsional inertia in the overlapped region and decrease in length, the torsional frequency increases as the outboard blade is retracted. The variation of torsional frequency with rotor speed is small; the frequency increases about 3 percent as the rotor speed is varied from zero to 216 radians per second.

The first two torsional modes of the TRAC blade are presented in Figure 30. Their general characteristics are not affected by the amount of blade retraction and by changes in rotor speed (not shown). The mode shape first derivative approaches zero at the blade tip since the torsional moment, which is proportional to the slope of the mode shape, is zero at a free end. The mode shapes are normalized by the blade tip displacement as was done for the flatwise and edgewise modes.

NORMAL MODE AEROELASTIC ANALYSIS

To provide the capability for predicting the time history of the aeroelastic response of a TRAC rotor, an aeroelastic analysis provided to the Army under Contract DAAJ02-71-C-0025 has been modified. The basic analysis is described in References 2 and 3. This program uses uncoupled blade modes in the solution of the blade equations of motion defining the blade response to air loads.

The analysis is essentially a digital flight simulator that can be used to determine the fully-coupled rotor/airframe response of a helicopter in free flight. This is accomplished by the numerical integration of the blade/airframe equations of motion on a digital computer. Efforts have been made to provide a modular computer program so that various facets of the analysis may be easily updated as more refined analytical techniques are developed. The principal technical assumptions and features of the analysis are listed below:

1. The blade elastic response is determined using a modal approach based on the equations defined in References 2, 6, and 7.

2. The aerodynamic modeling of the blade includes unsteady aerodynamic effects based on the equations and tabulations defined in Reference 7.

3. Provision is made for specifying a distribution of induced velocities (inflow) over the rotor disc. Such distribution for steady level flight can be computed from analyses available in the literature (Reference 8).

4. The response of each individual blade is considered.

5. The fuselage is a rigid (nonelastic) body having six degrees of freedom. Provisions for fixed wings are included. The aerodynamic forces on the wings are computed using simple, finite-span wing theory, neglecting stall and unsteady effects. Alternatively, the wings can be included with the fuselage aerodynamics and handled as described in assumption 6 below.

6. Fuselage aerodynamic forces and moments are determined using steady, nonlinear, empirical data loaded into the computer program via punched cards.

The modifications made to this analysis to make it applicable to the TRAC rotor provide a capability similar to the original analysis. The primary problem encountered in the modification was one of storage requirements in the computer. To provide the necessary storage, two changes were made:

1. The blade natural frequency program was written as a stand-alone program, providing punched-card output which was then used as input to the TRAC Normal Mode Blade Aeroelastic Analysis.

2. The TRAC Normal Mode Blade Aeroelastic Analysis is now applicable to articulated, semiarticulated, and nonarticulated rotors. The teetering or gimbaled rotor capability has been removed.

In addition, several other modifications were made to provide for the specific requirements of the TRAC rotor. These include the following:

3. A buffer program was written which defines fifteen blade segments along the torque tube and outboard blade. These are external segments, and are the only ones to which external aerodynamic loading is applied.

4. The modal constants defined for each blade mode have been modified to include the participation of all 52 lumped mass blade elements. The modal equations of motion use these constants to describe the blade modal properties.

5. The input to the program has been modified to include additional input requirements, such as the section modulus of all elements of the blade. These are used to provide blade stress values. A complete description of the input requirements and modifications is included in the User's Manual, Reference 5.

6. The output printout has been modified to include the azimuthal time history of the response of all 52 blade elements.

These are the modifications made to the program. It can be run in the same way as the original Normal Mode Aeroelastic Analysis, and provides the user with all of its capability except as noted above.

CORRELATION OF ANALYTICAL AND TEST RESULTS

Calculations of blade flatwise, edgewise, and torsional moments were made for six sample rotor operating conditions tested under Contract DAAJ02-68-C-0074. The conditions selected for analysis encompass (1) operation of the rotor in the pure helicopter mode, (2) operation at partially and fully reduced diameters, and (3) operation at an extremely high forward speed. The parameters defining the specific conditions are given in Table I.

Except where noted, the calculations were performed with the following principal assumptions:

1) Variable inflow effects due to rotor wake and fuselage interference could be neglected.

2) Unsteady aerodynamic and spanwise flow effects could be neglected.

3) Flatwise, edgewise and torsional modes having frequencies generally greater than about 10 to 13 times rotor frequency could be neglected. (The natural frequencies of the uncoupled modes used in each case are given in Table II.)

4) Measured rotor lift and shaft angle of attack were matched in the analysis. In addition, the rigid-body flapping with respect to the shaft was set to zero $\pm 1^\circ$, while in the test the flapping at the blade root was set to zero $\pm 1^\circ$.

The TRAC Blade Normal Mode Aeroelastic Analysis can account for variable inflow due to rotor wakes and for unsteady aerodynamics.

The flatwise moment correlations are presented in Figure 31 through 33. Figures 31 and 32 present the radial distributions of the ½ peak-to-peak flatwise moment amplitudes. For those conditions involving substantial overlap of the blade and torque tube, moments for both are shown. Also, for two conditions, analytical results obtained using the TRAC Blade Four-Element Segmented Analysis discussed in the Introduction are presented for comparison with the results of the Normal Mode Analysis developed under this contract. Figure 33 shows corresponding sample correlations of time histories at several radial stations. The principal results and conclusions indicated in these figures are summarized below:

1. The Normal Mode TRAC Analysis generally underpredicts the moment amplitudes for the articulated rotor conditions, particularly on the blade portion of the structure (see Figures 31 and 32).

2. The Normal Mode TRAC Analysis and the TRAC Blade Four-Element Segmented Analysis give comparable results, although the latter appears to predict higher moments for the inboard (or torque tube) part of the blade (see Figure 31). The two analyses differ most at the inboard end of the torque tube ($r = 0.15$), where segmented blade analysis appears to reflect more accurately the effects of large discontinuities in mass and stiffness distribution introduced by the non-scaled blade root fittings.

TABLE I. TEST CONDITIONS ANALYZED

Case Number	Velocity (kt)	Percent of Full Radius	Flap Hinge Boundary Condition	Shaft Angle (deg)	$\frac{C_T}{\sigma}$
1	90	100	Articulated	-12	0.078
2	90	100	Articulated	8	0.088
3	150	100	Articulated	-4	0.048
4	150	80	Articulated	2	0.018
5	150	60.8	Locked	-2	0.063
6	350	60.8	Articulated	0	0.082

TABLE II. BLADE NATURAL FREQUENCIES			
Case Number	Flatwise Modal Frequencies (cycles/rev)	Edgewise Modal Frequencies (cycles/rev)	Torsional Modal Frequencies (cycles/rev)
1	1.05 4.48 7.43 8.70	.32 3.09	11.6
2	1.05 4.48 7.43 8.70	.32 3.09	11.6
3	1.05 4.48 7.43 8.70	.32 3.09	11.6
4	1.07 5.36 7.88	.36 4.61	13.2
5	1.64 7.34 9.69	6.98	∞
6	1.07 4.04 10.20	.40 8.76	∞

3. For the single locked hinge condition investigated, the Normal Mode TRAC Analysis correlated very well with test data (see Figure 32).

4. Large changes in predicted flatwise moments result when the shaft angle of the rotor is altered by 5 degrees (see Figure 31, 1st panel). Since rotor flapping is nominally trimmed to zero, rotor shaft angle is a direct measure of tip path plane angle. Some of the discrepancy between predicted and measured results may therefore be due to small differences in the rotor tip path planes corresponding to the analytical and experimental conditions. Such differences may exist due to tolerances in trimming the flapping motion and due to the different trimming techniques used (i.e., trimming rigid-body flapping mode in analysis versus trimming the root flapping of the blade in test). It is estimated that the analytical and experimental tip path planes could differ by as much as 1 to 2 degrees. Other factors which could contribute to the discrepancy observed include the absence of unsteady aerodynamics, fuselage interference, and hub wake turbulence effects in the analysis.

5. The time history correlations presented in Figure 33 indicate generally reasonable agreement. The test data, as might be expected, tend to exhibit more high-frequency content. However, particularly good agreement is noted for the locked hinge condition (Figure 33d). Also, the analysis correctly predicts the existence of a 4-per-rev resonance at the 350-knot, articulated rotor condition of Figure 33e.

Edgewise moment results are less extensive. Figure 34 presents typical computed edgewise moments for some of the test conditions analyzed. No experimental results are presented, since as noted in Reference 1 the experimental results were compromised by the existence of a large 5.25/rev component due to a shaft imbalance. As a result, the experimental results were approximately five times larger than predicted values and, of course, exhibited completely different harmonic character.

Sample torsional moment results are presented in Table III. Only ½ peak-to-peak amplitude results are noted, as it is evident that the analysis significantly underestimates the magnitude of the measured moments. The exact reason for this is not known. Historically, torsional moments (which are reflected in control loads) have been difficult to predict. This difficulty has promoted much research which has shown that variable inflow and blade unsteady aerodynamic effects can be important factors. Detailed study of these effects was beyond the scope of this contract.

TABLE III. COMPARISON OF PREDICTED AND MEASURED TORSIONAL MOMENT AMPLITUDES (½ PEAK-TO-PEAK)

Case Number	$\bar{r}$	Measured (in.-lb)	Predicted
1	0.17	39	8
2	0.17	65	5
3	0.17	46	10
4	0.21	13	2
5	0.28	-	3
6	0.28	66	15

RESULTS AND CONCLUSIONS

1. A computer program has been developed which can predict the uncoupled flatwise, edgewise, and torsional natural frequencies of a telescoping rotor blade at any rotor speed or amount of blade retraction.

2. A modified version of the Normal Mode Aeroelastic Analysis (Y200) has been developed which can predict the time history response of a TRAC rotor using the blade modes predicted by the natural frequency program.

3. A study of the change in TRAC blade natural frequency with rotor speed and retraction showed the following:

   a) At low rotor speeds, where centrifugal effects are small, the natural frequencies calculated for the TRAC rotor blade compare quite well with the results obtained for a conventional rotor blade.

   b) At high rotor speeds, the compressive loading on the outboard section of the TRAC blade reduces the natural frequencies of elastic modes as compared to those of a conventional rotor blade.

   c) The TRAC blade natural frequencies increase as the outboard blade is retracted over the torque tube.

   d) The presence of the jackscrew and tension straps as additional structural components of the TRAC rotor introduces new blade modes which show predominant motions in these components.

4. Correlation of the TRAC Normal Mode Aeroelastic Analysis with model rotor test data showed generally reasonable correlation with measured flatwise bending moments, although predicted moment amplitudes were less than those measured. The analysis underpredicted blade torsional moments, and no conclusion could be drawn regarding edgewise moments because of extraneous signals in the available edgewise moment test data; however, the edgewise moments were generally small.

5. The TRAC Normal Mode Aeroelastic Analysis and the TRAC Four-Element Segmented Blade Analysis gave comparable flatwise moments for the fully-extended rotor conditions examined. Both analyses should be useful as design tools.

RECOMMENDATIONS

1. A more detailed correlation study should be conducted to examine the influence of unsteady aerodynamics and variable inflow on predicted blade moments.

2. Detailed blade shake tests should be conducted to confirm the predicted unique modal characteristics of TRAC type rotor blades.

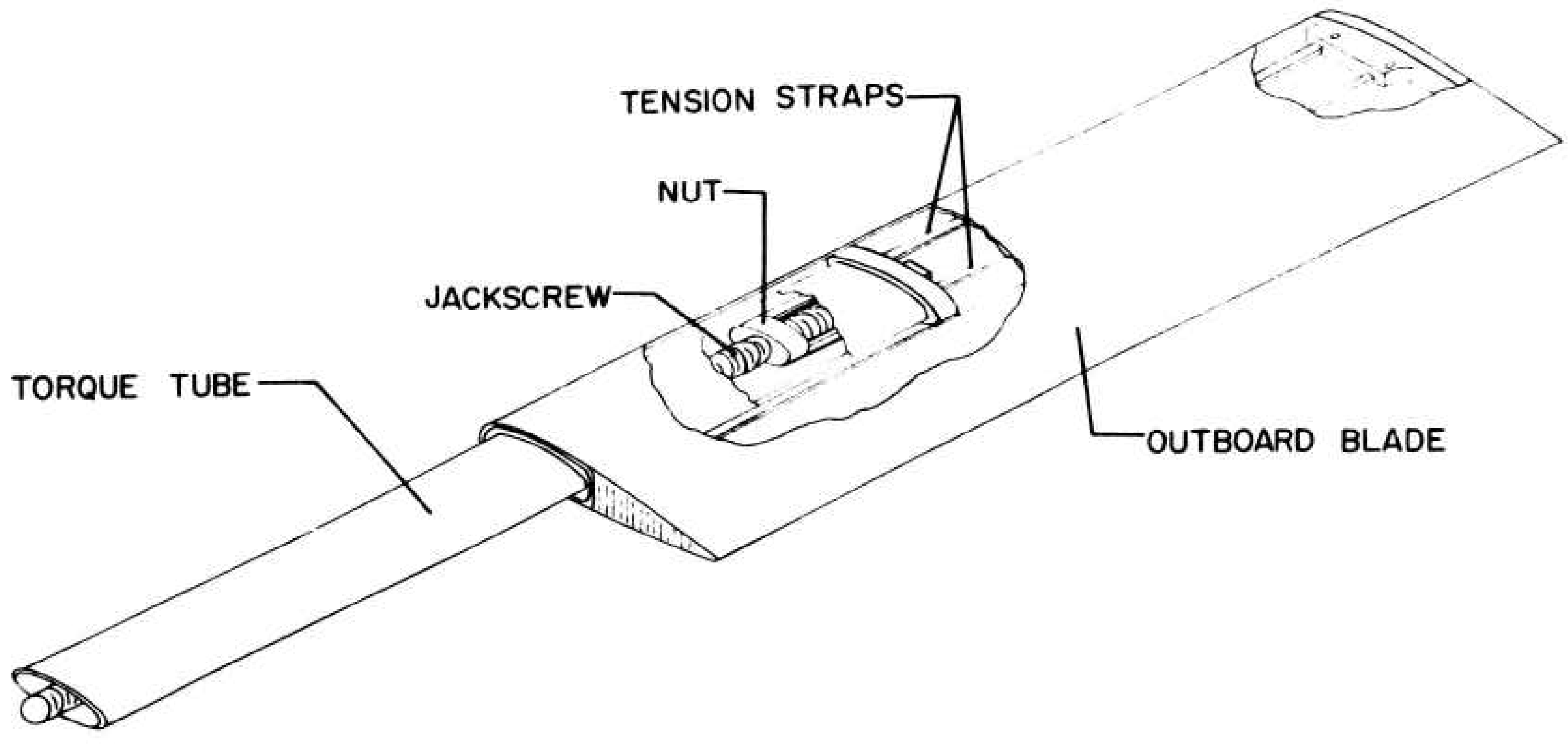

Figure 1. Schematic Drawing of a TRAC Variable-Diameter Rotor Blade.

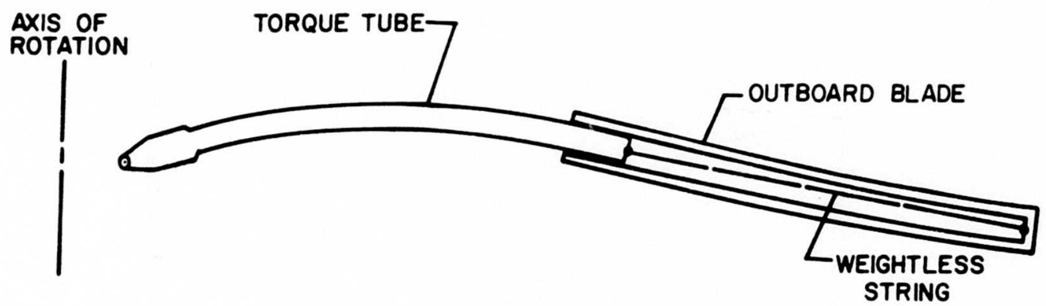

Figure 2. Preliminary Aeroelastic Representation of the TRAC Blade for the Two-Element Analysis (1964).

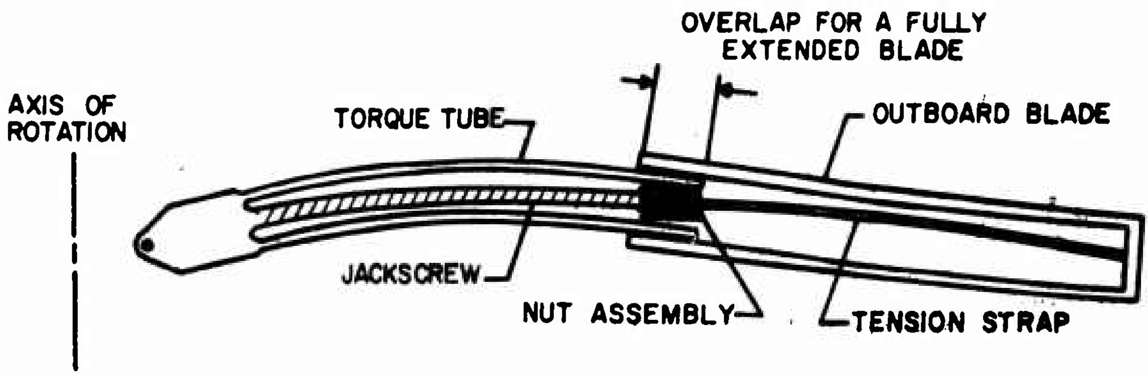

Figure 3. Extended Aeroelastic Representation of the TRAC Blade for the Four-Element Analysis (1967).

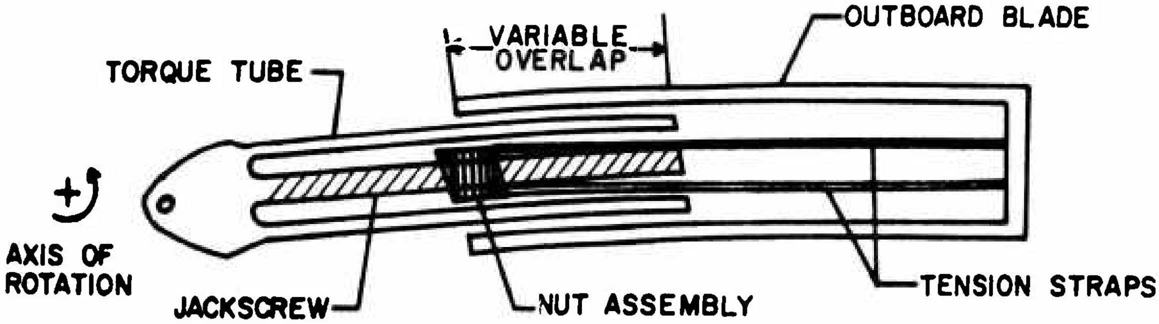

Figure 4. Present Aeroelastic Representation of the TRAC Blade for the "TRAC Aeroelastic Analysis" (1973).

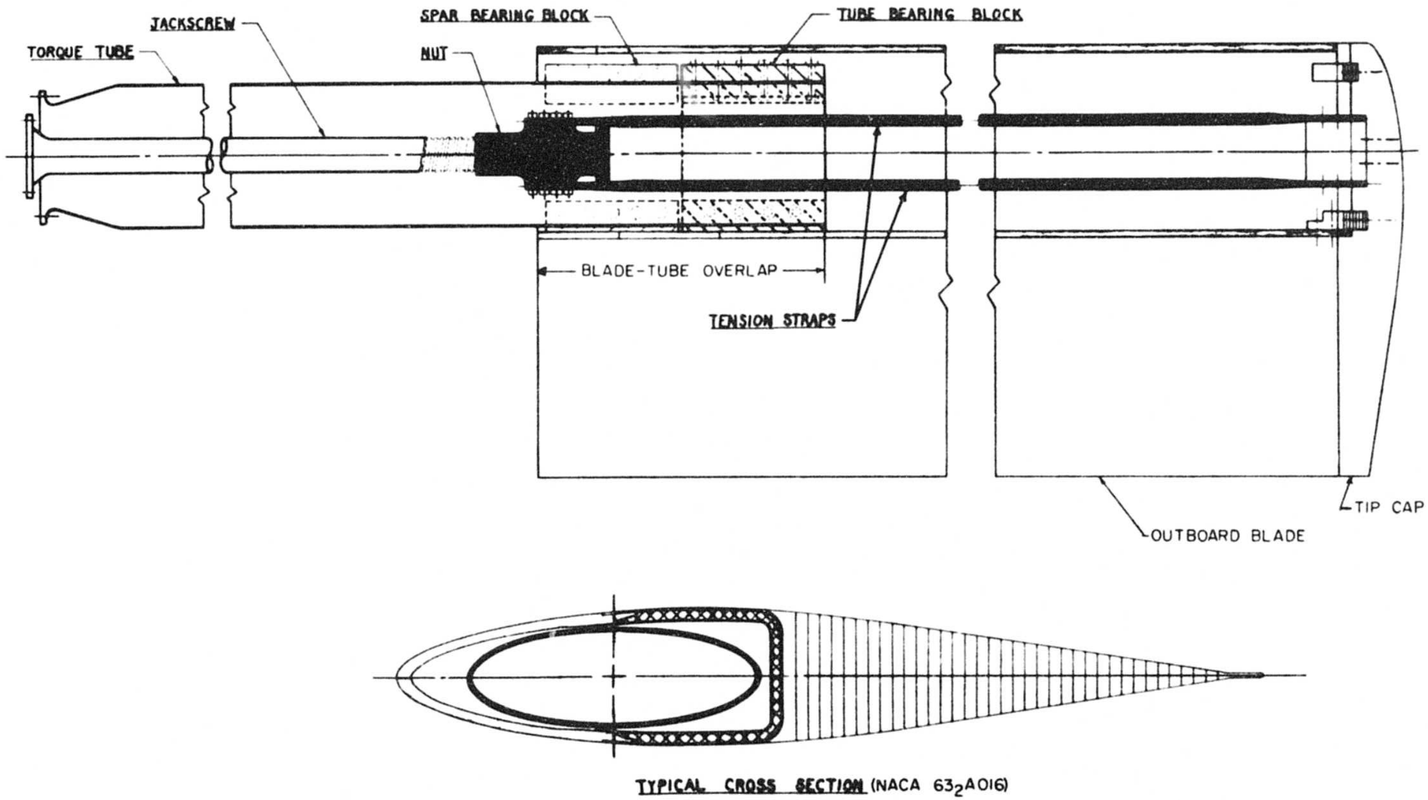

Figure 5. TRAC Blade Full-Scale Structure.

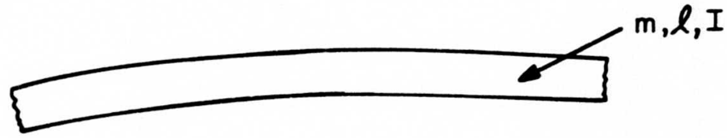

(a) SECTION OF ELASTIC BLADE ELEMENT

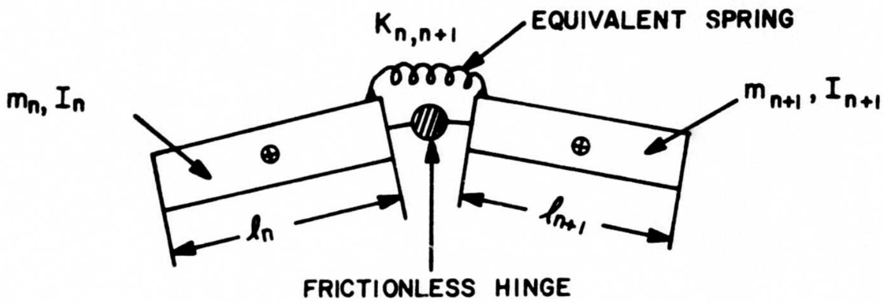

(b) MATHEMATICAL MODEL OF THE BLADE ELEMENT

Figure 6. Mathematical Model of a TRAC Blade Elastic Element.

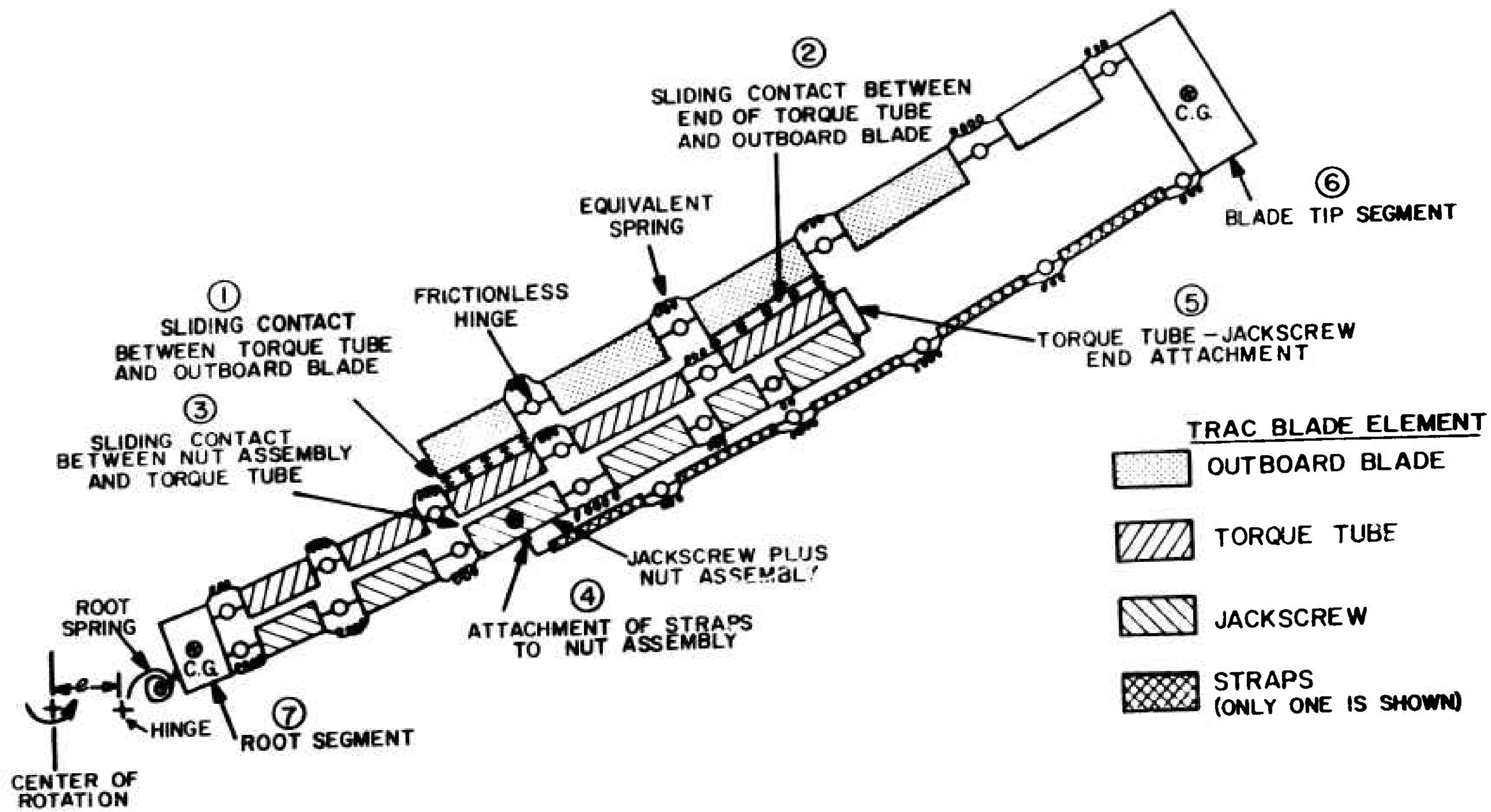

Figure 7. Complete Mathematical Model of the TRAC Blade.

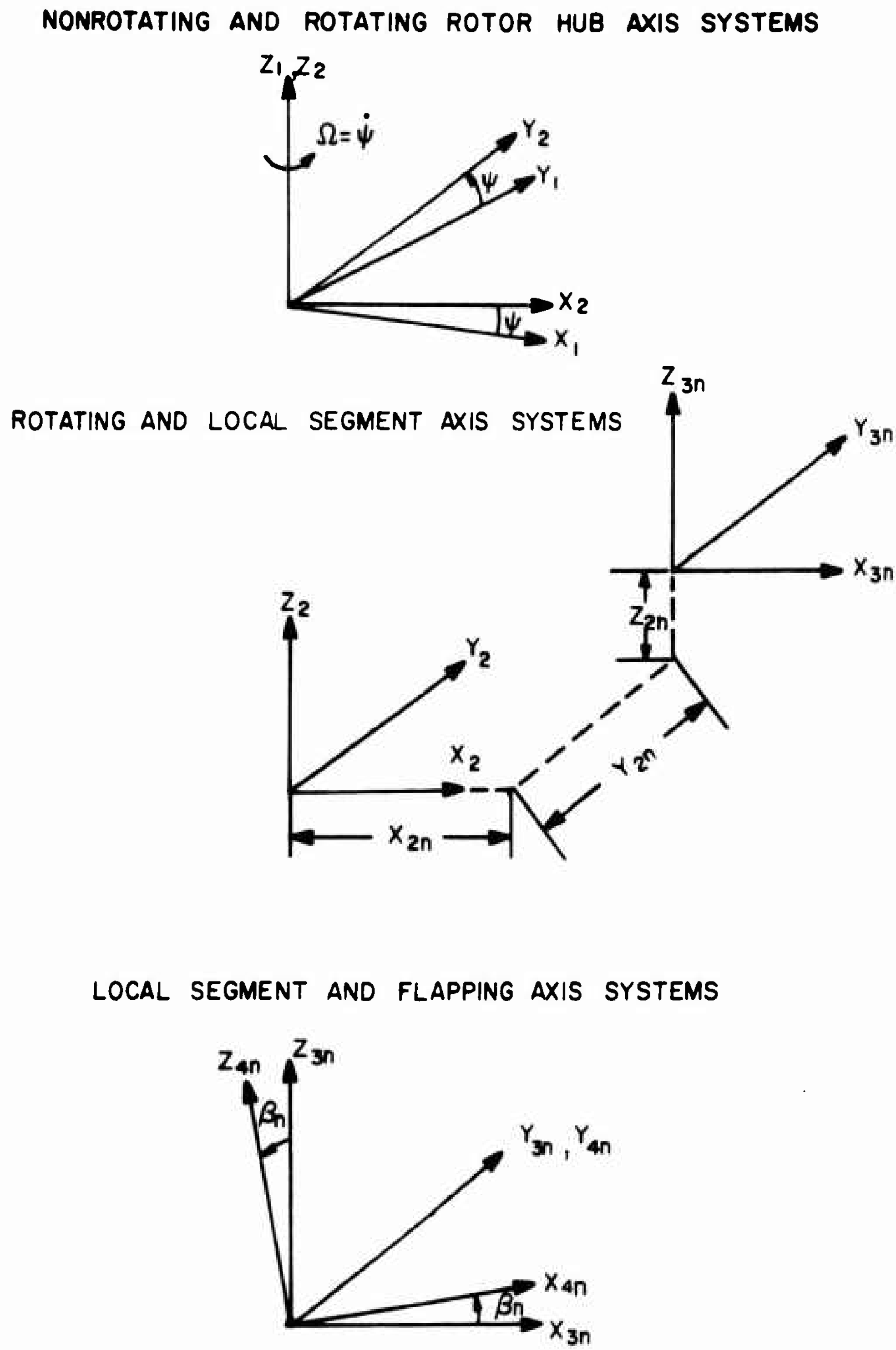

Figure 8. Coordinate Axis Systems for the Flatwise Equations of Motion.

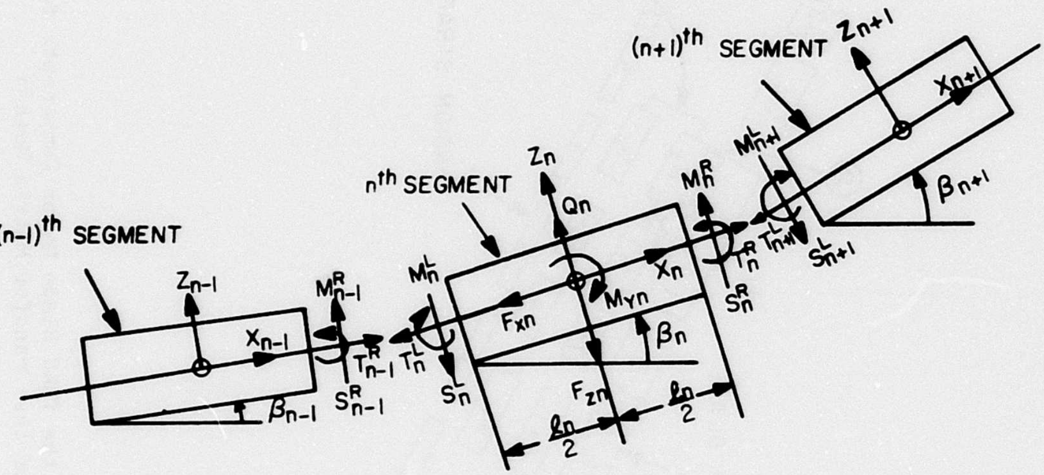

Figure 9. Free-Body Diagram of a TRAC Blade Segment for the Development of the Flatwise Equations of Motion.

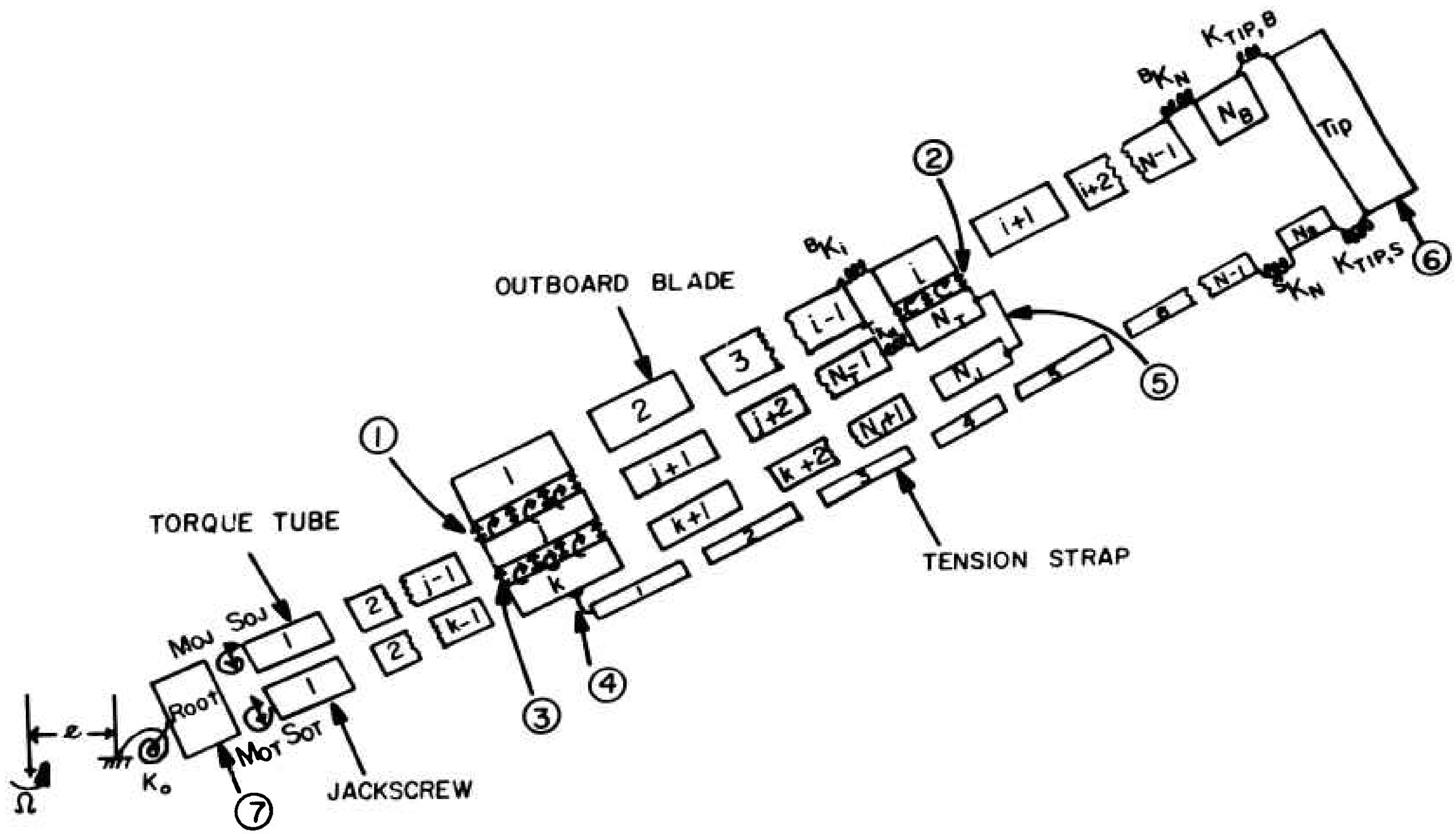

Figure 10. Schematic of the TRAC Blade Major Components for the Application of the Transfer Matrix Method.

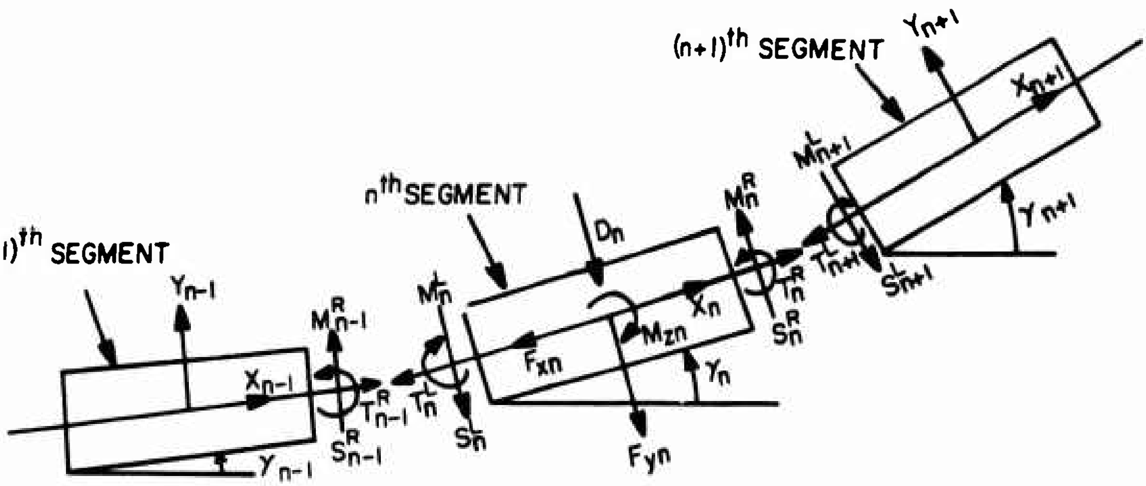

Figure 11. Free-Body Diagram of a TRAC Blade Segment for the Development of the Edgewise Equations of Motion.

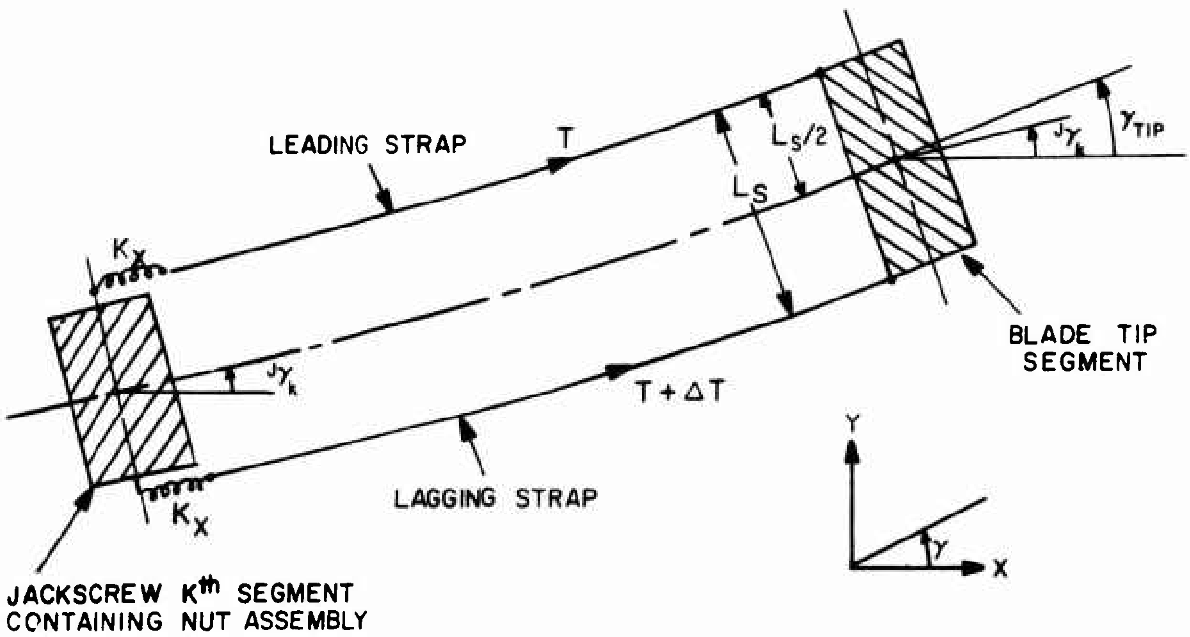

Figure 12. Schematic of Tension Straps Showing the Differential Tension Present With Inplane Bending of the Straps.

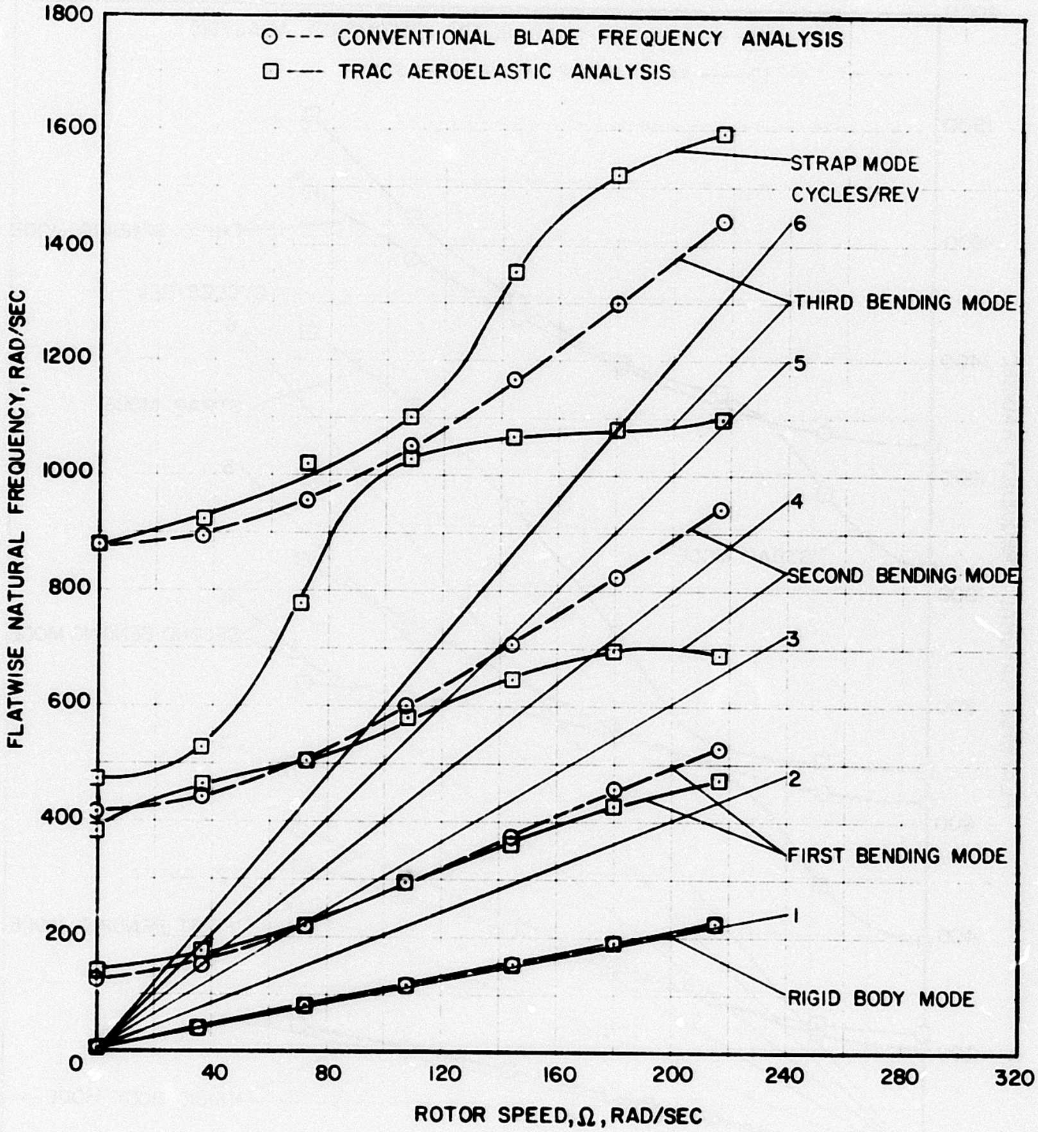

Figure 13. Flatwise Natural Frequencies for Fully-Extended TRAC Rotor.

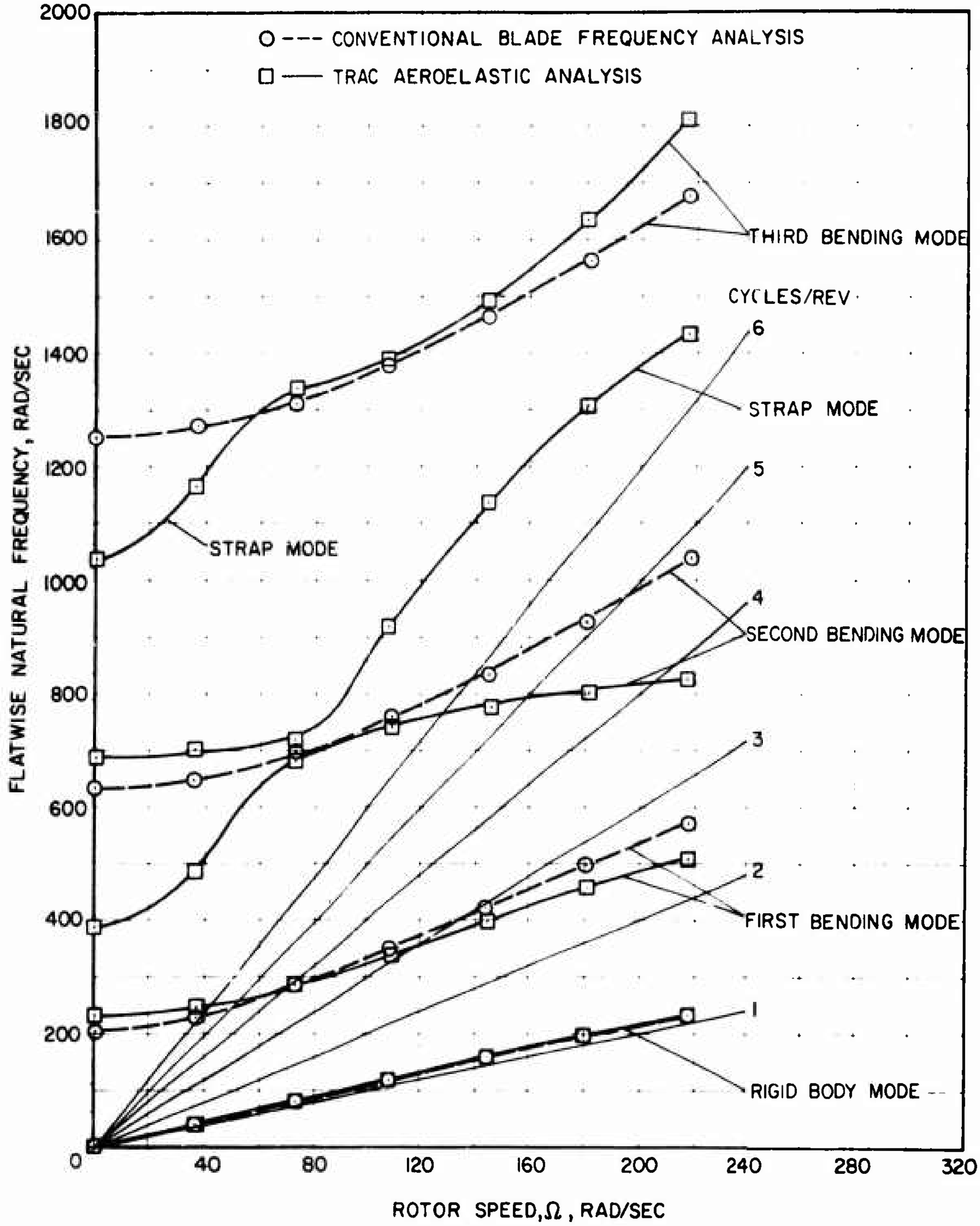

Figure 14. Flatwise Natural Frequencies for 80 Percent Extended TRAC Rotor.

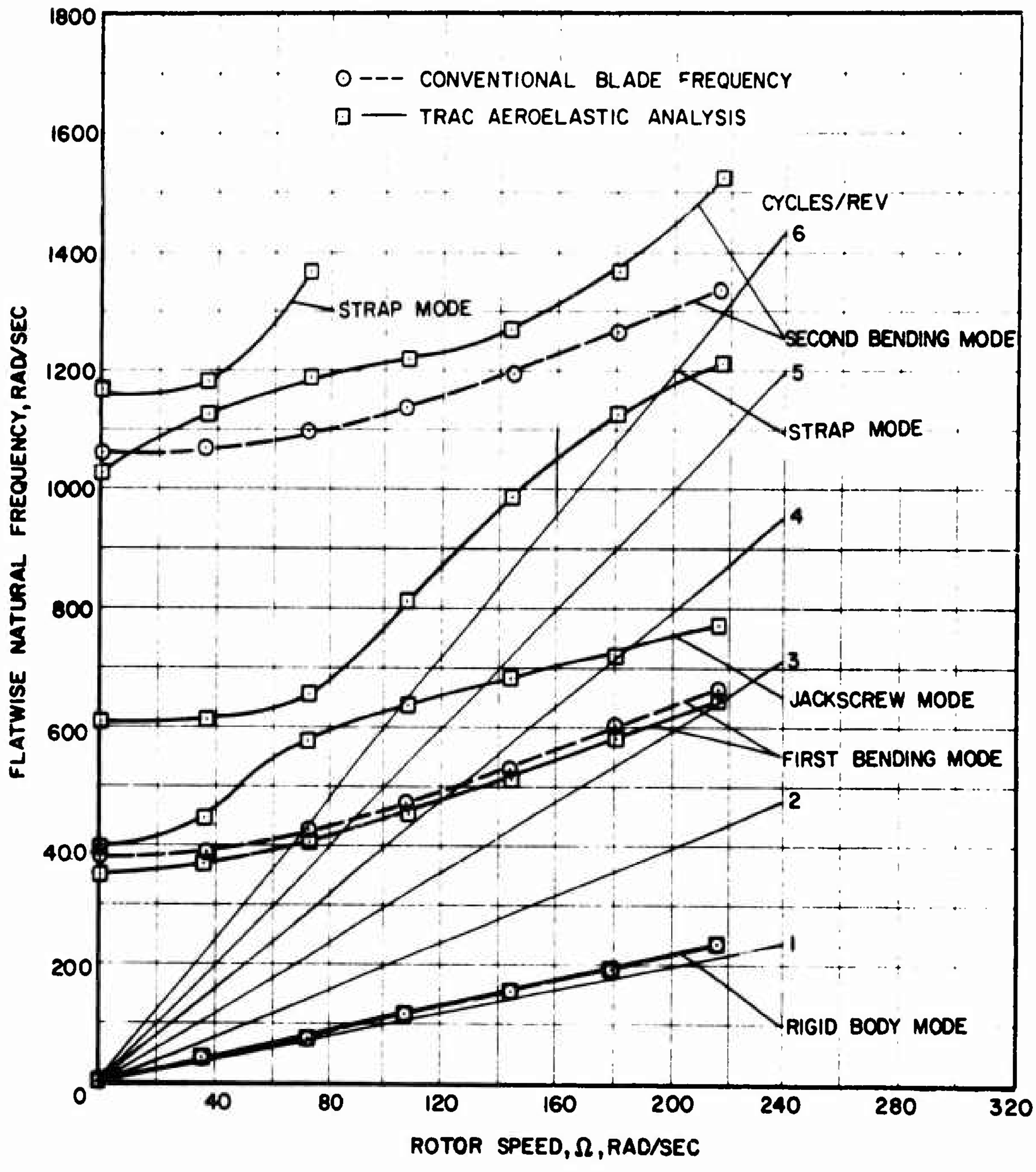

Figure 15. Flatwise Natural Frequencies for 62.5 Percent Extended TRAC Rotor.

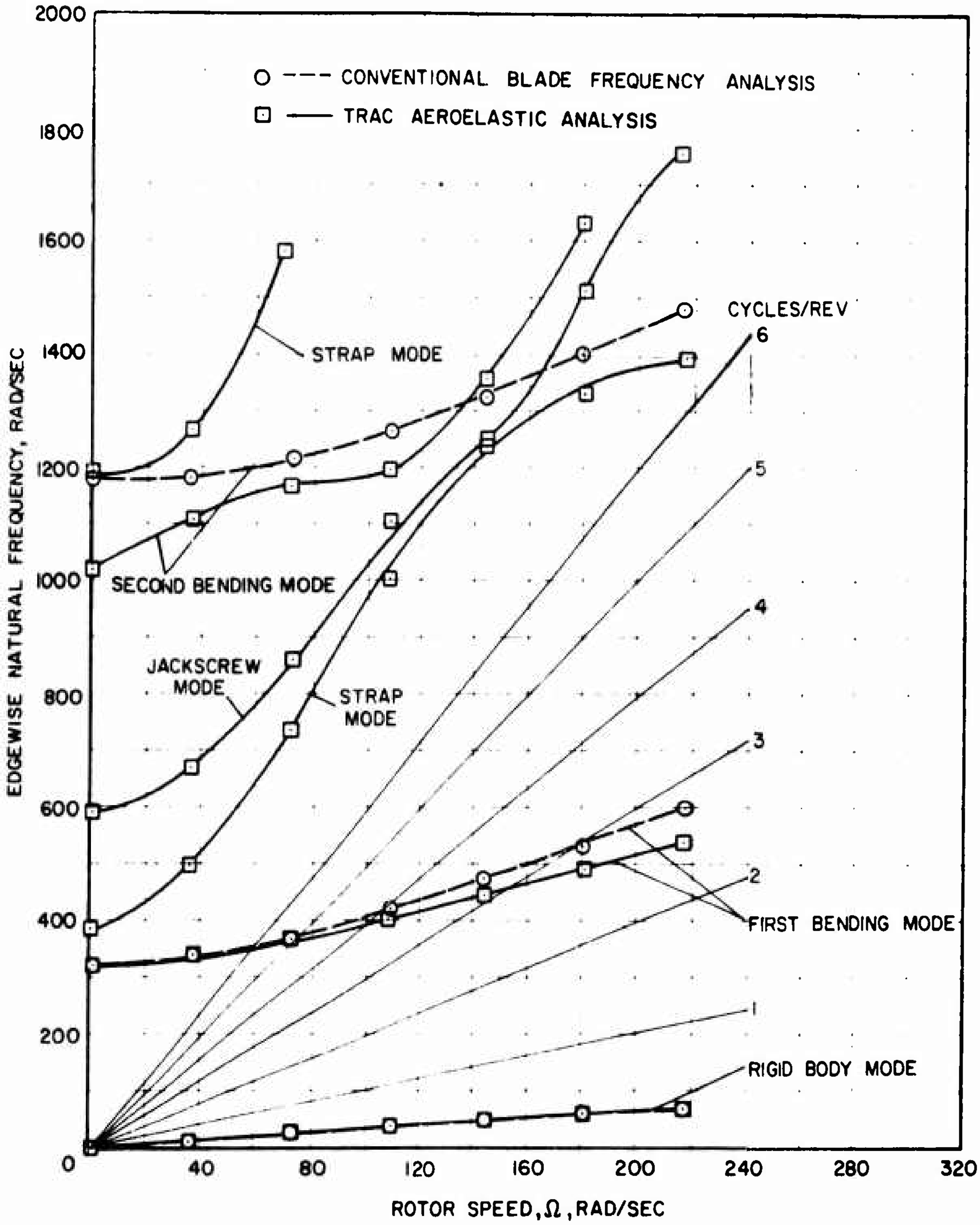

Figure 16. Edgewise Natural Frequencies for Fully-Extended TRAC Rotor.

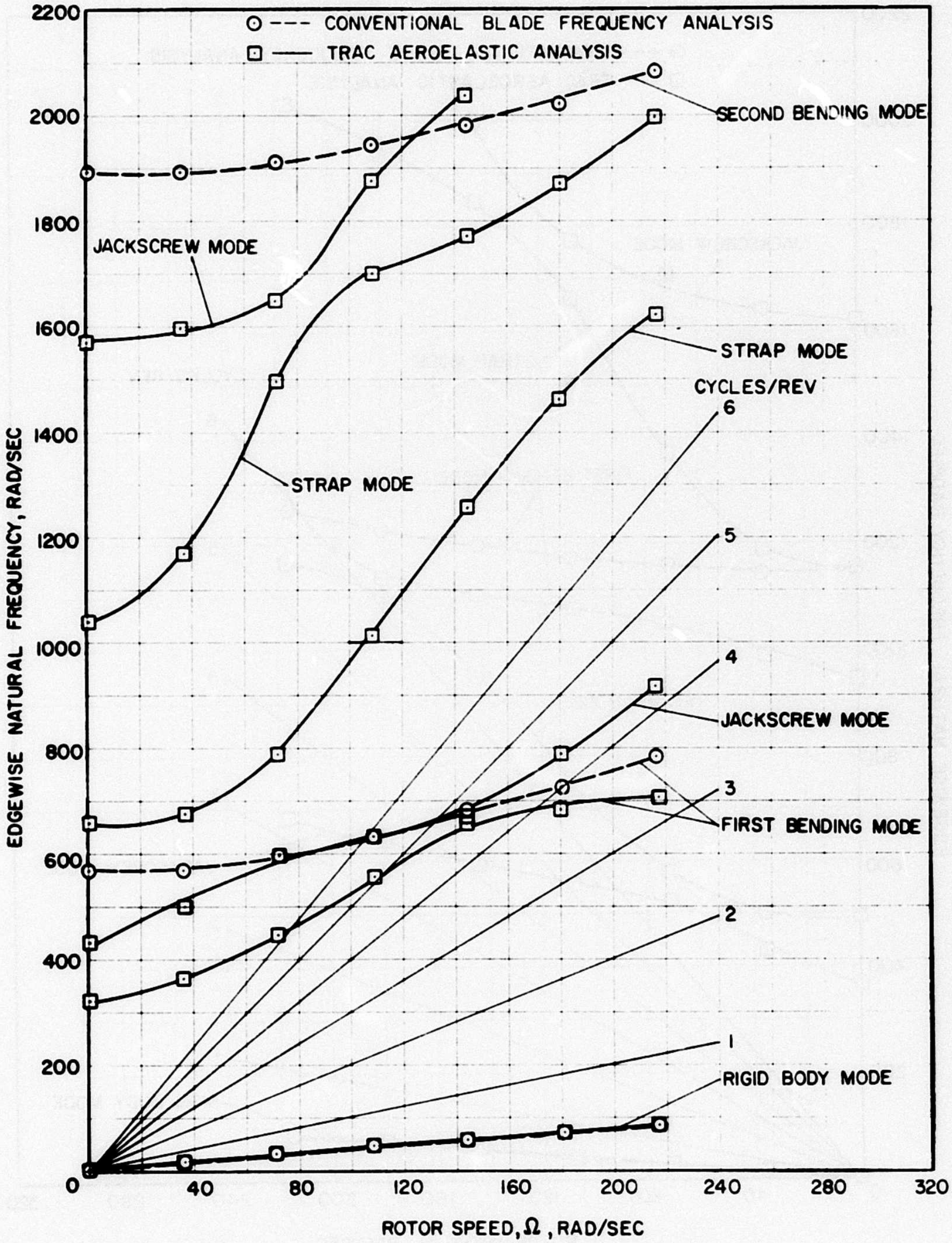

Figure 17. Edgewise Natural Frequencies for 80 Percent Extended TRAC Rotor.

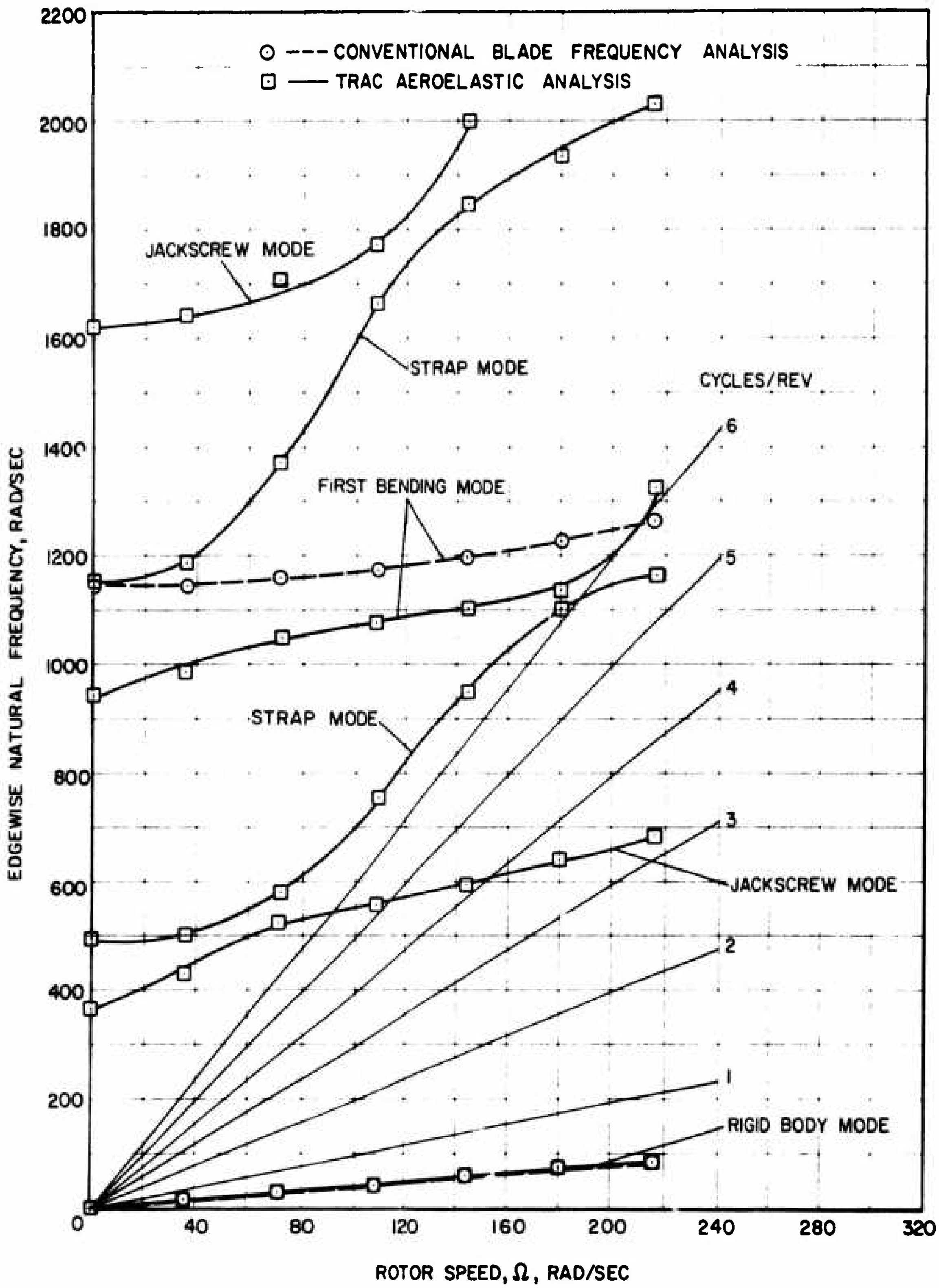

Figure 18. Edgewise Natural Frequencies for 62.5 Percent Extended TRAC Rotor.

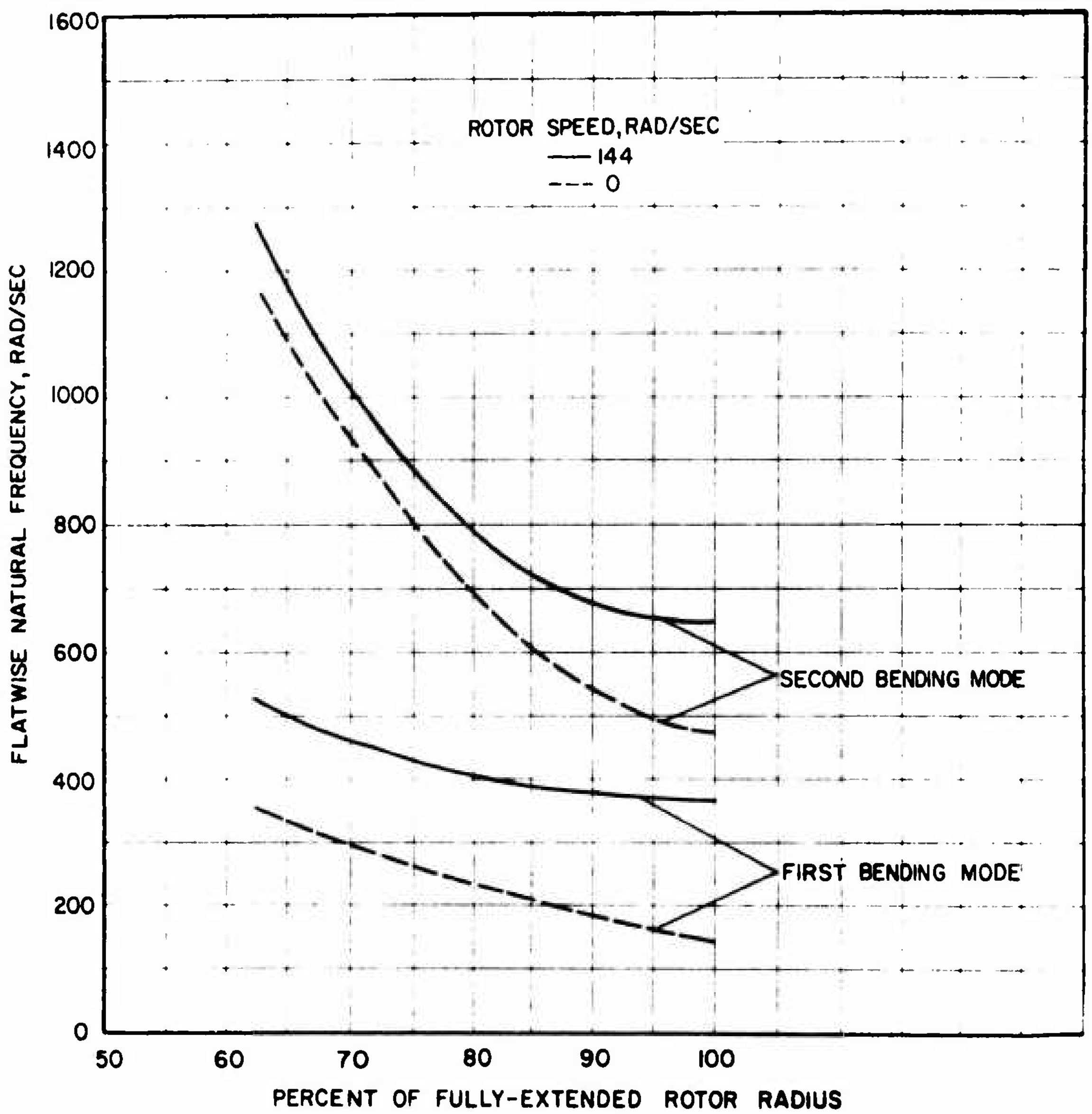

Figure 19. Effect of Rotor Retraction on the TRAC Blade Flatwise Natural Frequencies.

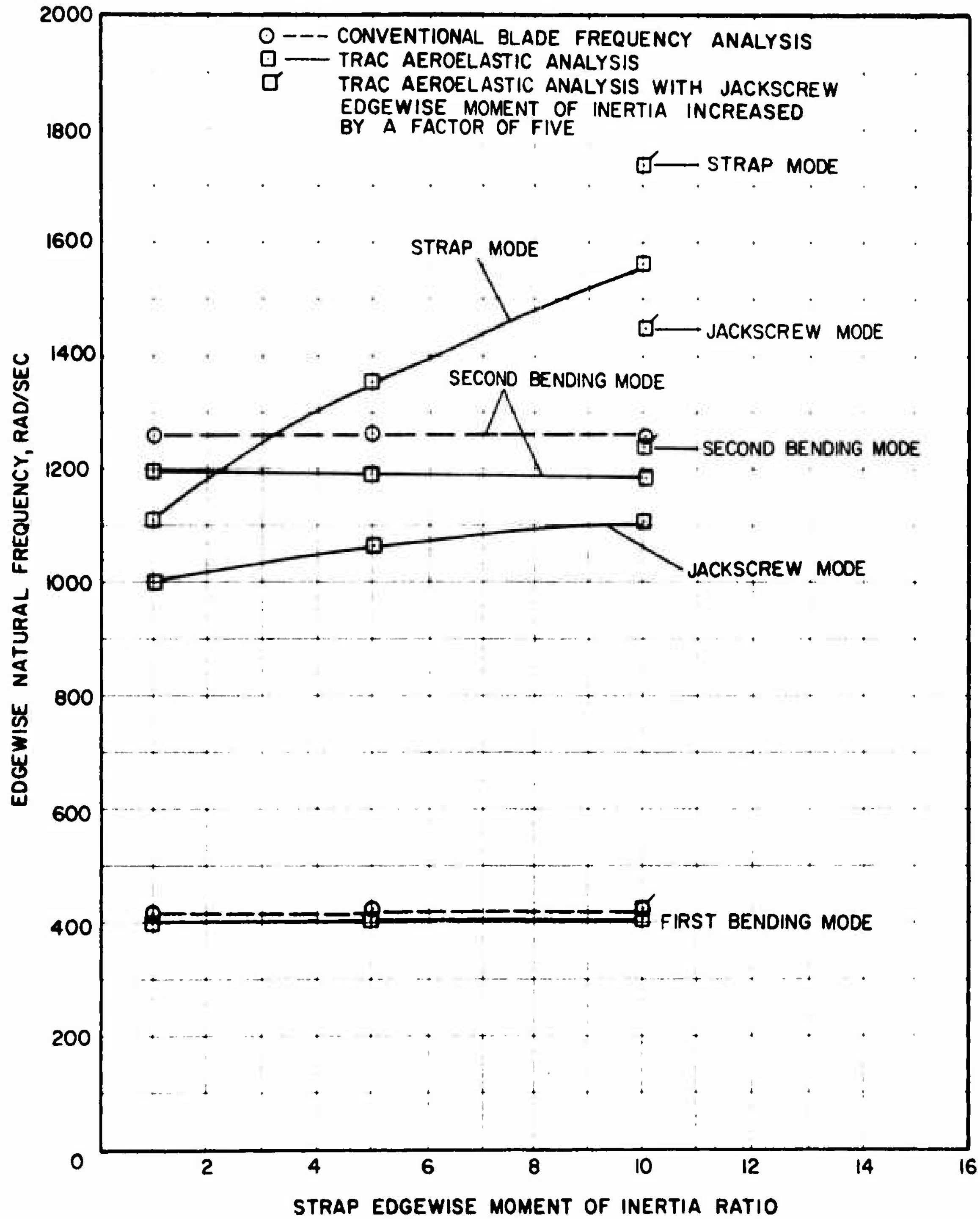

Figure 20. Effect of Strap and Jackscrew Edgewise Moment of Inertia on the TRAC Blade Edgewise Natural Frequencies, 100 Percent Radius, Ω = 108 Rad/Sec.

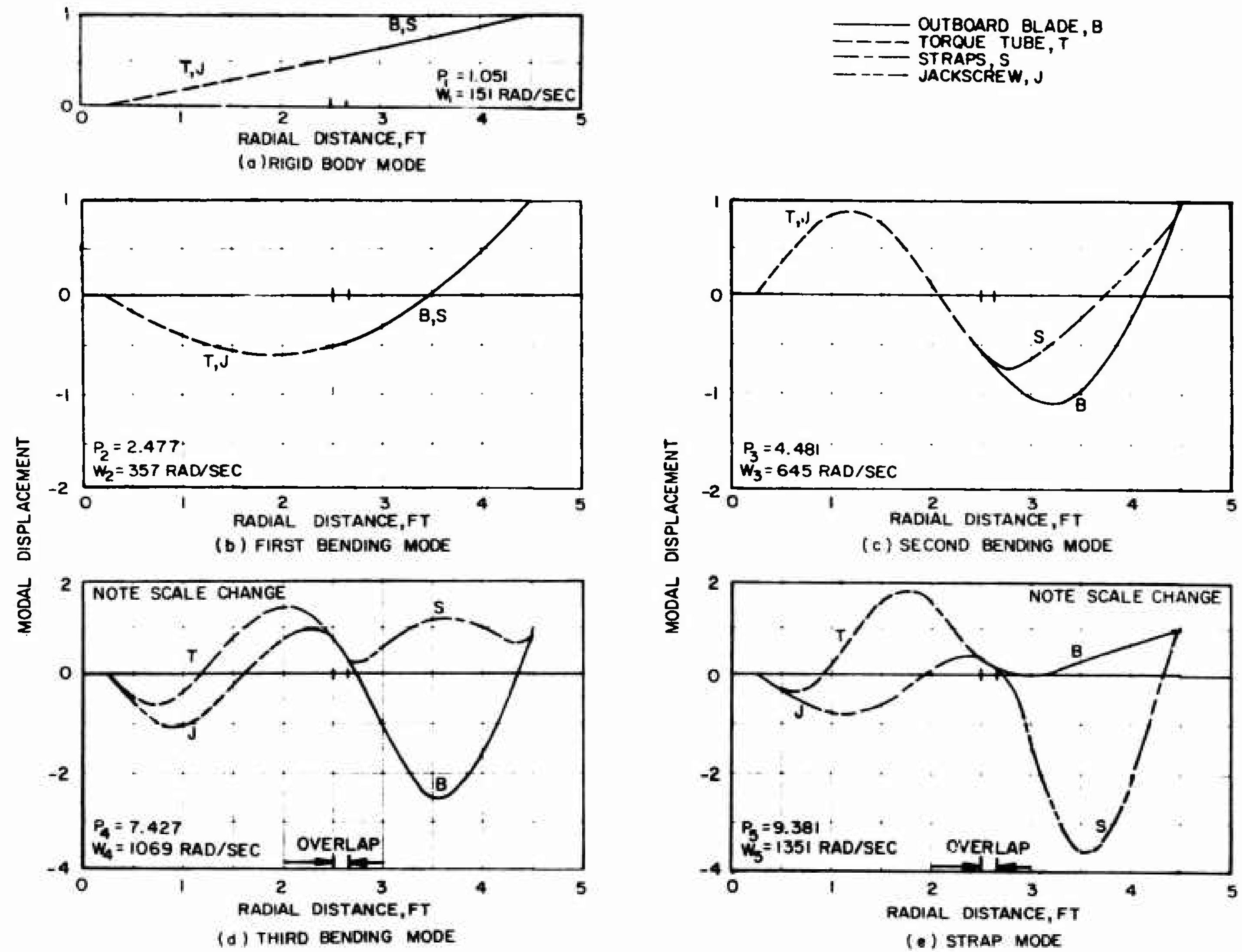

Figure 21. TRAC Blade Flatwise Mode Shapes for Fully-Extended Radius at a Rotor Speed of 144 Radians per Second.

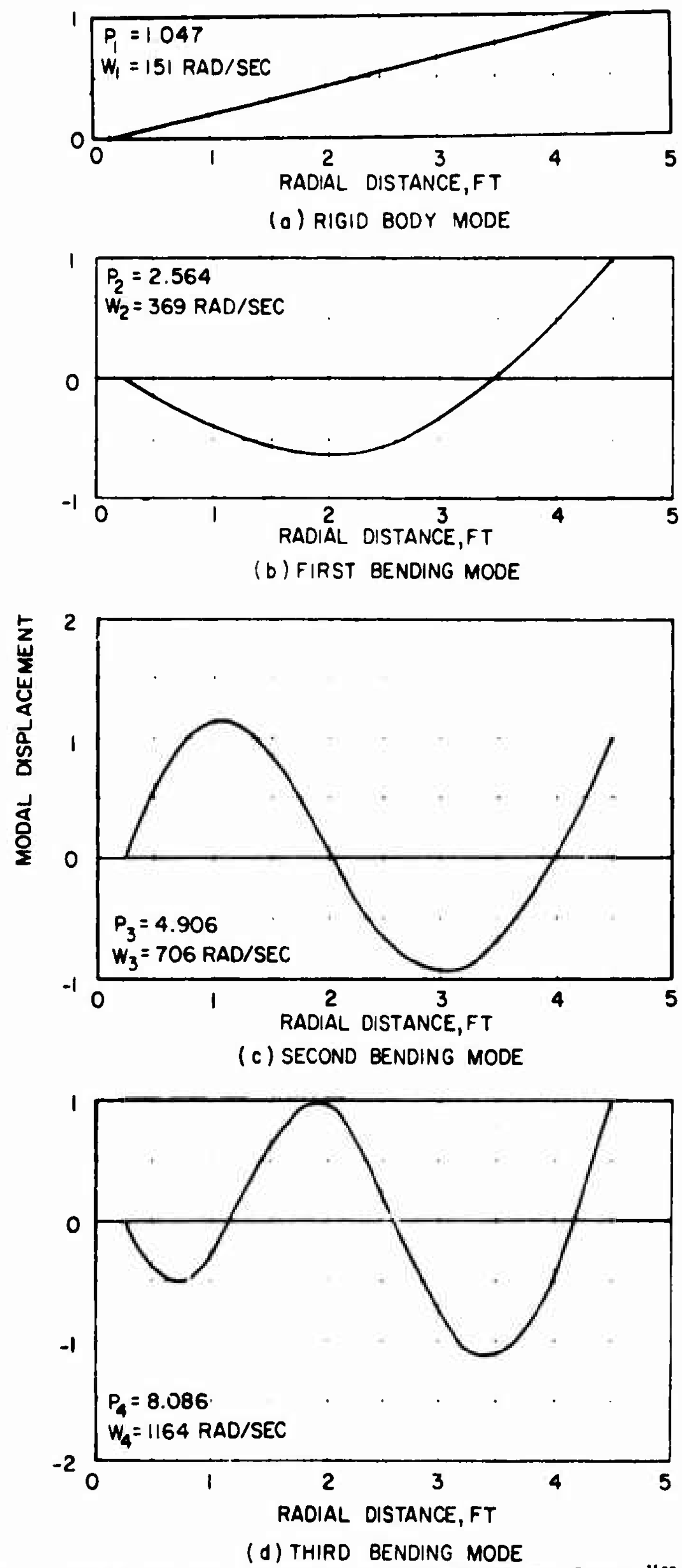

Figure 22. TRAC Blade Flatwise Mode Shapes from "Normal Modes Analysis" for Fully-Extended Radius at a Rotor Speed of 144 Radians per Second.

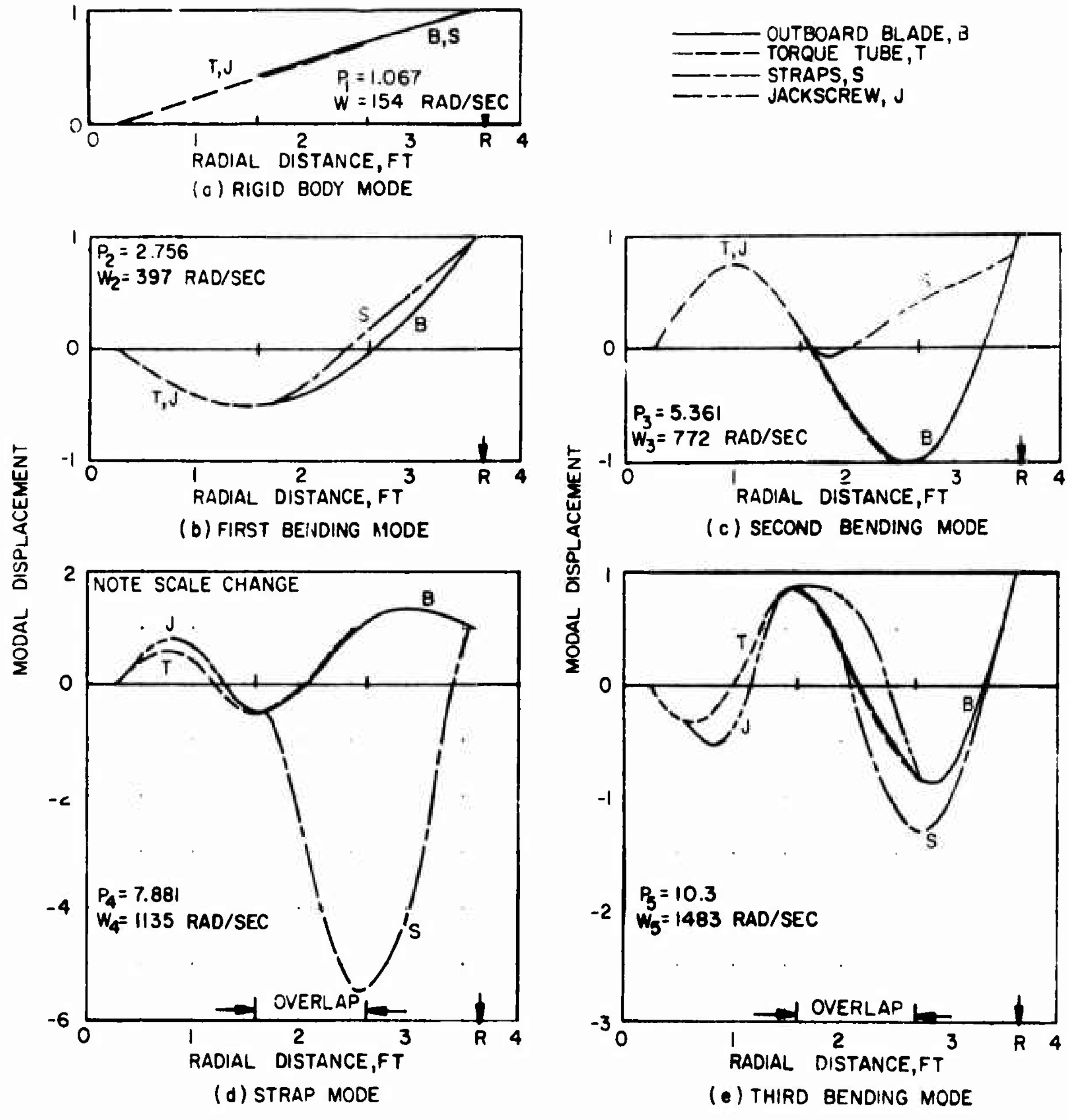

Figure 23. TRAC Blade Flatwise Mode Shapes for 80 Percent Extended Radius at a Rotor Speed of 144 Radians per Second.

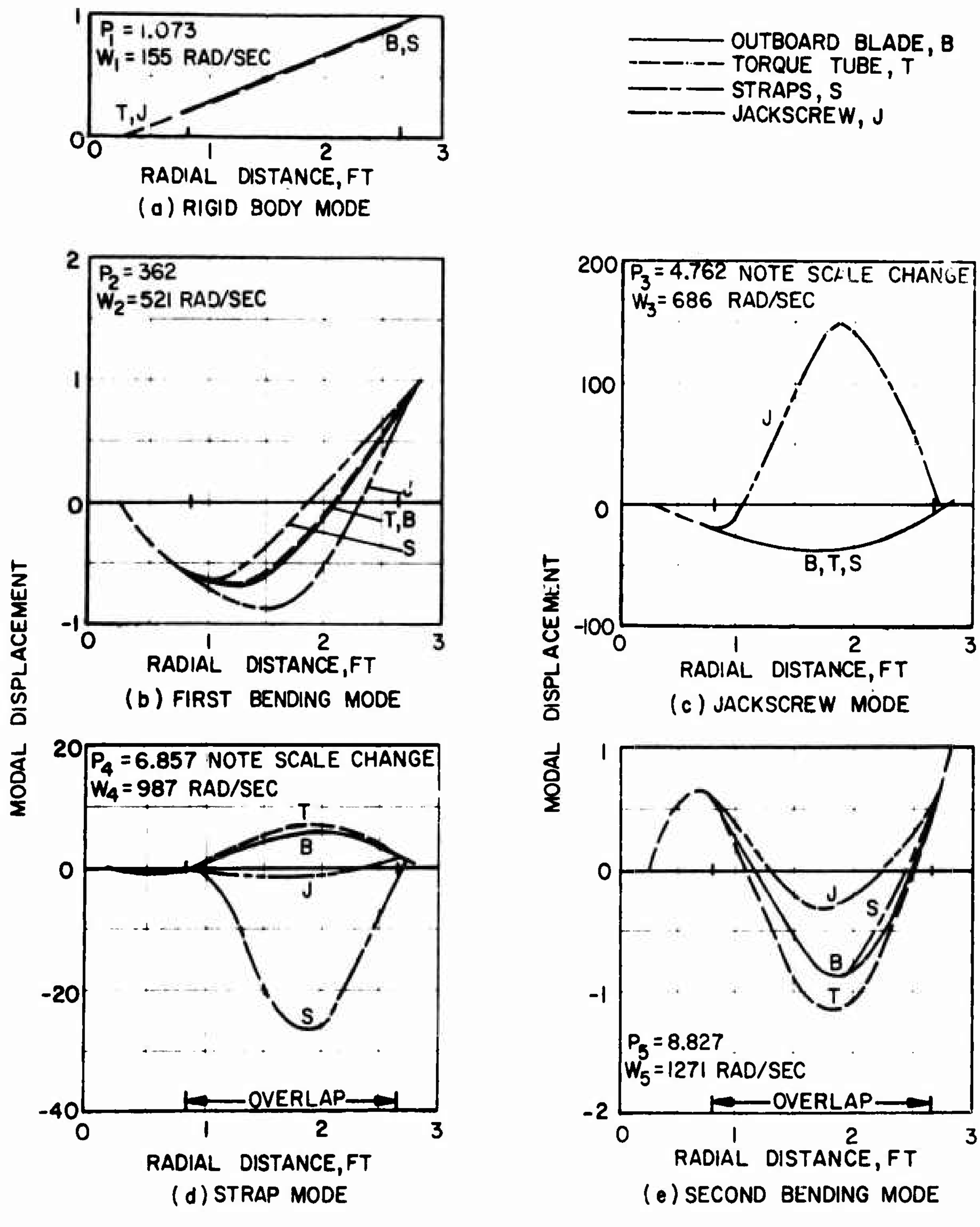

Figure 24. TRAC Blade Flatwise Mode Shapes for 62.5 Percent Extended Radius at a Rotor Speed of 144 Radians per Second.

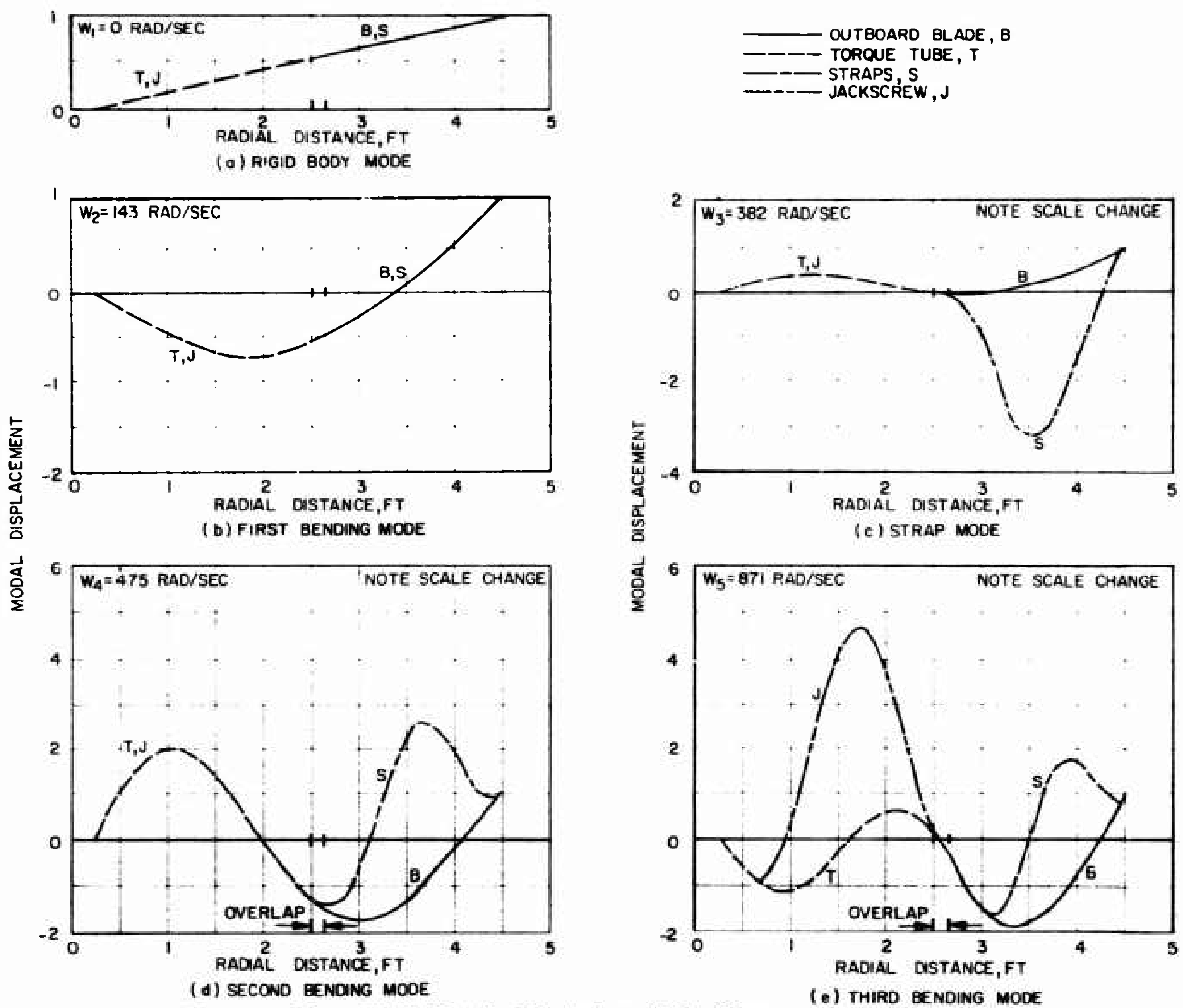

Figure 25. TRAC Blade Flatwise Mode Shapes for Fully-Extended Radius at Zero Rotor Speed.

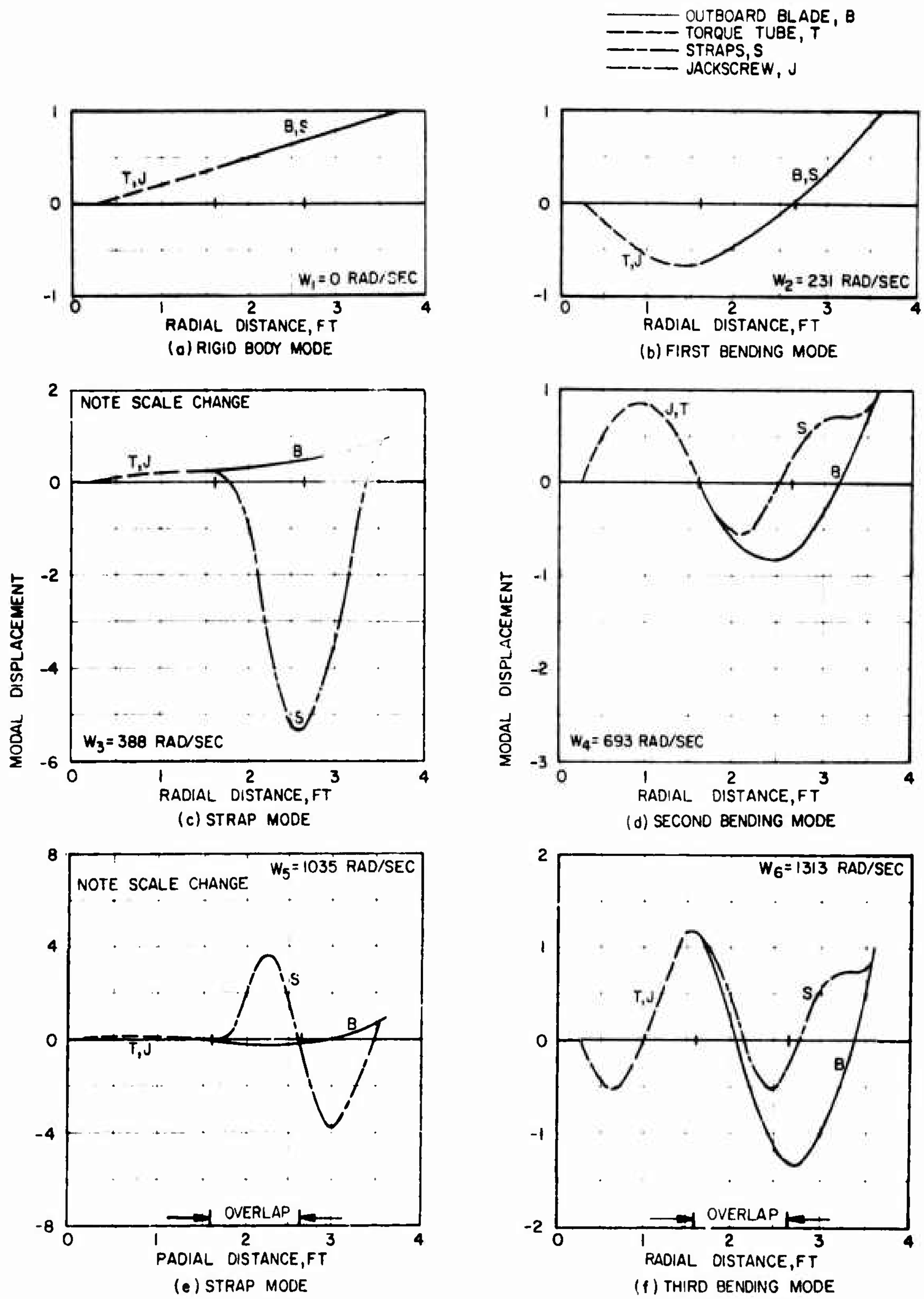

Figure 26. TRAC Blade Flatwise Mode Shapes for 80 Percent Extended Radius at Zero Rotor Speed.

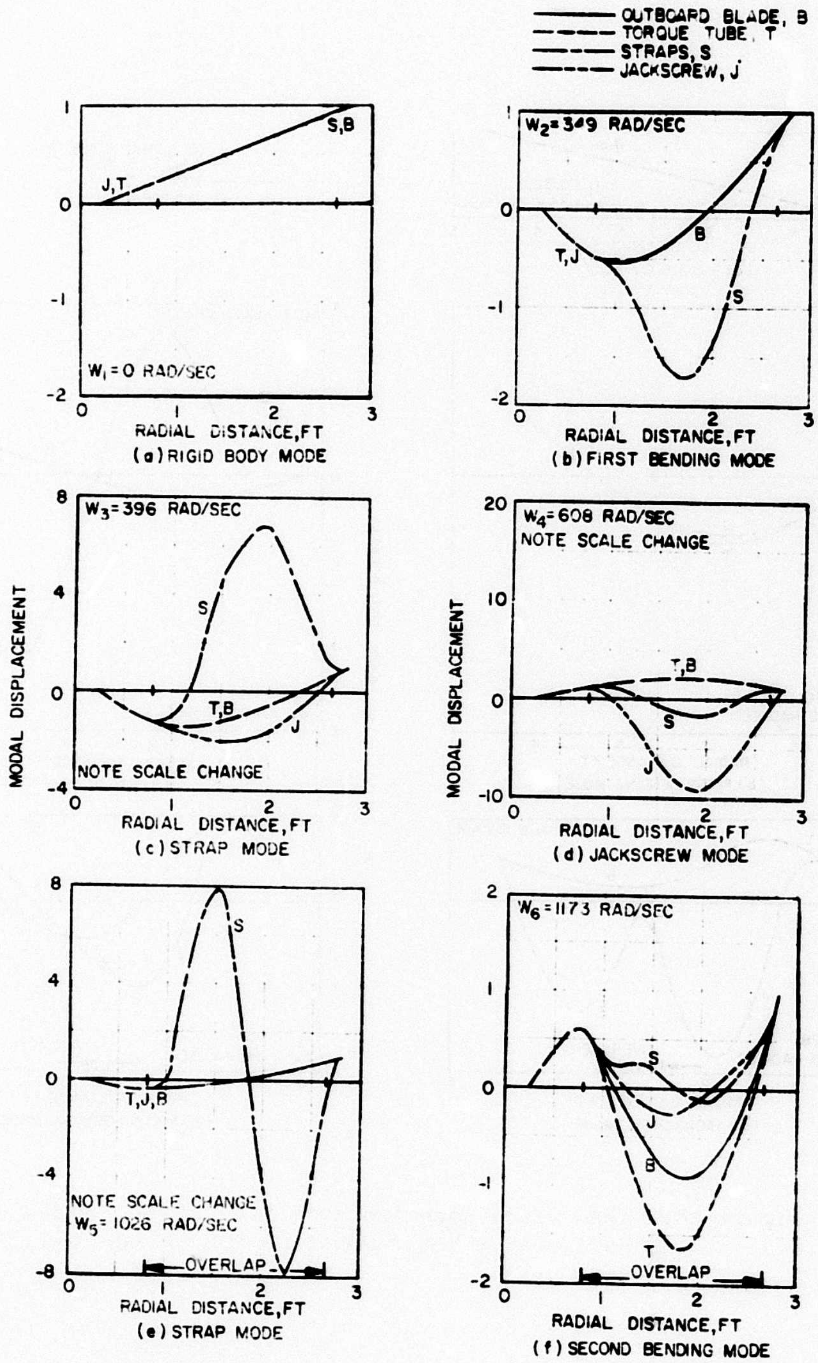

Figure 27. TRAC Blade Flatwise Mode Shapes for 62.5 Percent Extended Radius at Zero Rotor Speed.

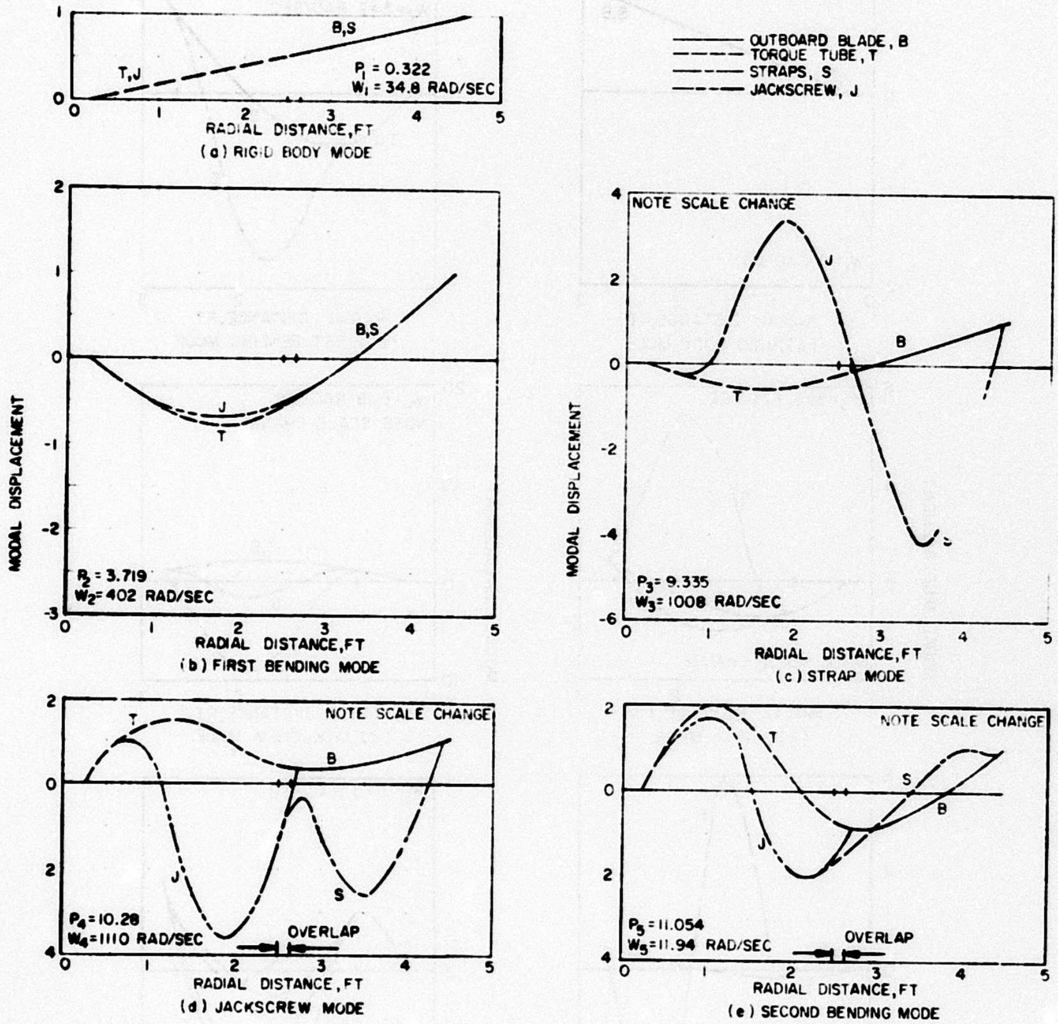

Figure 28. TRAC Blade Edgewise Mode for Fully-Extended Radius at a Rotor Speed of 108 Radians per Second.

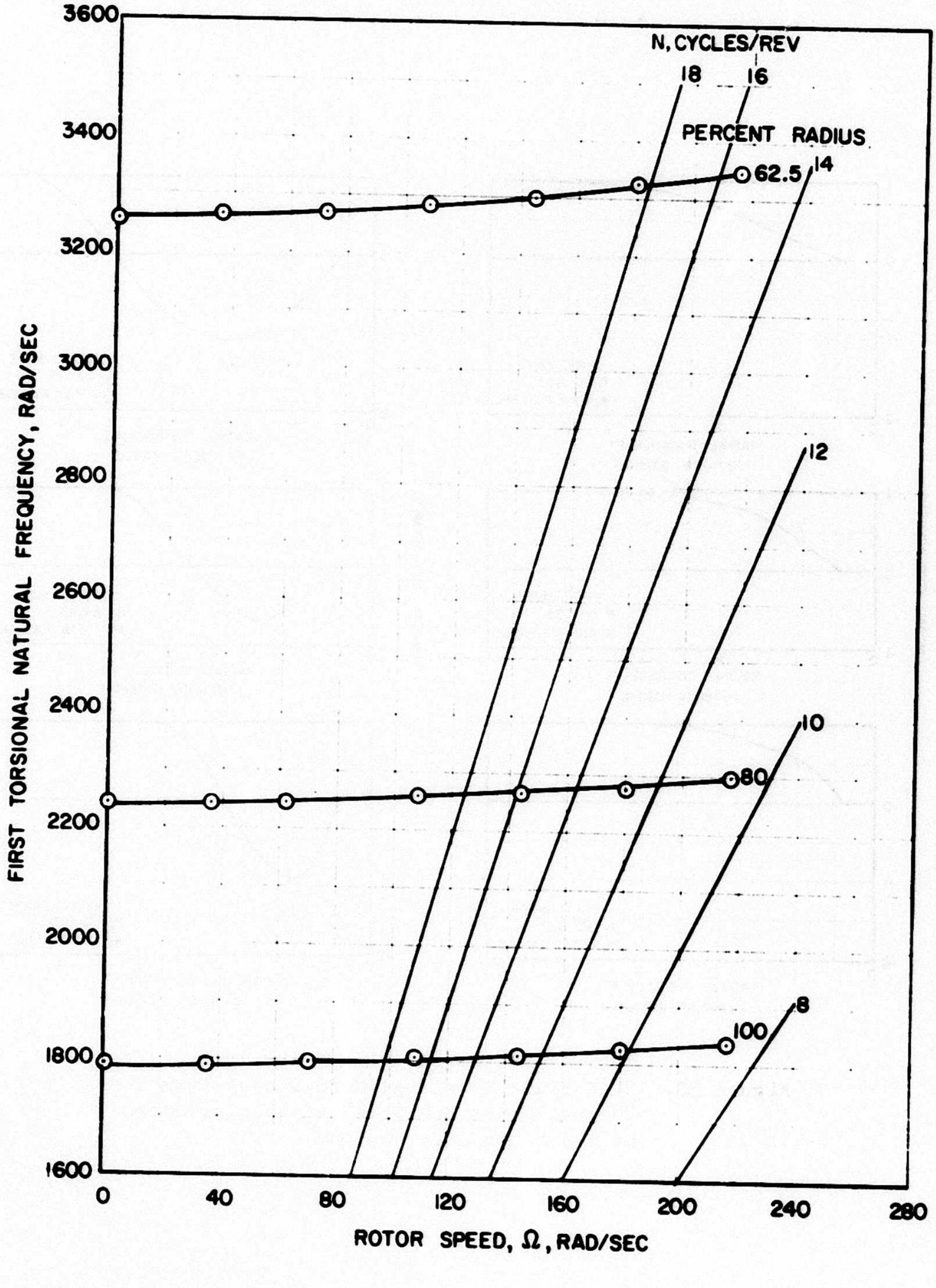

Figure 29. TRAC Blade First Torsional Natural Frequency.

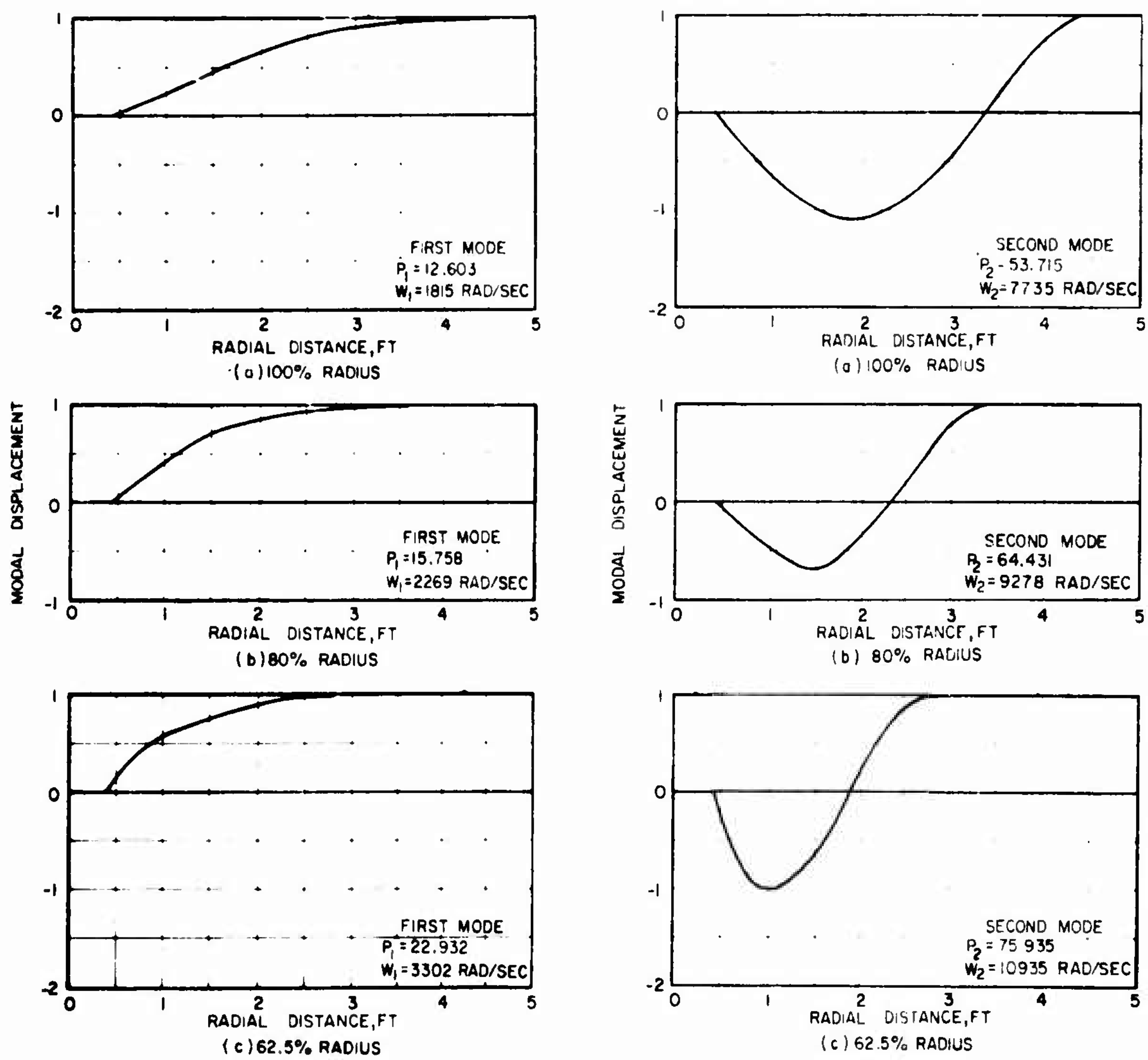

Figure 30. TRAC Blade Torsional Mode Shapes From the "Normal Modes Analysis" at a Rotor Speed of 144 Radians per Second.

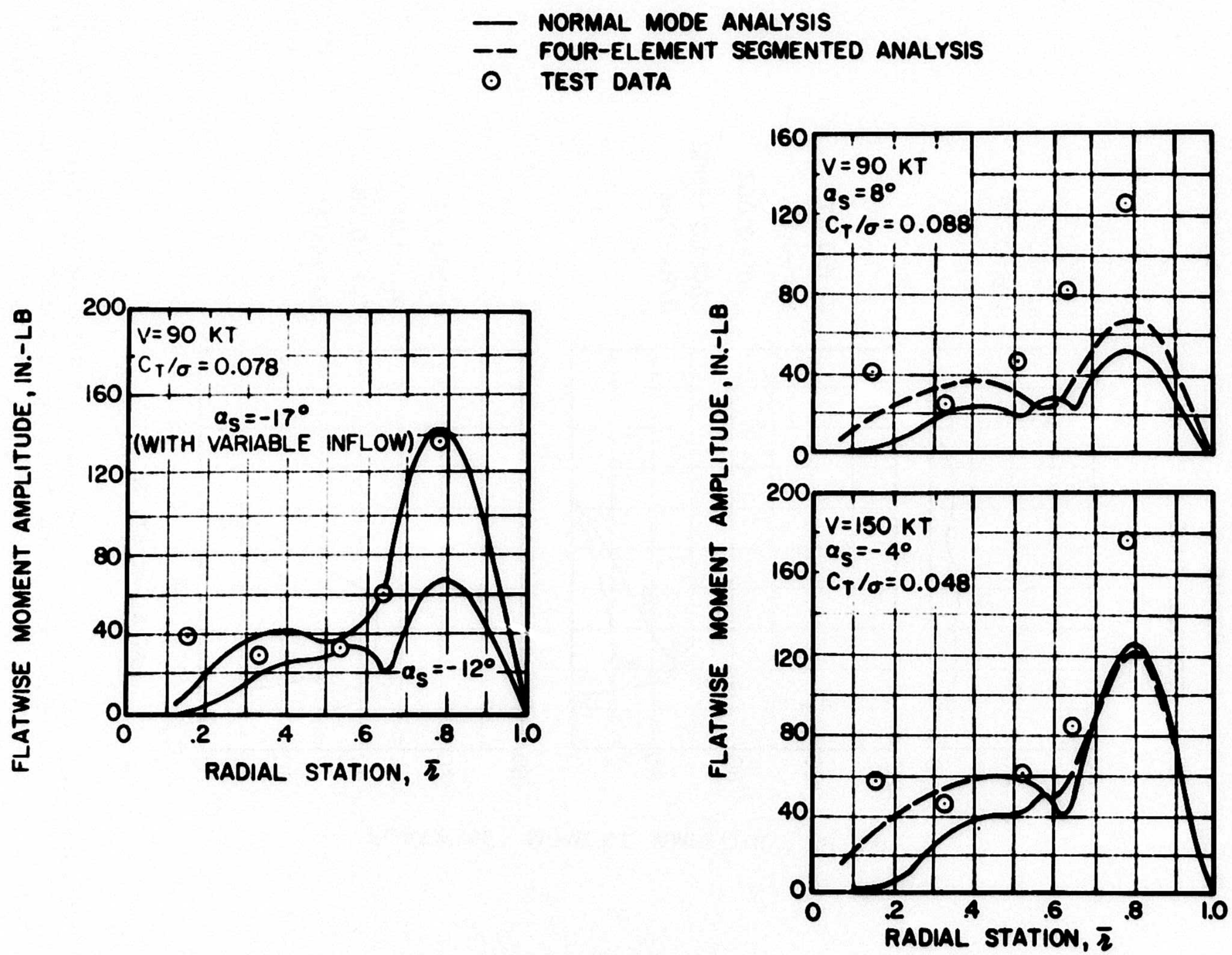

Figure 31. Comparison of Predicted and Measured Flatwise Moment Amplitudes for Fully-Extended Rotor Conditions.

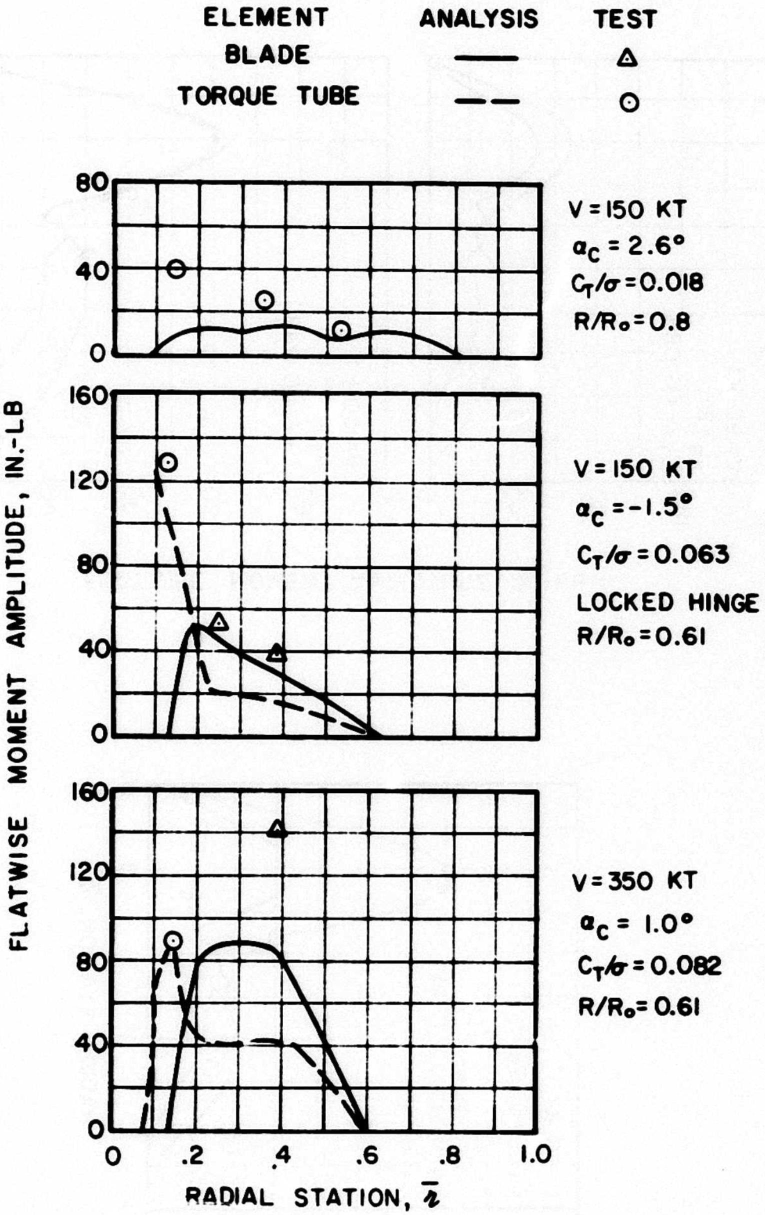

Figure 32. Comparison of Predicted and Measured Flatwise Moment Amplitudes for Reduced-Diameter Conditions.

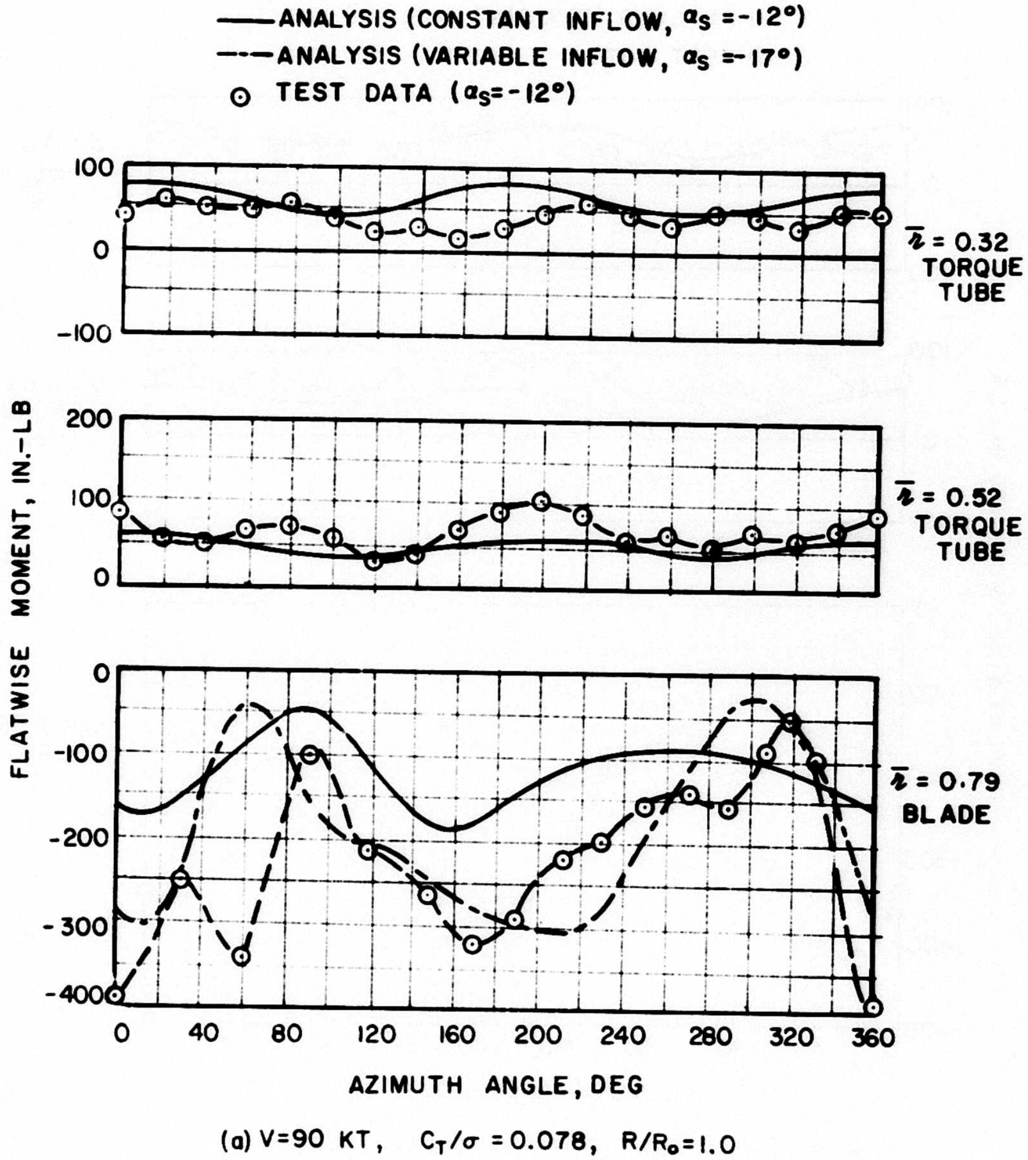

Figure 33. Comparison of Predicted and Measured Time Histories of Flatwise Moment.

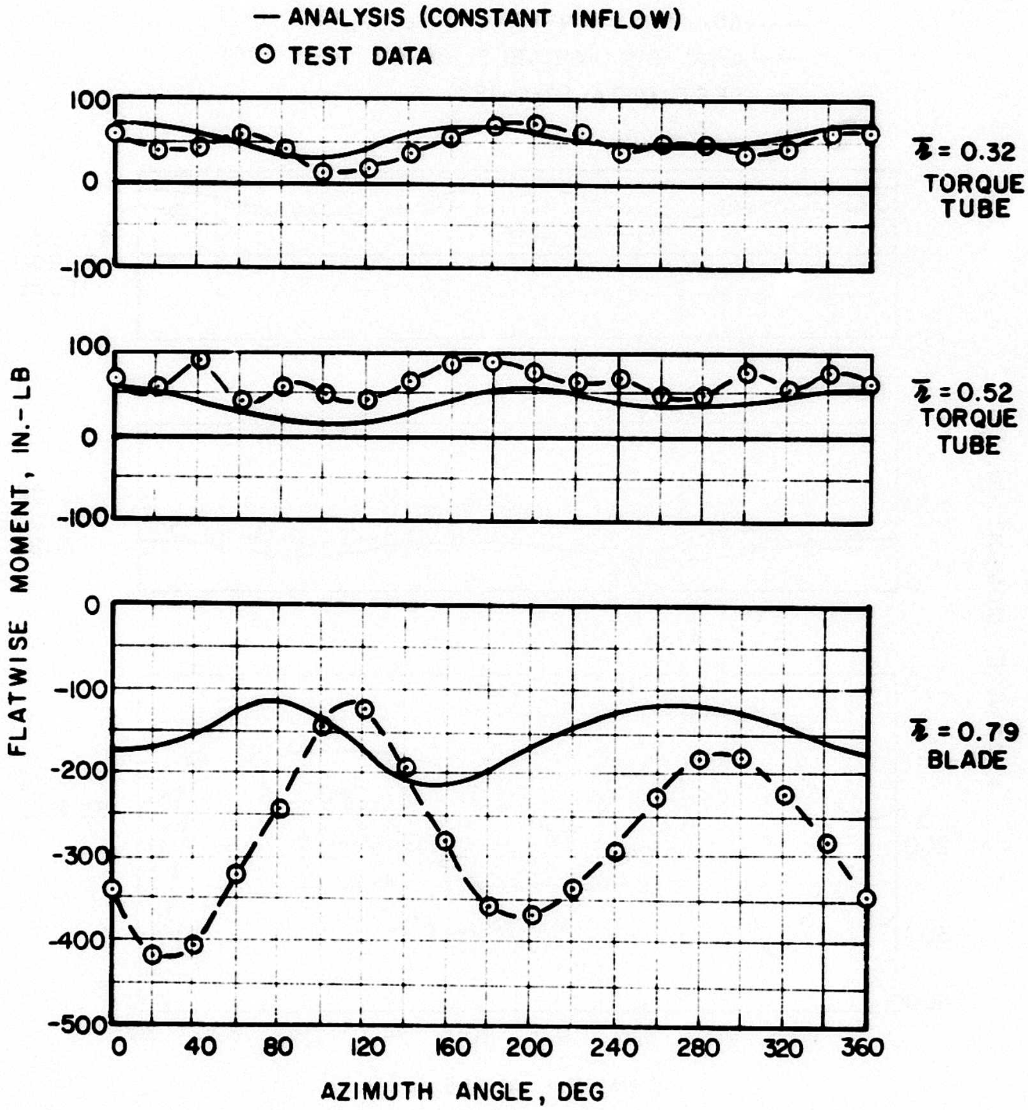

(b) V=90 KT, $a_S = 8°$, $C_T/\sigma = 0.088$, $R/R_o = 1.0$

Figure 33. Continued.

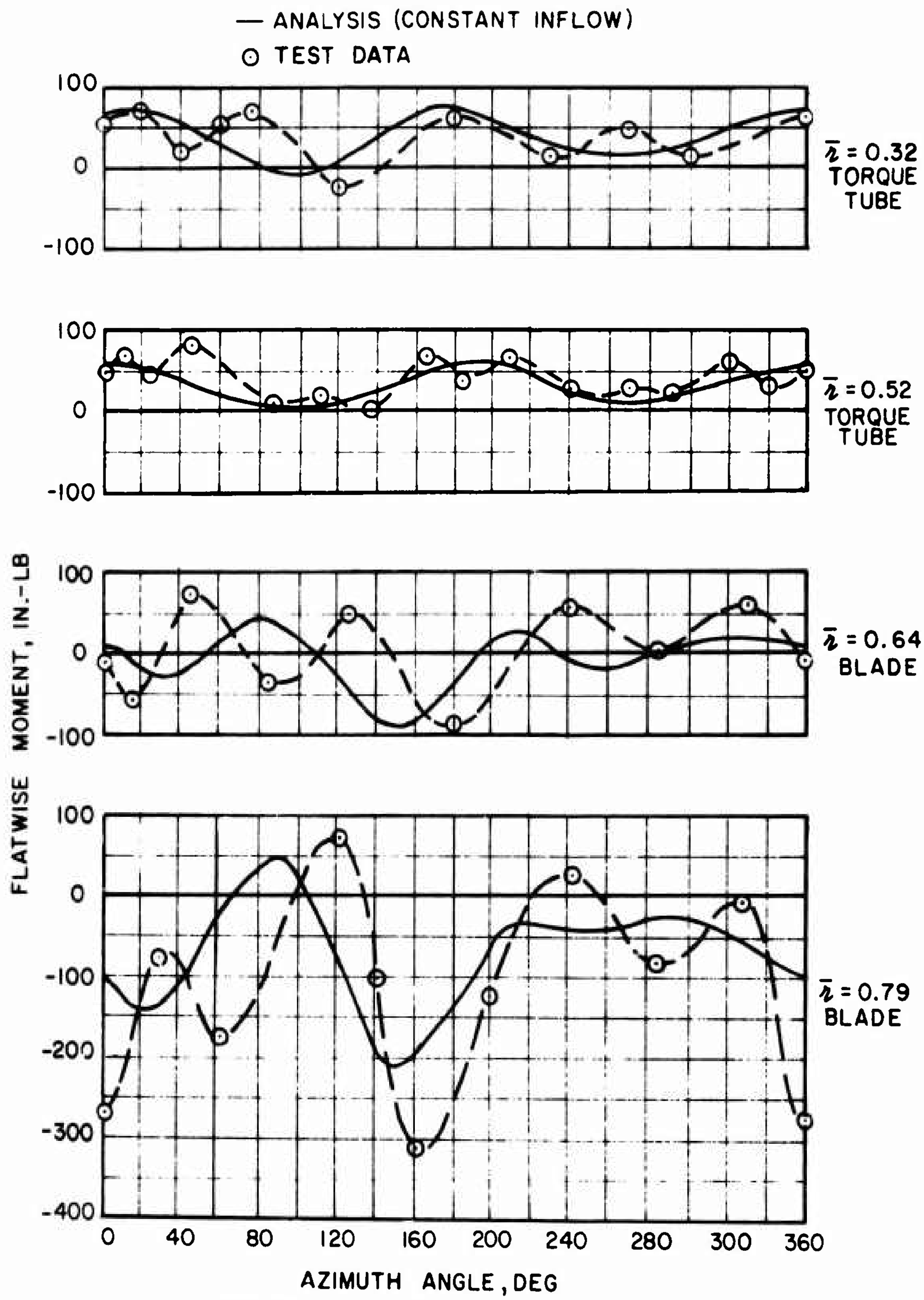

(c) V=150 KT, $a_S=-4°$, $C_T/\sigma=0.048$, $R/R_o=1.0$

Figure 33. Continued.

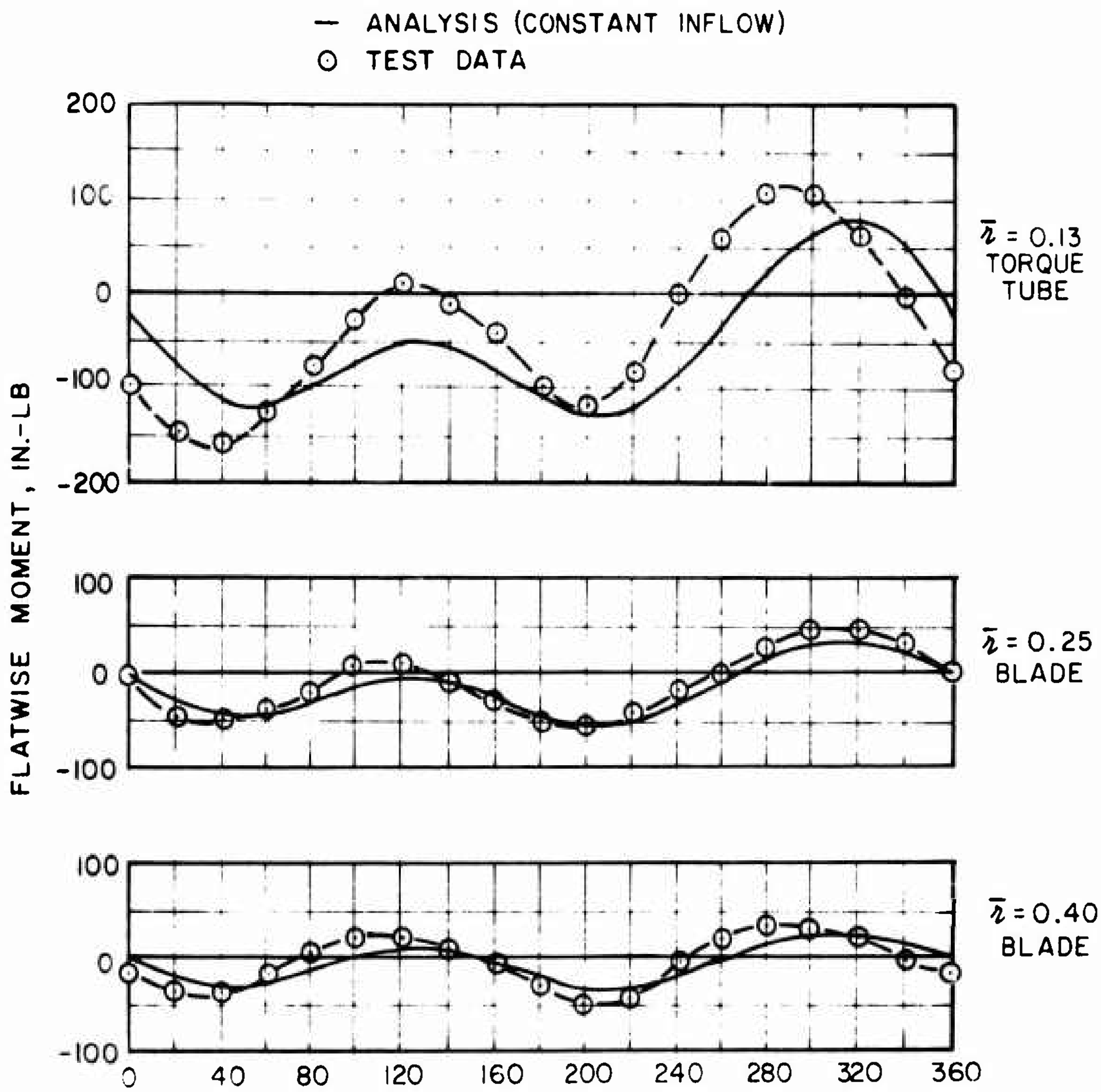

(d) V = 150 KT, $a_S = -2°$, $C_T/\sigma = 0.063$, $R/R_o = 0.61$, LOCKED HINGE

Figure 33. Continued.

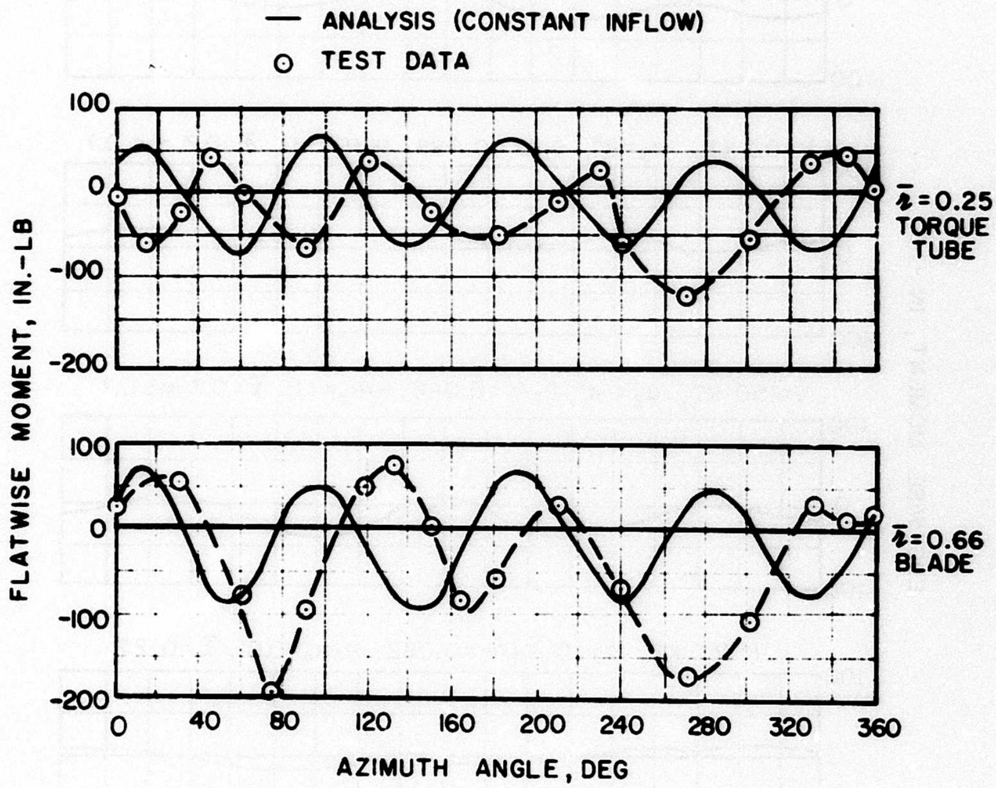

(e) V = 350 KT, $a_S = 0°$, $C_T/\sigma = 0.082$, $R/R_o = 0.61$

Figure 33. Concluded.

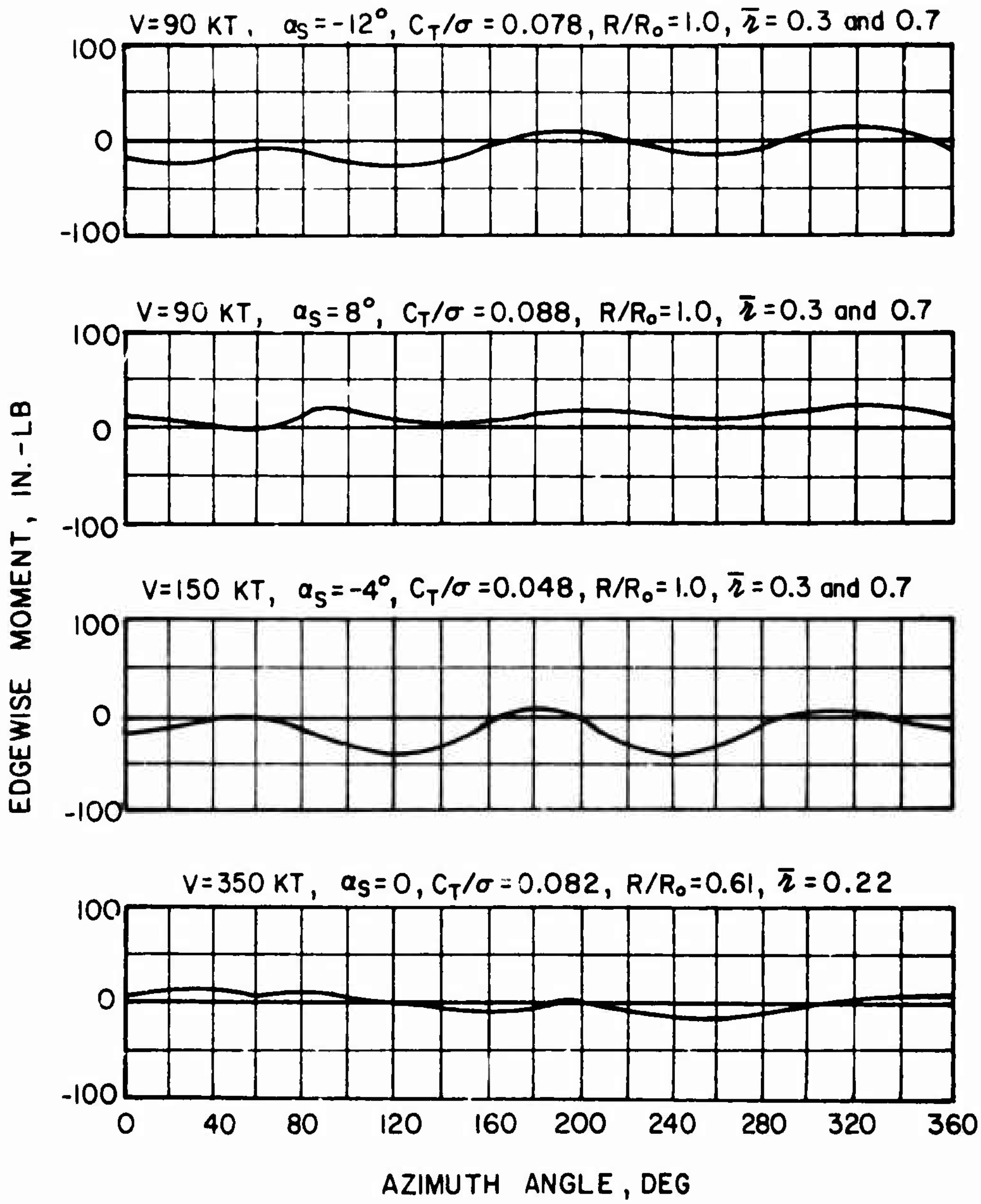

Figure 34. Predicted Edgewise Moments.

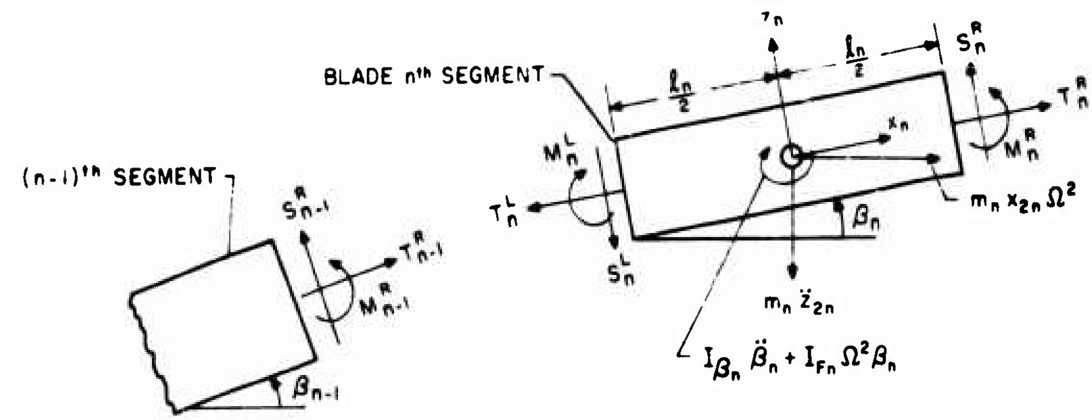

Figure 35. Free-Body Diagram of a Typical Blade Segment for the Development of the Flatwise Equations of Motion.

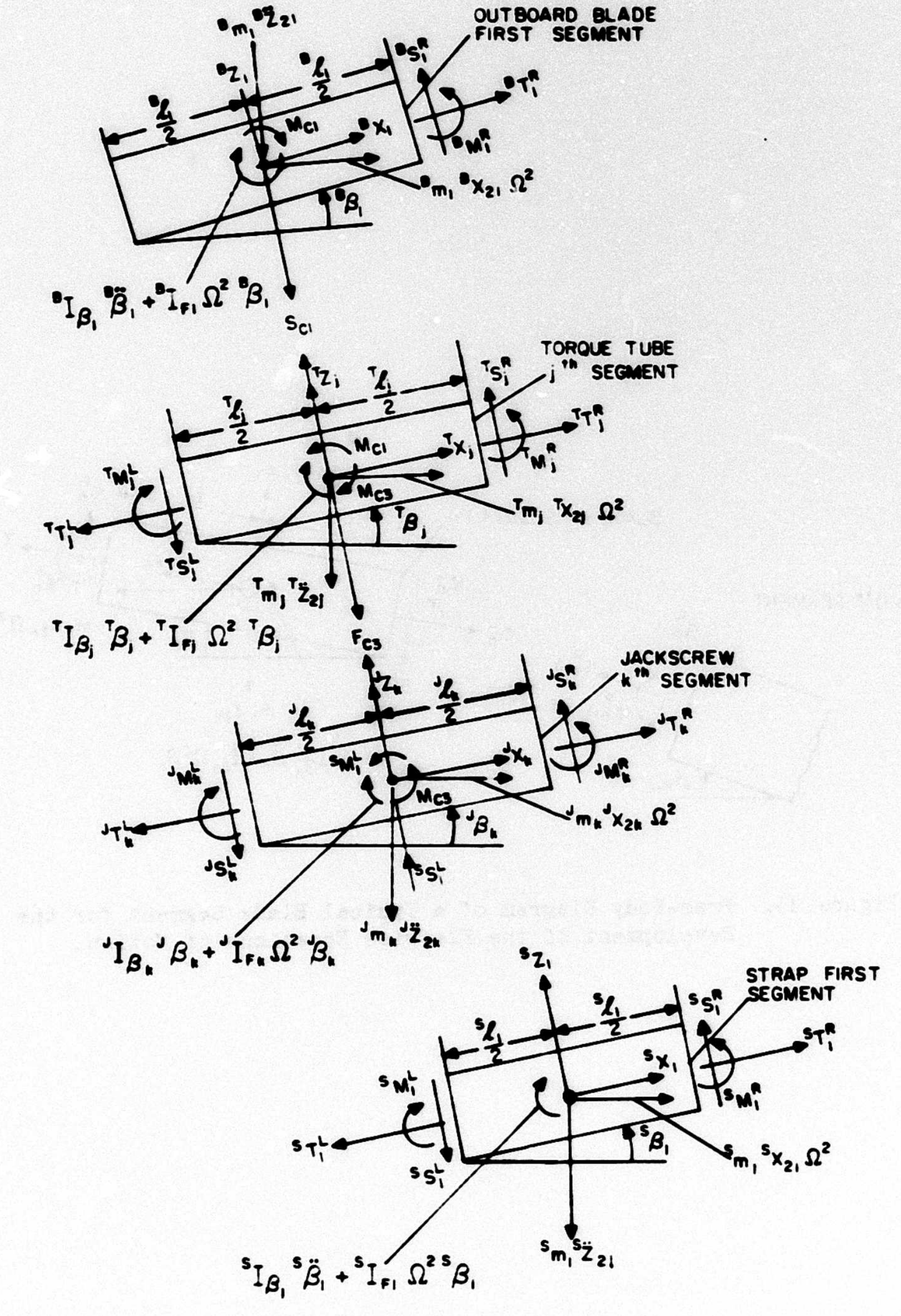

Figure 36. Free-Body Diagrams for Boundary Conditions 1, 3, and 4 (See Figure 7).

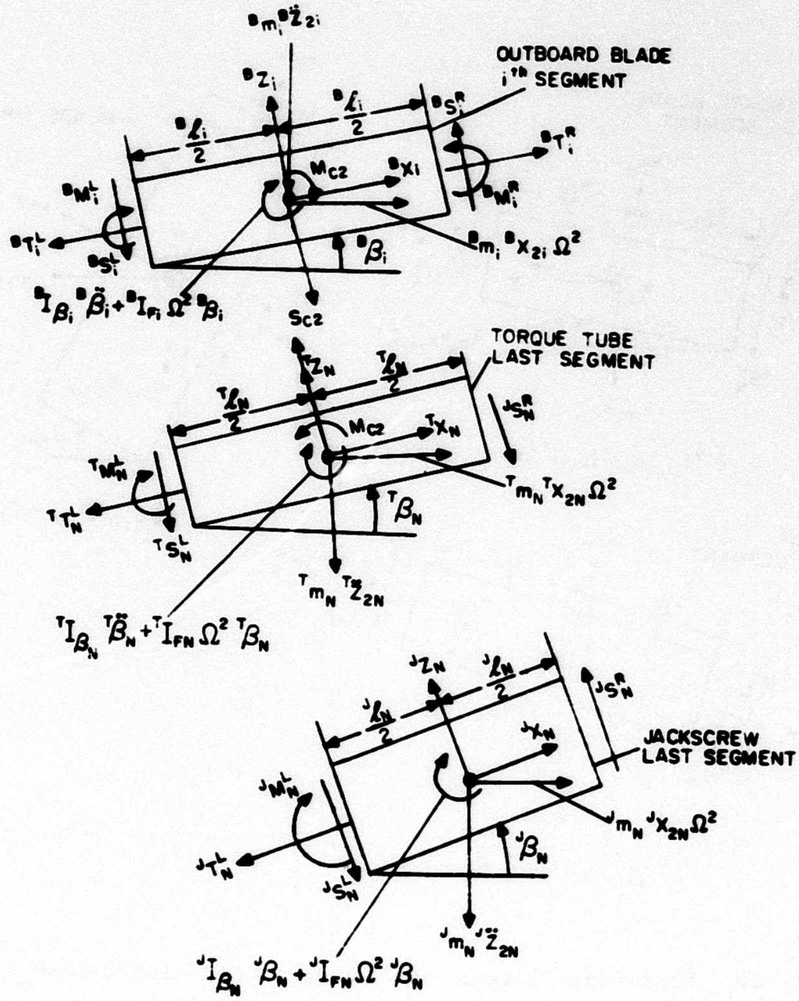

Figure 37. Free-Body Diagrams for Boundary Conditions 2 and 5 (See Figure 7).

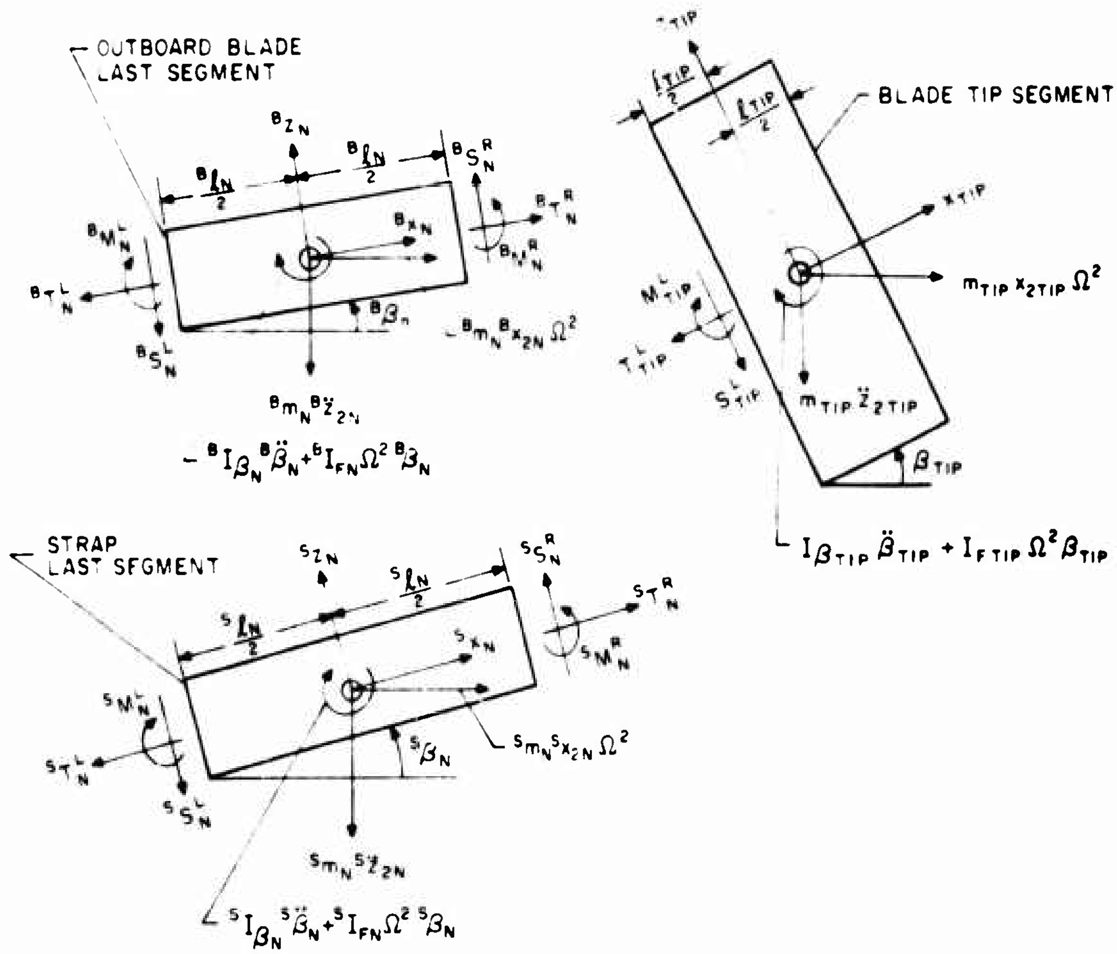

Figure 38. Free-Body Diagram for Boundary Condition 6 (See Figure 7).

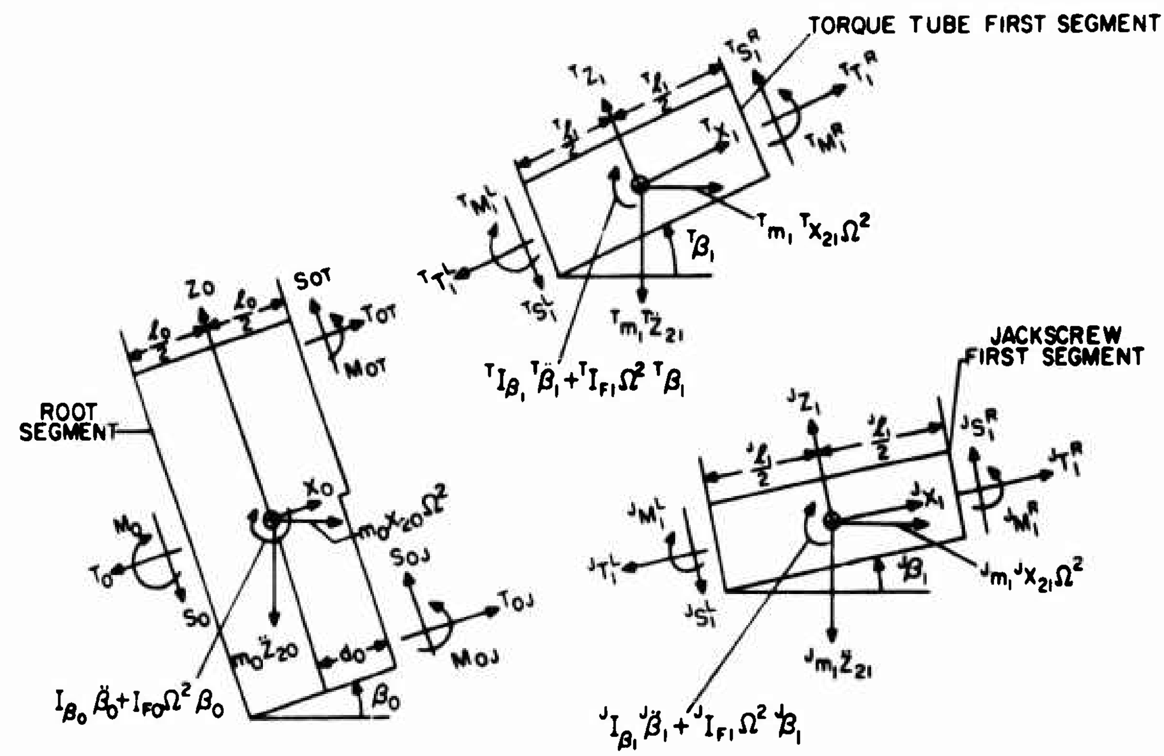

Figure 39. Free-Body Diagram for Boundary Condition 7 (See Figure 7).

LITERATURE CITED

1. Fradenburgh, E. A., Murrill, R. J., and Kiely, E. F., DYNAMIC MODEL WIND TUNNEL TESTS OF A VARIABLE-DIAMETER, TELESCOPING-BLADE ROTOR SYSTEM (TRAC ROTOR), Sikorsky Aircraft Division, United Aircraft Corporation; USAAMRDL Technical Report 73-32, Eustis Directorate, U. S. Army Air Mobility Research and Development Laboratory, Fort Eustis, Virginia, July 1973.

2. Arcidiacono, P. J., PREDICTION OF ROTOR INSTABILITY AT HIGH FORWARD SPEEDS, VOLUME I, STEADY FLIGHT DIFFERENTIAL EQUATIONS OF MOTION FOR A FLEXIBLE HELICOPTER BLADE WITH CHORDWISE MASS UNBALANCE, Sikorsky Aircraft Division, United Aircraft Corporation; USAAVLABS Technical Report 68-18A, U. S. Army Aviation Materiel Laboratories, Fort Eustis, Virginia, February 1969, AD685860.

3. Bergquist, R. R., HELICOPTER GUST RESPONSE INCLUDING UNSTEADY AERODYNAMIC STALL EFFECTS, Sikorsky Aircraft Division, United Aircraft Corporation; USAAMRDL Technical Report 72-68, Eustis Directorate, U. S. Army Air Mobility Research and Development Laboratory, Fort Eustis, Virginia, May 1973.

4. Pestel, E. C., and Leckie, F. A., MATRIX METHODS IN ELASTOMECHANICS, McGraw-Hill Book Co., Inc., New York, 1963.

5. Bergquist, R. R., USER'S MANUAL FOR THE NORMAL MODES AEROELASTIC ANALYSIS COMPUTER PROGRAM FOR THE TRAC ROTOR BLADE, February 1973.

6. Bergquist, R. R., and Thomas, G. C. USER'S MANUAL FOR NORMAL MODE BLADE AEROELASTIC COMPUTER PROGRAM, July 1972.

7. Arcidiacono, P. J., Carta, F. O., Casselini, L. M., and Elman, H. L., INVESTIGATION OF HELICOPTER CONTROL LOADS INDUCED BY STALL FLUTTER, Sikorsky Aircraft Division, United Aircraft Corporation; USAAVLABS Technical Report 70-2, U. S. Army Aviation Materiel Laboratories, Fort Eustis, Virginia, March 1970, AD869823.

8. Landgrebe, Anton J., AN ANALYTICAL METHOD FOR PREDICTING ROTOR WAKE GEOMETRY, United Aircraft Research Laboratories, Journal of the American Helicopter Society, Vol. 14, No. 4, October 1969, pp. 20-32.

APPENDIX I
DERIVATION OF FLATWISE EQUATIONS OF MOTION

The basic transfer matrix for two adjacent segments of a TRAC blade major component is given by relation (51), which is shown below:

$$\begin{Bmatrix} \beta_n \\ z_{2n} \\ S_n^R \\ M_n^R \end{Bmatrix} = \left[C_n \right] \begin{Bmatrix} \beta_{n-1} \\ z_{2(n-1)} \\ S_{n-1}^R \\ M_{n-1}^R \end{Bmatrix} \tag{109}$$

The matrix $[C_n]$, which will be referred to as the "standard " transfer matrix, is repeated below:

$$\left[C_n \right] = \begin{bmatrix} 1 & 0 & 0 & \frac{1}{K_n} \\ \frac{\ell_{n-1}+\ell_n}{2} & 1 & 0 & \frac{\ell_n}{2K_n} \\ C_{31,n} & -m_n \omega^2 & 1 & C_{34,n} \\ C_{41,n} & \frac{m_n \ell_n \omega^2}{2} & -\ell_n & C_{44,n} \end{bmatrix} \tag{110}$$

where

$$C_{31,n} = -m_n \left[\frac{\omega^2}{2} \left(\ell_{n-1} + \ell_n \right) - x_{2n} \Omega^2 \right]$$

$$C_{34,n} = -\frac{1}{K_n} \left[T_{n-1}^R + m_n \left(\frac{\omega^2}{2} \ell_n - x_{2n} \Omega^2 \right) \right]$$

$$C_{41,n} = -\frac{\ell_n}{2} C_{31,n} + I_{Fn} \Omega^2 - I_{\beta_n} \omega^2$$

$$C_{44,n} = 1 + \frac{1}{K_n} \left[-I_{\beta_n} \omega^2 + I_{Fn} \Omega^2 + \ell_n T_{n-1}^R + \frac{m_n \ell_n}{2} \left(\frac{\omega^2 \ell_n}{2} - x_{2n} \Omega^2 \right) \right]$$

The free-body diagram of a typical blade segment is presented in Figure 35. In the derivation of the equations of motion, it is necessary to differentiate among the five structural blade components. To this purpose, a left

superscript is introduced. The letter B refers to the outboard blade, T to the torque tube, J to the jackscrew, RS to the leading strap, and LS to the trailing strap. The schematic of the TRAC blade shown in Figure 10 should be used as a reference in the following presentation, in conjunction with the free-body diagrams shown in Figures 36 through 39.

The equations of motion of the blade tip segment showing the coupling with the last segments of the outboard blade and the straps (see Figure 36) are given below:

$$\begin{Bmatrix} \beta_{TIP} \\ z_{2(TIP)} \\ 0 \\ 0 \end{Bmatrix} = \left[C_{TIP,B}\right] {}^{B}\!\begin{Bmatrix} \beta_N \\ z_{2N} \\ S_N^R \\ M_N^R \end{Bmatrix} + \left[C_{TIP,RS}\right] {}^{RS}\!\begin{Bmatrix} \beta_N \\ S_N^R \end{Bmatrix} + \left[C_{TIP,LS}\right] {}^{LS}\!\begin{Bmatrix} \beta_N \\ S_N^R \end{Bmatrix} \tag{111}$$

where

$$\left[C_{TIP,B}\right] = \begin{bmatrix} 1 & 0 & 0 & \dfrac{1}{K_{TIP,B}} \\ \dfrac{\ell_{TIP} + {}^{B}\ell_N}{2} & 1 & 0 & \dfrac{\ell_{TIP}}{2K_{TIP,B}} \\ C_{31,TIP} & -m_{TIP}\,\omega^2 & 1 & C_{34,TIP} \\ C_{41,TIP} & \dfrac{m_{TIP}\,\ell_{TIP}\,\omega^2}{2} & -\ell_{TIP} & C_{44,TIP} \end{bmatrix} \tag{112}$$

and

$$C_{31,TIP} = -{}^{RS}T_N^R - {}^{LS}T_N^R - m_{TIP}\left[\frac{\omega^2}{2}\left(\ell_{TIP} + {}^{B}\ell_N\right) - X_{2(TIP)}\Omega^2\right]$$

$$C_{34,TIP} = -\frac{1}{K_{TIP,B}}\left[{}^{B}T_N^R + {}^{RS}T_N^R + {}^{LS}T_N^R + m_{TIP}\left(\frac{\omega^2 \ell_{TIP}}{2} - X_{2(TIP)}\Omega^2\right)\right]$$

$$\begin{aligned} C_{41,TIP} = {} & -\frac{\ell_{TIP}}{2} C_{31,TIP} + K_{TIP,RS} + K_{TIP,LS} + \frac{\ell_{TIP}}{2}\left({}^{RS}T_N^R + {}^{LS}T_N^R\right) \\ & - \omega^2 I_{\beta_{TIP}} + \Omega^2 I_{F\,TIP} \end{aligned}$$

$$\begin{aligned} C_{44,TIP} = {} & 1 + \frac{1}{K_{TIP,B}}\Big[\ell_{TIP}\left({}^{B}T_N^R + {}^{RS}T_N^R + {}^{LS}T_N^R\right) + K_{TIP,RS} + K_{TIP,LS} \\ & + \frac{m_{TIP}\,\ell_{TIP}}{2}\left(\frac{\omega^2 \ell_{TIP}}{2} - X_{2(TIP)}\Omega^2\right) - \omega^2 I_{\beta_{TIP}} + \Omega^2 I_{F,TIP} \end{aligned}$$

The coupling between the blade tip and the straps is present in the following matrices:

$$\left[C_{TIP,RS}\right] = \begin{bmatrix} 0 & 0 \\ 0 & 0 \\ {}^{RS}T_N^R & 1 \\ -\ell_{TIP}\,{}^{RS}T_N^R - K_{TIP,RS} & -\ell_{TIP} \end{bmatrix}, \quad \left[C_{TIP,LS}\right] = \begin{bmatrix} 0 & 0 \\ 0 & 0 \\ {}^{LS}T_N^R & 1 \\ -\ell_{TIP}\,{}^{LS}T_N^R - K_{TIP,LS} & -\ell_{TIP} \end{bmatrix} \quad (113)$$

In equation (111), the boundary condition stating that the blade tip is a free end was used; i.e., the tension, shear, and moment at the right-hand side of the tip segment are all zero.

By proceeding inboard along the outboard blade, the transfer matrix method results in the following equations describing the tip end variables in terms of the variables at the blade i^{th} segment:

$$^{B}\begin{Bmatrix} \beta_N \\ z_{2N} \\ S_N^R \\ M_N^R \end{Bmatrix} = {}^{B}\left[C_N\right]{}^{B}\left[C_{N-1}\right]\cdots{}^{B}\left[C_{i+1}\right]{}^{B}\begin{Bmatrix} \beta_i \\ z_{2i} \\ S_i^R \\ M_i^R \end{Bmatrix} \quad (114)$$

where the matrices ${}^{B}\left[C_N\right]$ through ${}^{B}\left[C_{i+1}\right]$ are forms of the standard transfer matrix.

As illustrated in Figure 37, the blade i^{th} segment is in sliding contact with the torque tube last segment. The assumption that the tube and spar walls are infinitely stiff in the normal direction leads to the condition that the vertical displacements of the two segments are the same, i.e., ${}^{B}z_{2i} = {}^{T}z_{2n}$. An equivalent angular spring, K_{C2}, is assumed to represent the component flexibility in the flapping direction. The moment present in the contact area, M_{C2}, is then defined by the relation $M_{C2} = K_{C2}\,({}^{B}\beta_i - {}^{T}\beta_N)$. We note that for walls of infinite stiffness, the relation above reduces to ${}^{B}\beta_i = {}^{T}\beta_N$. The normal shear and bending moments present in the contact area are eliminated by a simultaneous solution of the equations for the shear and moment of the two segments and the relations given above. The torque tube end is rigidly attached to the end of the jackscrew; the normal shear present between the two elements at this junction is denoted by the symbol ${}^{J}S_N^R$. The end bending moment for both the jackscrew and torque tube is zero. The above statements justify the form of the equations given below for the i^{th} blade segment.

$$
{}^{B}\begin{Bmatrix} \beta_i \\ Z_{2i} \\ S_i^R \\ M_i^R \end{Bmatrix} = {}^{B}[C_i]\,{}^{B}[C_{i-1}]\cdots{}^{B}[C_2]\;{}^{B}\begin{Bmatrix} \beta_1 \\ Z_{21} \\ S_1^R \\ M_1^R \end{Bmatrix} + {}^{T}[C_N]\;{}^{T}\begin{Bmatrix} \beta_{N-1} \\ S_{N-1}^R \\ M_{N-1}^R \end{Bmatrix} + {}^{J}[C_N]\,{}^{J}S_N^R \tag{115}
$$

where the matrices ${}^{B}[C_{i-1}]$ through ${}^{B}[C_2]$ are standard transfer matrices and the matrices ${}^{B}[C_i]$, ${}^{T}[C_N]$ and ${}^{J}[C_N]$ are listed below.

$$
{}^{B}[C_i] = \begin{bmatrix} 1 & 0 & 0 & \dfrac{1}{{}^{B}K_i} \\ \dfrac{{}^{B}l_{i-1} + {}^{B}l_i}{2} & 1 & 0 & \dfrac{{}^{B}l_i}{2\,{}^{B}K_i} \\ {}^{B}C_{31,i} & -\omega^2({}^{B}m_i + {}^{T}m_N) & 1 & {}^{B}C_{34,i} \\ {}^{B}C_{41,i} & \dfrac{\omega^2\,{}^{B}l_i}{2}({}^{B}m_i + {}^{T}m_N) & -{}^{B}l_i & {}^{B}C_{44,i} \end{bmatrix} \tag{116}
$$

where

$$
{}^{B}C_{31,i} = -{}^{B}m_i\left[\frac{\omega^2}{2}({}^{B}l_i + {}^{B}l_{i-1}) - {}^{B}x_{2i}\,\Omega^2\right] - {}^{T}m_N\frac{\omega^2}{2}({}^{B}l_i + {}^{B}l_{i-1})
$$

$$
{}^{B}C_{34,i} = -\frac{1}{{}^{B}K_i}\left[{}^{B}T_{i-1}^R + {}^{B}m_i\left(\omega^2\frac{{}^{B}l_i}{2} - {}^{B}x_{2i}\,\Omega^2\right) + {}^{T}m_N\,\omega^2\,\frac{{}^{B}l_i}{2}\right]
$$

$$
{}^{B}C_{41,i} = -\frac{{}^{B}l_i}{2}\,{}^{B}C_{31,i} - \omega^2\,{}^{B}I_{\beta_i} + \Omega^2\,{}^{B}I_{Fi} + \frac{C_{c2}D_N + C_{c2}^2}{D_N}
$$

$$
{}^{B}C_{44,i} = 1 + \frac{1}{{}^{B}K_i}\left[{}^{B}l_i\,{}^{B}T_{i-1}^R + {}^{B}I_{Fi}\,\Omega^2 - {}^{B}I_{\beta_i}\,\omega^2 + \frac{{}^{B}m_i\,{}^{B}l_i}{2}\left(\omega^2\frac{{}^{B}l_i}{2} - {}^{B}x_{2i}\,\Omega^2\right) + \frac{{}^{T}m_N\,{}^{B}l_i^2\,\omega^2}{4} + \frac{C_{c2}D_N + C_{c2}^2}{D_N}\right]
$$

$$
{}^{T}[C_N] = \begin{bmatrix} 0 & 0 & 0 \\ 0 & 0 & 0 \\ {}^{T}T_{N-1}^R & 1 & 0 \\ \dfrac{{}^{B}l_i\,{}^{T}T_{N-1}^R(C_{c2}-D_N)}{2D_N} & \dfrac{{}^{B}l_i(C_{c2}-D_N)}{2D_N} & -\dfrac{C_{c2}}{D_N} \end{bmatrix} \tag{117}
$$

$$
{}^{J}[C_N] = \begin{bmatrix} 0 \\ 0 \\ 1 \\ -\dfrac{{}^{B}l_i(D_N + C_{c2})}{2D_N} \end{bmatrix} \tag{118}
$$

In the matrices above, the quantity D_N is given by

$$D_N = {}^T I_{\beta_N} \omega^2 - {}^T I_{FN} \Omega^2 - \frac{{}^B l_i}{2} {}^T T_{N-1}^R - C_{c2} \tag{119}$$

It should be pointed out that the analysis requires that the two sliding segments have the same length, i.e., ${}^B l_i = {}^T l_N$. This relation has been used in the derivation of equation (115).

The two additional equations for the last segment of the torque tube are

$${}^T\beta_N = {}^T\beta_{N-1} + \frac{{}^T M_{N-1}^R}{{}^T K_N} \tag{120}$$

$${}^T z_{2N} = {}^T z_{2(N-1)} + \frac{{}^T l_{N-1}}{2} {}^T\beta_{N-1} + \frac{{}^T l_N}{2} {}^T\beta_N \tag{121}$$

Substitution for ${}^T\beta_N$ from the moment equation and for ${}^T z_{2N}$ and ${}^T l_n$ reduces the above relations to

$$\begin{aligned} 0 = {}^T\beta_{N-1}\left[-\frac{{}^B l_i}{2} {}^T T_{N-1}^R - D_N\right] - \frac{{}^B l_i}{2} {}^T S_{N-1}^R \\ + \frac{{}^T M_{N-1}^R}{{}^T K_N}\left({}^T K_N + D_N\right) + \frac{{}^T l_i}{2} {}^T S_N^R - C_{c2} {}^B\beta_i \end{aligned} \tag{122}$$

$${}^B z_{2i} = \frac{{}^T\beta_{N-1}}{2}\left({}^T l_{N-1} + {}^B l_i\right) + {}^T z_{2(N-1)} + \frac{{}^B l_i \, {}^T M_{N-1}^R}{2 \, {}^T K_N} \tag{123}$$

The derivation of the equations of motion which are directly applicable to the outboard blade has been completed.

The derivation of the equations for both straps is handled in the same manner. The left supercript, S, refers to either strap. Since no additional contacts are present along the entire length of the straps, the transfer matrix method results in the following equations:

$${}^S\begin{Bmatrix} \beta_N \\ z_{2N} \\ S_N^R \\ M_N^R \end{Bmatrix} = {}^S[C_N]\,{}^S[C_{N-1}] \cdots {}^S[C_2]\,{}^S\begin{Bmatrix} \beta_1 \\ z_{21} \\ S_1^R \\ M_1^R \end{Bmatrix} \tag{124}$$

where the matrices ${}^S[C_N]$ through ${}^S[C_2]$ are standard forms of the transfer matrix.

From Figure 10 it is seen that the inboard end of the straps is attached rigidly to the center of the jackscrew k^th segment which contains the nut assembly (point 4). The boundary conditions at this point are then

$$ {}^{S}\beta_1 = {}^{J}\beta_k \tag{125} $$

and

$$ {}^{S}z_{21} - \frac{{}^{S}\ell_1}{2}\beta_1 = {}^{J}z_{2k} \tag{126} $$

In addition,we have two relations between the last segment of the strap and the blade tip. They are

$$ {}^{S}M_N^{R} = K_{TIP,S}\left[\beta_{TIP} - {}^{S}\beta_N\right] \tag{127} $$

and

$$ {}^{S}z_{2N} + \frac{{}^{S}\ell_N}{2}\,{}^{S}\beta_N = z_{2(TIP)} - \frac{\ell_{TIP}}{2}\beta_{TIP} \tag{128} $$

Equations (124) through (128) are applicable to either strap.

The next element to be analyzed is the torque tube. The equations for the last segment of the torque tube have already been used in the derivation of equation (115) for contact point 2. The rigid attachment between the outboard ends of the tube and the jackscrew, which is illustrated by point 5 in Figure 10, provides the following relation:

$$ {}^{J}z_{2N} + \frac{{}^{J}\ell_N}{2}\,{}^{J}\beta_N = {}^{T}z_{2N} + \frac{{}^{T}\ell_N}{2}\,{}^{T}\beta_N \tag{129} $$

No relation is assumed to be present between the flapping angles of the two segments. Proceeding inboard along the torque tube, the following equations apply:

$$
{}^{T}\begin{Bmatrix} \beta_{N-1} \\ z_{N-1} \\ S^{R}_{N-1} \\ M^{R}_{N-1} \end{Bmatrix} = {}^{T}\left[C_{N-1}\right] {}^{T}\left[C_{N-2}\right] \cdots {}^{T}\left[C_{j+1}\right] {}^{T}\begin{Bmatrix} \beta_j \\ z_j \\ S_j^{R} \\ M_j^{R} \end{Bmatrix} \tag{130}
$$

where the matrices ${}^{T}\left[C_{N-1}\right]$ through ${}^{T}\left[C_{j+1}\right]$ are all standard forms of the transfer matrix.

The equations for the torque tube j^{th} segment which is in contact with the first segment of the outboard blade (point 1 in Figure 10) and with the nut assembly (point 3) are derived in the same manner as that used for contact number 2, using Figure 38. Use of the relations

$$
M_{C1} = C_{C1}\left[{}^{B}\beta_1 - {}^{T}\beta_j\right] \tag{131}
$$

$$
{}^{T}z_{2j} = {}^{B}z_{21} \tag{132}
$$

$$
{}^{T}\beta_j\, C_{C1} = D_1\, {}^{B}\beta_1 - \frac{{}^{B}\ell_1}{2}\, {}^{B}S_1^{R} - {}^{B}M_1^{R} \tag{133}
$$

where

$$
D_1 = -\omega^2\, {}^{B}I_{\beta_1} + \Omega^{2}\, {}^{B}I_{F1} + C_{C1} \tag{134}
$$

gives

$$
{}^{T}\begin{Bmatrix} \beta_j \\ z_{2j} \\ S_j^{R} \\ M_j^{R} \end{Bmatrix} = {}^{T}\left[C_j\right] {}^{T}\left[C_{j-1}\right] \cdots {}^{T}\left[C_2\right] {}^{T}\begin{Bmatrix} \beta_1 \\ z_{21} \\ S_1^{R} \\ M_1^{R} \end{Bmatrix} + {}^{B}\left[C_1\right] {}^{B}\begin{Bmatrix} \beta_1 \\ S_1^{R} \end{Bmatrix} + \left[M_1\right] \begin{Bmatrix} F_{C3} \\ M_{C3} \end{Bmatrix} \tag{135}
$$

The normal force F_{C3} and the bending moment M_{C3} are present between the tube and the jackscrew k^{th} segment which contains the nut assembly. This contact is present only in the flatwise equations of motion. The matrices ${}^{T}\left[C_{j-1}\right]$ through ${}^{T}\left[C_2\right]$ in equation (135) are standard matrices, while the matrices ${}^{T}\left[C_j\right]$, ${}^{B}\left[C_1\right]$, and $\left[M_1\right]$ are as follows:

$$
{}^T[C_j] = \begin{bmatrix} 1 & 0 & 0 & \dfrac{1}{{}^TK_j} \\ \dfrac{{}^T\ell_{j-1} + {}^T\ell_j}{2} & 1 & 0 & \dfrac{{}^T\ell_j}{2\,{}^TK_j} \\ {}^Tc_{31,j} & -\omega^2({}^Bm_1 + {}^Tm_j) & 1 & {}^Tc_{34,j} \\ {}^Tc_{41,j} & \omega^2 \dfrac{{}^T\ell_j}{2}({}^Bm_1 + {}^Tm_j) & -{}^T\ell_j & {}^Tc_{44,j} \end{bmatrix} \tag{136}
$$

where

$$
{}^Tc_{31,j} = -{}^Bm_1 \frac{\omega^2}{2}({}^T\ell_{j-1} + {}^T\ell_j) - {}^Tm_j\left[\frac{\omega^2}{2}({}^T\ell_{j-1} + {}^T\ell_j) - {}^Tx_{2j}\,\Omega^2\right]
$$

$$
{}^Tc_{34,j} = -\frac{1}{{}^TK_j}\left[{}^TT_{j-1}^R + {}^Tm_j\left(\frac{\omega^2}{2}{}^T\ell_j - {}^Tx_{2j}\,\Omega^2\right) + {}^Bm_1 \frac{\omega^2}{2}\,{}^T\ell_j\right]
$$

$$
{}^Tc_{41,j} = -\frac{{}^T\ell_j}{2}\,{}^Tc_{31,j} - \omega^2\,{}^TI_{\beta_j} + \Omega^2\,{}^TI_{Fj} + C_{c1}
$$

$$
{}^Tc_{44,j} = 1 + \frac{1}{{}^TK_j}\left[-\omega^2\,{}^TI_{\beta_j} + \Omega^2\,{}^TI_{Fj} + {}^T\ell_j\,{}^TT_{j-1}^R + {}^Bm_1\,{}^T\ell_j^2\,\frac{\omega^2}{4} + \frac{{}^Tm_j\,{}^T\ell_j}{2}\left(\frac{\omega^2\,{}^T\ell_j}{2} - {}^Tx_{2j}\,\Omega^2\right) + C_{c1}\right]
$$

$$
{}^B[C_1] = \begin{bmatrix} 0 & 0 \\ 0 & 0 \\ {}^Bm_1\,{}^Bx_{21}\,\Omega^2 & -1 \\ -\dfrac{{}^Bm_1\,{}^Bx_{21}\,{}^T\ell_j\,\Omega^2}{2} - C_{c1} & \dfrac{{}^T\ell_j}{2} \end{bmatrix} \tag{137}
$$

$$
[M_1] = \begin{bmatrix} 0 & 0 \\ 0 & 0 \\ 1 & 0 \\ -\dfrac{{}^T\ell_j}{2} & 1 \end{bmatrix} \tag{138}
$$

The relations between the first segment of the torque tube and the root segments are presented below, using Figure 39.

$$
{}^T\begin{Bmatrix} \beta_1 \\ z_{21} \\ S_1^R \\ M_1^R \end{Bmatrix} = {}^T[C_1] \begin{Bmatrix} \beta_c \\ S_{cT} \\ M_{cT} \end{Bmatrix} \tag{139}
$$

where β_0 is the root flapping angle, S_{OT} is the normal shear, and M_{OT} is the bending moment between the tube and the root segment. The matrix ${}^{T}[C_1]$ is given below:

$$
{}^{T}\left[C_1\right] = \begin{bmatrix} 1 & 0 & \dfrac{1}{{}^{T}K_1} \\ \ell_0 + \dfrac{{}^{T}\ell_1}{2} & 0 & \dfrac{{}^{T}\ell_1}{2\,{}^{T}K_1} \\ {}^{T}C_{31,1} & 1 & {}^{T}C_{33,1} \\ {}^{T}C_{41,1} & -{}^{T}\ell_1 & {}^{T}C_{43,1} \end{bmatrix} \tag{140}
$$

where

$$
{}^{T}C_{31,1} = -{}^{T}m_1\left[\omega^2\left(\ell_c + \frac{{}^{T}\ell_1}{2}\right) - {}^{T}x_{21}\Omega^2\right]
$$

$$
{}^{T}C_{33,1} = -\frac{1}{{}^{T}K_j}\left[T_{CT} + {}^{T}m_1\left(\omega^2\frac{{}^{T}\ell_1}{2} - {}^{T}x_{21}\Omega^2\right)\right]
$$

$$
{}^{T}C_{41,1} = -\frac{{}^{T}\ell_1}{2}\,{}^{T}C_{31,1} - {}^{T}I_{\beta_1}\omega^2 + {}^{T}I_{F1}\Omega^2
$$

$$
{}^{T}C_{43,1} = 1 + \frac{1}{{}^{T}K_1}\left[{}^{T}\ell_1 T_{CT} + \frac{{}^{T}m_1\,{}^{T}\ell_1}{2}\left(\frac{\omega^2\,{}^{T}\ell_1}{2} - {}^{T}x_{21}\Omega^2\right) - {}^{T}I_{\beta_1}\omega^2 + {}^{T}I_{F1}\Omega^2\right]
$$

We have now completed the derivation of the torque tube equations. The jackscrew equations are derived next.

The flatwise equations of motion for the last segment of the jackscrew with zero bending moment on the right-hand side are listed below:

$$
{}^{J}\left[A_N\right]{}^{J}\begin{Bmatrix} \beta_N \\ z_{2N} \\ S_N^R \end{Bmatrix} = {}^{J}\left[B_N\right]{}^{J}\begin{Bmatrix} \beta_{N-1} \\ z_{2(N-1)} \\ S_{N-1}^R \\ M_{N-1}^R \end{Bmatrix} \tag{141}
$$

where the matrices ${}^{J}[A_N]$ and ${}^{J}[B_N]$ are

$$
{}^{J}\left[A_N\right] = \begin{bmatrix} {}^{J}m_N\left(\dfrac{{}^{J}\ell_N}{2}\omega^2 - {}^{J}x_{2N}\Omega^2\right) + {}^{J}T_{N-1}^R & 0 & 1 \\ -\dfrac{{}^{J}\ell_N}{2} & 1 & 0 \\ {}^{J}I_{\beta_N}\omega^2 - {}^{J}I_{FN}\Omega^2 - \dfrac{{}^{J}\ell_N}{2}\,{}^{J}T_{N-1}^R & 0 & \dfrac{{}^{J}\ell_N}{2} \\ 1 & 0 & 0 \end{bmatrix} \tag{142}
$$

$$
{}^{J}\left[B_N\right] = \begin{bmatrix} \dfrac{{}^{J}T_{N-1}^{R} - {}^{J}m_N\,{}^{J}\ell_{N-1}\,\omega^2}{2} & -{}^{J}m_N\,\omega^2 & 1 & 0 \\ \dfrac{{}^{J}\ell_{N-1}}{2} & 1 & 0 & 0 \\ -\dfrac{{}^{J}\ell_N\,{}^{J}T_{N-1}^{R}}{2} & 0 & -\dfrac{{}^{J}\ell_N}{2} & 1 \\ 1 & 0 & 0 & \dfrac{1}{{}^{J}K_N} \end{bmatrix} \tag{143}
$$

By proceeding inboard along the jackscrew, the following relations are obtained:

$$
{}^{J}\begin{Bmatrix} \beta_{N-1} \\ z_{2(N-1)} \\ S_{N-1}^{R} \\ M_{N-1}^{R} \end{Bmatrix} = {}^{J}\left[C_{N-1}\right]\,{}^{J}\left[C_{N-2}\right]\cdots{}^{J}\left[C_{k+1}\right]\,{}^{J}\begin{Bmatrix} \beta_k \\ z_{2k} \\ S_k^{R} \\ M_k^{R} \end{Bmatrix} \tag{144}
$$

where the matrices ${}^{J}\left[C_{N-1}\right]$ through ${}^{J}\left[C_{k+1}\right]$ are standard forms of the transfer matrix.

For the jackscrew segment containing the nut assembly, it is found that

$$
{}^{J}\begin{Bmatrix} \beta_k \\ z_{2k} \\ S_k^{R} \\ M_k^{R} \end{Bmatrix} = {}^{J}\left[C_k\right]\cdots{}^{J}\left[C_2\right]\,{}^{J}\begin{Bmatrix} \beta_1 \\ z_{21} \\ S_1^{R} \\ M_1^{R} \end{Bmatrix} + {}^{RS}\left[C_1\right]\,{}^{RS}\begin{Bmatrix} S_1^{R} \\ M_1^{R} \end{Bmatrix} + {}^{LS}\left[C_1\right]\,{}^{LS}\begin{Bmatrix} S_1^{R} \\ M_1^{R} \end{Bmatrix} + \left[M_2\right]\begin{Bmatrix} F_{C3} \\ M_{C3} \end{Bmatrix} \tag{145}
$$

where the matrices ${}^{J}\left[C_{k-1}\right]$ through ${}^{J}\left[C_2\right]$ are standard matrices and the remaining matrices are given below:

$$
{}^{J}\left[C_k\right] = \begin{bmatrix} 1 & 0 & 0 & \dfrac{1}{{}^{J}K_k} \\ \dfrac{{}^{J}\ell_{k-1} + {}^{J}\ell_k}{2} & 1 & 0 & \dfrac{{}^{J}\ell_k}{2\,{}^{J}K_k} \\ {}^{J}c_{31,k} & {}^{J}c_{32,k} & 1 & {}^{J}c_{34,k} \\ {}^{J}c_{41,k} & {}^{J}c_{42,k} & {}^{J}\ell_k & {}^{J}c_{44,k} \end{bmatrix} \tag{146}
$$

where

$$^{J}C_{31,k} = \Omega^2\left[{}^{J}m_k\,{}^{J}x_{2k} + {}^{RS}m_1\,{}^{RS}x_{21} + {}^{LS}m_1\,{}^{LS}x_{21}\right] - \frac{\omega^2}{2}\left[{}^{J}m_k\left({}^{J}\ell_{k-1} + {}^{J}\ell_k\right) + {}^{RS}m_1\left({}^{J}\ell_{k-1} + {}^{J}\ell_k + {}^{RS}\ell_1\right) + {}^{LS}m_1\left({}^{J}\ell_{k-1} + {}^{J}\ell_k + {}^{LS}\ell_1\right)\right]$$

$$^{J}C_{32,k} = -\omega^2\left[{}^{J}m_k + {}^{RS}m_1 + {}^{LS}m_1\right]$$

$$^{J}C_{34,k} = -\frac{1}{{}^{J}K_k}\left\{-\Omega^2\left({}^{J}m_k\,{}^{J}x_{2k} + {}^{RS}m_1\,{}^{RS}x_{21} + {}^{LS}m_1\,{}^{LS}x_{21}\right) + \frac{\omega^2}{2}\left[{}^{J}\ell_k\,{}^{J}m_k + {}^{RS}m_1\left({}^{RS}\ell_1 + {}^{J}\ell_k\right) + {}^{LS}m_1\left({}^{LS}\ell_1 + {}^{J}\ell_k\right)\right] + {}^{J}T_{k-1}^{R}\right\}$$

$$^{J}C_{41,k} = -\frac{{}^{J}\ell_k}{2}\,{}^{J}C_{31,k} + \Omega^2\left[{}^{J}I_{Fk} + {}^{RS}I_{F1} + {}^{LS}I_{F1} + \frac{{}^{RS}m_1\,{}^{RS}\ell_1\,{}^{RS}x_{21}}{2} + \frac{{}^{LS}m_1\,{}^{LS}\ell_1\,{}^{LS}x_{21}}{2}\right] - \omega^2\left[\frac{{}^{RS}m_1\,{}^{RS}\ell_1}{4}\left({}^{J}\ell_{k-1} + {}^{J}\ell_k + {}^{RS}\ell_1\right) + \frac{{}^{LS}m_1\,{}^{LS}\ell_1}{4}\left({}^{J}\ell_{k-1} + {}^{J}\ell_k + {}^{LS}\ell_1\right) + {}^{J}I_{\beta k} + {}^{RS}I_{\beta 1} + {}^{LS}I_{\beta 1}\right]$$

$$^{J}C_{42,k} = \frac{\omega^2}{2}\left[{}^{J}m_k\,{}^{J}\ell_k + {}^{RS}m_1\left({}^{J}\ell_k - {}^{RS}\ell_1\right) + {}^{LS}m_1\left({}^{J}\ell_k - {}^{LS}\ell_1\right)\right]$$

$$^{J}C_{44,k} = 1 + \frac{1}{{}^{J}K_k}\left\{{}^{J}\ell_k\,{}^{J}T_{k-1}^{R} + \Omega^2\left[{}^{J}I_{Fk} + {}^{RS}I_{F1} + {}^{LS}I_{F1} + \frac{{}^{RS}m_1\,{}^{RS}x_{21}}{2}\left({}^{RS}\ell_1 - {}^{J}\ell_k\right) + \frac{{}^{LS}m_1\,{}^{LS}x_{21}}{2}\left({}^{LS}\ell_1 - {}^{J}\ell_k\right) - \frac{{}^{J}\ell_k}{2}\,{}^{J}m_k\,{}^{J}x_{2k}\right] - \omega^2\left[{}^{J}I_{\beta k} + {}^{RS}I_{\beta 1} + {}^{LS}I_{\beta 1} + \frac{{}^{RS}m_1}{4}\left({}^{RS}\ell_1^2 - {}^{J}\ell_k^2\right) + \frac{{}^{LS}m_1}{4}\left({}^{LS}\ell_1^2 - {}^{J}\ell_k^2\right) - \frac{{}^{J}\ell_k^2}{4}\,{}^{J}m_k\right]\right\}$$

$$^{RS}[C_1] = \begin{bmatrix} 0 & 0 \\ 0 & 0 \\ -1 & 0 \\ \frac{{}^{J}\ell_k}{2} - {}^{RS}\ell_1 & 1 \end{bmatrix}, \quad {}^{LS}[C_1] = \begin{bmatrix} 0 & 0 \\ 0 & 0 \\ -1 & 0 \\ \frac{{}^{J}\ell_k}{2} - {}^{LS}\ell_1 & 1 \end{bmatrix}, \quad [M_2] = \begin{bmatrix} 0 & 0 \\ 0 & 0 \\ -1 & 0 \\ \frac{{}^{J}\ell_k}{2} & -1 \end{bmatrix} \qquad (147)$$

To satisfy the assumption that the contact between the jackscrew and torque tube is rigid, the following boundary conditions must be met:

$$ {}^{T}\beta_j = {}^{J}\beta_k \tag{148}$$

$$ {}^{T}z_{2j} = {}^{J}z_{2k} \tag{149}$$

The equations relating the first segment of the jackscrew and the blade root are summarized as follows:

$$ {}^{J}\begin{Bmatrix} \beta_1 \\ z_{21} \\ S_1^R \\ M_1^R \end{Bmatrix} = {}^{J}\left[C_1\right] \begin{Bmatrix} \beta \\ S_{OJ} \\ M_{OJ} \end{Bmatrix} \tag{150}$$

where S_{OJ} and M_{OJ} are the normal shear and bending moment respectively between the jackscrew first segment and the blade root. The matrix ${}^{J}\left[C_1\right]$ is shown below:

$$ {}^{J}\left[C_1\right] = \begin{bmatrix} 1 & 0 & \dfrac{1}{{}^{J}K_1} \\ \dfrac{{}^{J}l_1 + l_0}{2} + d_0 & 0 & \dfrac{{}^{J}l_1}{2\,{}^{J}K_1} \\ {}^{J}c_{31,1} & 1 & {}^{J}c_{33,1} \\ {}^{J}c_{41,1} & -{}^{J}l_1 & {}^{J}c_{43,1} \end{bmatrix} \tag{151}$$

where

$$ {}^{J}c_{31,1} = -{}^{J}m_1\left[\omega^2\left(\frac{l_0}{2} + d_0 + \frac{{}^{J}l_1}{2}\right) - {}^{J}x_{21}\Omega^2\right]$$

$$ {}^{J}c_{33,1} = -\frac{1}{{}^{J}K_1}\left[T_{OJ} + {}^{J}m_1\left(\omega^2\frac{{}^{J}l_1}{2} - {}^{J}x_{21}\Omega^2\right)\right]$$

$$ {}^{J}c_{41,1} = -\frac{{}^{J}l_1}{2}\,{}^{J}c_{31,1} - {}^{J}I_{\beta_1}\omega^2 + {}^{J}I_{F1}\Omega^2$$

$$ {}^{J}c_{43,1} = 1 + \frac{1}{{}^{J}K_1}\left[{}^{J}l_1 T_{OJ} + \frac{{}^{J}m_1\,{}^{J}l_1}{2}\left(\omega^2\frac{{}^{J}l_1}{2} - {}^{J}x_{21}\Omega^2\right) - {}^{J}I_{\beta_1}\omega^2 + {}^{J}I_{F1}\Omega^2\right]$$

The root segment length is l_0 while d_0 is the distance from the center of the root segment to the left side of the jackscrew first segment.

The flatwise equations of motion for the blade root segment are given below:

$$\beta_0 m_0 \left[-x_{20}\Omega^2 + \frac{\ell_0 \omega^2}{2} \right] = S_0 - S_{OJ} - S_{OT} \tag{152}$$

and

$$\beta_0 \left[-I_{F0}\Omega^2 + I_{F0}\omega^2 - K_0 \right] + M_{OJ} = -\frac{\ell_0}{2} S_0 - d_0 S_{OJ} - \frac{\ell_0}{2} S_{OT} - M_{OT} \tag{153}$$

In equation (153), the angular spring about the flapping **hinge** has a stiffness of K_o foot-pounds per radian. For an articulated **blade**, K_o is zero. The shear S_o acts at the flapping hinge.

Sixty-five equations have been derived to describe the **flatwise** motion of the TRAC blade five major structural components. The **variables** retained in the analysis must add up to 65 for a fully defined **system of equations. A** summary of the variables present in the flatwise equation **is provided** in the chart below:

TRAC BLADE VARIABLES FOR THE FLATWISE EQUATIONS OF MOTION

Number	Outboard Blade	Leading Strap	Lagging Strap	Torque Tube	Jack-Screw	Tip Segment	Root Segment	Others
1	β_N	β_N	β_N	β_{N-1}	β_N	β_{TIP}	β_0	F_{C3}
2	z_{2N}	z_{2N}	z_{2N}	$z_{2(N-1)}$	z_{2N}	$z_{2(TIP)}$	S_0	M_{C3}
3	S_N^R	S_N^R	S_N^R	S_{N-1}^R	S_N^R		S_{OJ}	
4	M_N^R	M_N^R	M_N^R	M_{N-1}^R	β_{N-1}		S_{OT}	
5	β_i	β_1	β_1	β_j	$z_{2(N-1)}$		M_{OJ}	
6	z_{2i}	z_{21}	z_{21}	z_{2j}	S_{N-1}^R		M_{OT}	
7	S_i^R	S_1^R	S_1^R	S_j^R	M_{N-1}^R			
8	M_i^R	M_1^R	M_1^R	M_j^R	β_k			
9	β_1			β_1	z_k			
10	z_{21}			z_{21}	S_k^R			
11	S_1^R			S_1^R	M_k^R			
12	M_1^R			M_1^R	β_1			
13					z_{21}			
14					S_1^R			
15					M_1^R			
Total No.	12	8	8	12	15	2	6	2

APPENDIX II
DERIVATION OF EDGEWISE EQUATIONS OF MOTION

The system of 65 equations derived in Appendix I for the flatwise motion of the TRAC blade can be used to describe the edgewise motion with the following modifications:

1. The linear displacement z_n is replaced by y_n and the angular displacement β_n by γ_n.
2. Replace ω^2 by $(\omega^2 + \Omega^2)$ with the exception that the inertial term $I_{\beta_n}\omega^2$ appearing in the moment equations becomes $I_{\gamma_n}\omega^2$.
3. Set I_{Fn} to zero.
4. Set F_{C3} and M_{C3} to zero and eliminate the boundary conditions specified in equations (148) and (149).
5. Add to the moment equation of the blade tip segment (equation (111)) the following term:

$$\frac{K_x L_s^2}{2}\left[{}^{\beta}\gamma_N + \frac{{}^{\beta}M_N^R}{{}^{\beta}K_{TIP,\beta}} - {}^{J}\gamma_k\right]$$

6. Add to the moment equation of the jackscrew k^{th} segment (equation (145)) the following term:

$$-\frac{K_x L_s^2}{2}\gamma_{TIP}$$

7. In relation (146), add to the coefficient ${}^{J}C_{41,k}$ the term $\frac{K_x L_s^2}{2}$ and to the coefficient ${}^{J}C_{44,k}$ the term $\frac{K_x L_s^2}{2\,{}^{J}K_R}$.

These modifications were discussed in more detail in the section <u>Derivation of the Edgewise Equations of Motion for the TRAC Blade</u>.

APPENDIX III
SOLUTION OF THE BLADE TENSION EQUATIONS

As seen in Appendix I, the tensions present in each major component are needed in order to solve the system of 65 equations for the blade frequencies and mode shapes. The tension equation (43), which is valid for both flatwise and edgewise motions, is repeated below:

$$T_n^R = T_{n-1}^R - m_n x_{2n} \Omega^2 \tag{154}$$

The continuity equation for the tension force is that

$$T_n^L = T_{n-1}^R \tag{155}$$

The boundary conditions which must be satisfied by the tension equations are listed below using Figure 10:

Point 1: $${}^B T_1^L = 0 \tag{156}$$

Point 2: $${}^T T_N^R = 0 \tag{157}$$

Point 4: $${}^J T_k^R = {}^J T_{k-1}^R - {}^J m_k\, {}^T x_{2k} \Omega^2 - {}^{RS}T_1^L - {}^{LS}T_1^L \tag{158}$$

Point 5: $${}^J T_N^R = 0 \tag{159}$$

Point 6: $$T_{TIP}^R = 0\,, \quad T_{TIP}^L = {}^B T_N^R + {}^{RS}T_N^R + {}^{LS}T_N^R \tag{160}$$

Point 7: $$T_O^R = T_{OJ} + T_{OT}\,, \quad T_O^L = T_O \tag{161}$$

The tension equations (154) and (155) and the boundary conditions listed above are now applied to the TRAC blade major components.

BLADE ROOT

Equations (154), (155), and (161) give

$$T_O = T_{OJ} + T_{OT} + m_O x_{2O} \Omega^2 \tag{162}$$

where

$$x_{2O} = e + \frac{l_O}{2} \tag{163}$$

TORQUE TUBE

Equations (154), (155), and (157) result in the following expression for the tension at any segment, n, of the torque tube:

$$ {}^{T}T_{n}^{R} = \Omega^{2} \sum_{i=n+1}^{N_T} {}^{T}m_{i} {}^{T}x_{2i} \tag{164} $$

Thus the tension at the left side of the tube first segment, T_{OT}, is

$$ T_{OT} = \Omega^{2} \sum_{i=1}^{N_T} {}^{T}m_{i} {}^{T}x_{2i} \tag{165} $$

JACKSCREW

Combining equations (154), (155), (158), and (159) yields, for the tension of a jackscrew segment inboard of the strap attachment,

$$ {}^{J}T_{n}^{R} = \Omega^{2} \left[\sum_{i=n+1}^{N_J} {}^{J}m_{i} {}^{J}x_{2i} \right] + {}^{RS}T_{1}^{L} + {}^{LS}T_{1}^{L} \tag{166} $$

and thus the tension at the left side of the first segment of the jackscrew becomes

$$ T_{OJ} = \Omega^{2} \left[\sum_{i=1}^{N_J} {}^{J}m_{i} {}^{J}x_{2i} \right] + {}^{RS}T_{1}^{L} + {}^{LS}T_{1}^{L} \tag{167} $$

The tension at the k^{th} segment containing the nut assembly is given by equation (158), which is

$$ {}^{J}T_{k}^{R} = {}^{J}T_{k-1}^{R} - {}^{J}m_{k} {}^{J}x_{2k} \Omega^{2} - {}^{RS}T_{1}^{L} - {}^{LS}T_{1}^{L} \tag{168} $$

The tension at any segment outboard of the k^{th} segment is

$$ {}^{J}T_{n}^{R} = \Omega^{2} \sum_{i=n+1}^{N_J} {}^{J}m_{i} {}^{J}x_{2i} \tag{169} $$

OUTBOARD BLADE

The tension equations (154) and (155) and the boundary condition (156) at the inboard end result in the expression below for the blade tension at

any segment:

$$ {}^{B}T_{n}^{R} = -\Omega^{2} \sum_{i=1}^{n} {}^{B}m_{i} {}^{B}x_{2i} \tag{170} $$

Thus, the tension at the outboard end is

$$ {}^{B}T_{N}^{R} = -\Omega^{2} \sum_{i=1}^{N_B} {}^{B}m_{i} {}^{B}x_{2i} \tag{171} $$

An inspection of equations (164) and (170) for the tension along the torque tube and the outboard blade respectively reveals that the centrifugal loading produces a tensile force in the torque tube and a compressive force in the outboard blade.

TENSION STRAPS

Equations (154) and (155) yield for the tension along the leading tension strap,

$$ {}^{RS}T_{n}^{R} = {}^{RS}T_{1}^{L} - \Omega^{2} \sum_{i=1}^{n} {}^{RS}m_{i} {}^{RS}x_{2i} \tag{172} $$

Application of the equation above at the end of the strap gives

$$ {}^{RS}T_{N}^{R} = {}^{RS}T_{1}^{L} - \Omega^{2} \sum_{i=1}^{N_{RS}} {}^{RS}m_{i} {}^{RS}x_{2i} \tag{173} $$

The above expressions are also applicable to the trailing strap. Thus,

$$ {}^{LS}T_{n}^{R} = {}^{LS}T_{1}^{L} - \Omega^{2} \sum_{i=1}^{n} {}^{LS}m_{i} {}^{LS}x_{2i} \tag{174} $$

and

$$ {}^{LS}T_{N}^{R} = {}^{LS}T_{1}^{L} - \Omega^{2} \sum_{i=1}^{N_{LS}} {}^{LS}m_{i} {}^{LS}x_{2i} \tag{175} $$

BLADE TIP

The tension equation (154) in conjunction with the boundary conditions (160) results in the following relation for the blade tip tension:

$$ T_{TIP}^{L} = {}^{B}T_{N}^{R} + {}^{RS}T_{N}^{R} + {}^{LS}T_{N}^{R} = m_{TIP}\, x_{2(TIP)}\, \Omega^{2} \tag{176} $$

An investigation of the tension equations shows that the number of variables present is six, and they are:

$$T_C, T_{CJ}, {}^{RS}T_1^L, {}^{LS}T_1^L, {}^{RS}T_N^R, {}^{LS}T_N^R \tag{177}$$

The number of equations available is five, as given by equations (162), (167), (173), (175), and (176). An additional equation is needed; it is provided by the condition

$${}^{LS}T_N^R = {}^{RS}T_N^R \tag{178}$$

Thus, the tension at the outboard ends of the straps is the same for either strap. This statement is correct when dealing with the flatwise motion of the TRAC blade. However, when the blade bends in the inplane direction, the tension in the straps can be different as discussed in Figure 12. The differential tension is

$$\Delta T = K_x L_S \left(\gamma_{Tip} - {}^J\gamma_k \right) \tag{179}$$

and then equation (178) becomes

$${}^{LS}T_N^R = {}^{RS}T_N^R + K_x L_S \left(\gamma_{Tip} - {}^J\gamma_k \right) \tag{180}$$

We note that the differential tension is a first-order quantity in the inplane angular displacement. It is then consistent with the linearization procedure adopted in this analysis to assume that ΔT is small compared to the strap tension. It should also be pointed out that the contribution of ΔT to the shear force (equation (94)) would be a second-order term which can be neglected.

The final six equations are solved simultaneously to give the following results:

$${}^{RS}T_N^R = {}^{LS}T_N^R = \frac{\Omega^2}{2}\left[m_{Tip} x_{2(Tip)} + \sum_{i=1}^{N_B} {}^B m_i \, {}^B x_{2i} \right] \tag{181}$$

$${}^{RS}T_1^L = \frac{\Omega^2}{2}\left[m_{Tip} x_{2(Tip)} + \sum_{i=1}^{N_B} {}^B m_i \, {}^B x_{2i} + 2 \sum_{i=1}^{N_{RS}} {}^{RS} m_i \, {}^{RS} x_{2i} \right] \tag{182}$$

$$ {}^{LS}T_1^{L} = \frac{\Omega^2}{2}\left[m_{TIP}\, x_{2(TIP)} + \sum_{i=1}^{NB} {}^{B}m_i^{B}\, x_{2i} + 2 \sum_{i=1}^{N_{LS}} {}^{LS}m_i^{LS}\, x_{2i} \right] \tag{183} $$

$$ T_{CJ} = \Omega^2 \left[\sum_{i=1}^{N_J} {}^{J}m_i^{J}\, x_{2i} + \sum_{i=1}^{NB} {}^{B}m_i^{B}\, x_{2i} + \sum_{i=1}^{N_{RS}} {}^{RS}m_i^{RS}\, x_{2i} + \sum_{i=1}^{N_{LS}} {}^{LS}m_i^{LS}\, x_{2i} + m_{TIP}\, x_{2(TIP)} \right] \tag{184} $$

$$ \begin{aligned} T_C = \Omega^2 \Bigg[& m_0 x_{20} + \sum_{i=1}^{N_T} {}^{T}m_i^{T}\, x_{2i} + \sum_{i=1}^{N_J} {}^{J}m_i^{J}\, x_{2i} + \sum_{i=1}^{NB} {}^{B}m_i^{B}\, x_{2i} \\ & + \sum_{i=1}^{N_{RS}} {}^{RS}m_i^{RS}\, x_{2i} + \sum_{i=1}^{N_{LS}} {}^{LS}m_i^{LS}\, x_{2i} + m_{TIP}\, x_{2(TIP)} \Bigg] \end{aligned} \tag{185} $$

The displacement, x_{2n}, for any element is calculated from the continuity equation

$$ x_{2n} = x_{2(n-1)} + \frac{\ell_{n-1} + \ell_n}{2} \tag{186} $$